CO-AXIAL TURBULENT DIFFUSION FLAMES WITH DIRECTED OXYGEN INJECTION

by

Dadmehr Rezaei

A dissertation submitted to the faculty of
The University of Utah
in partial fulfillment of the requirements for the degree of

Doctor of Philosophy

Department of Chemical Engineering

The University of Utah

May 2013

The University of Utah Graduate School

STATEMENT OF DISSERTATION APPROVAL

The dissertation of Dadmehr Rezaei

has been approved by the following supervisory committee members:

Jost O.L. Wendt	, Chair	**10-24-2012** Date Approved
Eric G. Eddings	, Member	**10-24-2012** Date Approved
Terry A. Ring	, Member	**10-24-2012** Date Approved
Philip J. Smith	, Member	**10-24-2012** Date Approved
Lawrence E. Bool	, Member	**10-24-2012** Date Approved

and by **JoAnn Lighty**, Chair of the Department of **Chemical Engineering**

and by Donna M. White, Interim Dean of The Graduate School.

ABSTRACT

Oxy-coal combustion technology has been suggested as the most promising strategy for retrofitting conventional coal power plants to generate electric power while capturing carbon dioxide. The current research addresses three issues in oxy-coal combustion, namely:

1- What is the effect of coal composition on the stability of co-axial turbulent diffusion oxy-flames?

2- What are the stability criteria for turbulent diffusion oxy-coal flames in an advanced triple concentric co-axial burner allowing directed streams of pure oxygen to be introduced into the combustion mix?

3- How does minimization of CO_2 diluent affect radiant heat flux in the combustion chamber?

It is hoped that data produced in this investigation can be used for validation of advanced simulations of the appropriate configurations considered.

In order to address Issue #1 listed above, the consequences of differences in coal composition on flame stability for two types of coal in oxy-combustion were explored: Utah Skyline Bituminous and Illinois #6 Bituminous. Differences in flame stand-off distances at equivalent experimental input conditions were interpreted through differences in the structure of the two coals as well as differences in their pyrolysis

behavior, as determined by fundamental solid state ^{13}C NMR and Thermal Gravimetric Analysis (TGA), respectively.

In addressing Issue #2, the consequences of segregating all the input oxygen into one stream composed of 100% oxygen were determined using the co-axial burners with different oxygen stream configurations. Flame stability, heat flux, and NO_x formation measurements were taken to evaluate the differences. Flame stability was quantified through flame probability density functions (PDF) of the stand-off distance (determined using photo-imaging techniques). The PDFs obtained from these simplified prototype configurations led to physical insight into coal flame attachment mechanisms and the significant effects of fine coal particles and their radial transportation by large eddies on flame stability.

Finally, in addressing Issue #3, impacts of reducing the amount of injected diluent CO_2 (mimicking the minimization of the recycle ratio) on the radiation heat flux were explored. Radiant heat flux, gas temperature, and wall temperature measurements were taken, and a simple radiation model was developed to correlate the average gas temperature and radian heat flux. This study provided a better understanding of the radiation mechanism and the significant effects of soot radiation on the total heat transfer in the next generation of oxy-coal combustion.

CONTENTS

LIST OF TABLES

LIST OF FIGURES

NOMENCLATURE

f_a, The fraction of carbon atoms that are sp2 hybridized (aromaticity).

f_a^C, The fraction of carbon atoms that are in carboxyl or carbonyl groups.

f_a^0, The fraction of carbon atoms that are in a carbonyl group (aldehydes and ketones).

f_a^{00}, The fraction of carbon atoms that are in a carboxyl group (acids, esters, amides).

$f_{a\prime}$, The fraction of carbon atoms that are sp2 hybridized excluding (corrected aromaticity).

f_a^H, The fraction of carbon atoms that are protonated aromatics.

f_a^N, The fraction of carbon atoms that are non-protonated aromatics.

f_a^P, The fraction of carbon atoms that are aromatic with an oxygen atom attached.

f_a^S, The fraction of carbon atoms that are aromatic with a carbon chain attached (also includes biaryl carbons).

f_a^B, The fraction of carbon atoms that are aromatic and a bridgehead carbon.

f_{al}, The fraction of carbon atoms that are sp3 hybridized (aliphatic).

f_{al}^H, The fraction of carbon atoms that are aliphatic but not methyls.

f_{al}^*, The fraction of carbons that are aliphatic and methyls

f_{al}^O, The fraction of carbon atoms that are aliphatic and attached to an oxygen atom.

χ_b, The mole fraction of bridgehead carbon atoms.

C, The average aromatic cluster size.

$\sigma+1$, The average number of attachments on an aromatic cluster.P_0, The fraction of attachments that don't end in a side chain (methyl group).

B.L., The average number of attachments on an aromatic cluster that are bridges or loops (a loop is a bridge back to the same cluster).

S.C., The average number of side chains on an aromatic cluster.

MW, The average molecular weight of an aromatic cluster including side-chains and bridges.

M_{δ}, The average mass of a side chain or one-half of a bridge.

ACKNOWLEDGMENTS

First and foremost, I would like to thank my parents, Reza Mohammadrezaei and Zahra Khoshbin, for their lifelong support in everything, but most significantly, for their encouragement to pursue a higher education. Additionally, my siblings, Daryoush and Roya Mohammadrezaei, were an integral part of my success.

I would also like to express my most sincere gratitude to Prof. Jost O. L. Wendt for his continual guidance, patience and support throughout my years in the program. It has been such a pleasure for me to work with Prof. Wendt. Prof. Eric Eddings, Prof. Terry Ring., Prof. Phil Smith, and Dr. Lawrence Bool, who were also much appreciated members of my defense committee.

I am also thankful to Prof. Ronald Pugmire and Dr. Mark Solum for their encouragements and technical suggestions as well as for providing outstanding NMR data. The help of Dr. Yuegui Zhou of Shanghai Jiao Tong University in the early stages of the research was unforgettable. Kerry Kelly is also much appreciated for contributing to the success of the integration of the photo-imaging technique and analyzing the length and stability of flame. Working with all of these professionals has been a great pleasure and a learning experience

The help of Dana Overacker, Ryan Okerlund, Dave Wagner, and Brian Nelson in the lab is appreciated. Without their indispensable help, the experimentation portion

would have been significantly drawn out. Additionally, I would like to thank Charles German, Colby Ashcroft, Taylor Geisler, and Travis LeGrande for their help in the lab.

This work is based upon work supported by the Department of Energy under Award Number FC26-08NT0005015 through the Clean Coal Center (UC^3). The O_2 and CO_2 supply during the test were provided at no cost to the project by Praxair Inc.

1. INTRODUCTION

1.1 Background

The generation of electricity from fossil fuels has caused the emission of greenhouse gases. Previous research has shown global warming is the result of greenhouse gases. Among the greenhouse gases, CO_2 is known as the most dominant contributor. It is believed that greenhouse emissions can be reduced by the use of renewable energy sources. However, until the time these energy sources can be developed adequately to generate the required amount of energy, fossil fuels are the most robust energy sources available. Coal is an abundant resource in the United States. To lower the emission of the greenhouse gases from coal power plants, several technologies have been suggested using amine absorption: 1) CO_2 capture from power plants by scrubbers 2) Integrated Gasification Combustion Cycle (IGCC) 3) Chemical Looping Combustion, and 4) Oxy-Fuel Combustion [1]. Abraham et al. [2] in 1982 proposed the technology of oxy-coal combustion to produce CO_2 for Enhanced Oil Recovery (EOR) . Wang et al. [3] explored the feasibility of burning pulverized coal in O_2/CO_2 atmosphere. Oxy-Fuel Combustion technology has been suggested as the most promising strategy for conventional coal power plants to generate electric power [4].

1.2 Oxy-Coal Combustion Technology Description

In oxy-coal combustion, a mixture of pure oxygen with purity of greater than 95% and the recycled flue gas are used for combustion of coal. The product of this combustion

is a gas consisting of mostly water and CO_2. The recycled flue gas is considered as an inert gas to modulate the combustion temperature as well as distribute the heat of combustion in the furnace [1,4]. The required oxygen is provided from an air separation unit (ASU). A part of the flue gas, not recycling, will go through the desulfurization unit and water condensation unit. After condensation of the moisture, the flue gas is a gas containing nearly 95% CO_2. This gas will be liquefied and can be applied for EOR or other industrial purposes. A schematic of oxy-fuel combustion is provided in Figure 1[5].

The differences between air and oxy-combustion are:

1) Combustion medium (O_2/N_2 in air-firing and O_2/CO_2 in oxy-firing)
2) Composition of combustion products and particulate concentration
3) Thermal properties such as heat capacity, density, and viscosity as well as radiative properties of the furnace gases
4) Radiant and convective heat flux profiles in oxy-combustion

Due to the similarity of the oxy-firing and air-firing systems, oxy-fuel combustion is known as one of the most promising remedies for retrofitting conventional power plans; however, there are issues that need to be resolved:

1) O_2 supply
2) Corrosion due to recirculation of flue gas
3) Purity of CO_2 in flue gas
4) Heat transfer
5) Need for submodels and simulation of the oxy-fuel combustion
6) Oxy-combustion cost
7) Burner aerodynamics and oxygen injection

1.3 Ignition and Flame Stability in Oxy-Coal Combustion

When a coal particle is placed in a furnace, it is heated to a temperature at which pyrolysis starts. During this process, the volatile contents of the coal particle get released. The pyrolysis temperature depends on the coal and the heating rate of the particle. The pyrolysis and ignitibility of coal volatile species and their transport from a particle to its surrounding determines whether the ignition of an isolated coal particle occurs either heterogeneously or homogeneously (in gas ignition) [6]. Homogeneous reaction occurs when the volatiles eject early due to the environment conditions, they react with oxygen, and start the ignition before oxygen reaches the particle surface. In the cases where combustion is incomplete or liberation of volatiles is retarded, oxygen can reach the particle surface and have a heterogeneous reaction with the particle.

Katalambula et al. [7] studied the effect of the volatile matter cloud surrounding a single coal particle on the ignition mechanism. They found that the amount of volatiles surrounding a coal particle being influenced by natural or forced convection affects the ignition mechanism and temperature. Volatile matter content has a significant effect on the ignition temperature, and is almost negligible under forced convection. Additionally, Katalambula and his colleagues showed that the ignition temperature increases correspondingly with the coal particle size. Kharbat and Annamalai [6] applied a digital image processing technique to investigate the ignition and combustion characteristics of isolated coal particles as well as the interactive combustion of a binary coal array. Their experiment concluded that the ignition of high, medium, and low volatile coals is always heterogeneous, and the release of volatiles and secondary gas ignition happened after

heterogeneous ignition. They suggested radiative interaction between the particles might have occurred in group particle ignition [8].

Du and Annamalia [9] applied a theory, known as Thermal Explosion Theory, to define the criterion of heterogeneous ignition. According to Thermal Explosion Theory, ignition starts if the rate of heat release caused by chemical reaction is larger than the rate of heat loss of the coal particle. They derived a method to determine heterogeneous char ignition temperature using Thermal Explosion Theory, and determined that heterogeneous ignition is a great function of coal particle ignition activation energy and the surface temperature of the coal particle. These two factors are highly influenced by the heat of ambient gas, radiant heat transfer from the wall to the particle surface, heat of reaction, and activation energy of particle ignition (this factor is a function of coal composition), the particle heat loss during its ignition.

Shaddix and Molina [4] claimed the presence of CO_2 retards single particle coal ignition. Particle devolatilization proceeds faster with higher O_2 concentrations; however, the existence of CO_2 decreases the devolatilization rate due to its negative influence on the mass diffusion of O_2 and volatiles in the CO_2 environment. Qiao et al. [10] proved the impact of the thermal conductivity of CO_2 as another factor for the weaker ignition of coal in O_2/CO_2 environments. Wall and Buhre et al. [1] in their review present the impact of CO_2 on coal ignition retardation as well as improvement of flame stability due to pure O_2 injection. Shaddix et al. [11], in a different study, found that O_2 concentration decreases ignition delay in a manner that could be used to counteract the retardant effects of CO_2. Kimura et al. [12] showed that the flame propagation speed is much lower in an O_2/CO_2 atmosphere than in O_2/N_2 and O_2/Ar, and that in O_2/Ar, it was the highest. The

propagation speed increases as oxygen concentration increases in all cases, as expected. Nozaki et al. injected 15% to 20% of the total oxygen into the furnace directly [13]. His group at IHI found hydrogen cyanide (HCN) formation in the near burner zone increases in O_2/CO_2 with oxygen injection, and he claimed that devolatilization becomes more active at higher gas temperatures realized near the burner by oxygen injection.

1.4 Sulfur and Recycled Flue Gas (RFG)

As mentioned previously, one of the focuses of this research is on the effects of minimization of recycle ratio on the radiant heat flux in oxy-coal combustion. It has been proven that due to the existence of high recycle ratio in oxy-coal combustion, the amount of SO_2 in the system increases. One of the major issues in oxy-coal combustion is corrosion resulting from SO_2 and SO_3 formed due to the flue gas recirculation. Therefore, a brief description regarding sulfur issues in oxy-coal combustion is provided in this section. It is important to note that SO_2 emissions in an oxy-case are lower than in an air case in terms of the total sulfur mass output; however, the in-furnace SO_2 concentration has been reported to increase significantly during O2/RFG combustion. The SO_3 concentration is approximately 2.5 to 3.0 times higher in the oxy-case than in the air case [14]. A consequence of reducing volumetric flow and introducing recycled flue gas during oxy-fuel fired combustion is an increase in SO_2 concentration in the flue gas. Ochs et al. [15] calculated a rise in SO_2 levels from 200 ppm under air-fired combustion to 900 ppm under oxy-firing. Also, pilot scale experimental results by CANMET, Argonne National Laboratory, and IEA Green House R&D report an increase in SO_2 from air-firing to oxy-firing about 2 to 4 times. In addition, there are arguments regarding condensation of H_2O

prior to recycle [14]. Weller reported wet recycle of flue gas has shown an increase in SO_2 compared to dry recycle [16].

Oxy-fuel technique is one of the CCS techniques, and as mentioned before, the captured CO_2 can be used for other industrial purposes such as EOR. Therefore, the quality and purity of CO_2 becomes an important factor. Li et al. [17] calculated the energy for purification and compression of oxy-fuel gas. They proved the significant effects of SO_2 on energy for compression, distillation, and final CO_2 purification. In the radiative section of the furnace, the formation of H_2S and COS can contribute to corrosion if the flame is not well managed. In the convective section, the formation of SO_3 impacts the ash deposit and enhances the transfer of iron from heat transfer surfaces. Furthermore, it reacts with NO_2 and generates sticky compounds of ammonium bisulfate, which also fouls heat exchanger elements. In sections of the furnace where the flue gas temperature is below the dew point of the flue gas, the formation of H_2SO_4 is very undesirable because of its corrosive potential [14]. Methods have been suggested to control SO_x in oxy-fuel combustion such as the use of low sulfur and high calcium coals, limestone injection, sulfur scrubbers, condensers in flue gas line, etc. However, performing any of these changes requires consideration of the cost and energy consumption, which make oxy-fuel combustion less efficient compared to other techniques.

In addition, it is reported that generally the fly ash produced in the oxy-case contains slightly more sulfur and the furnace deposits contain significantly more sulfur compared to air case samples [14].

1.5 NO_X Formation

In this study, the effects of directed oxygen injection in triple co-axial turbulent diffusion flames on NO_x formation was investigated; therefore, a brief description regarding the history of research on NO_x formation in both air and oxy-combustion was provided. In conventional air combustion, the generally accepted path ways for NO_x formation are the following three mechanisms [18]. Thermal NO_x is the production of reactions between O_2 and N_2. These reactions are temperature-dependent in a sensitive manner, and at temperatures above 1500 ºC, they become more important. Thermal NO_x formation reactions are described in detail by the Zeldovich mechanism.

$$N_2 + O \leftrightarrow NO + N$$

$$N + O_2 \leftrightarrow NO + O$$

$$N + OH \leftrightarrow NO + H$$

The nitrogen of fuel exists in the char and volatile matter of fuel. Char nitrogen reacts through heterogeneous reaction chains and converts to either N_2 or NO. The nitrogen of volatiles is released during devolatilization, and volatiles further decompose into cyanide and amine species. These intermediate species may react to produce N_2 or NO. Prompt NO_x is the product of the reaction of hydrocarbon radicals with N_2 in the fuel-rich zone of the jet. These products are in the cyanide form that will turn into NO after reacting with O_2. Due to the nature of oxy-coal combustion, the amount of the molecular nitrogen existing in the furnace is very small or theoretically zero. Therefore, one can consider only formation of the fuel NO_x in oxy-fuel combustion. Not only has carbon

capture and sequestration been a great motivation to pursue oxy-fuel combustion, but the potential for reducing the NO_x emissions from power plants considerably compared to conventional power plants has been one of the key drivers in the oxy-fuel combustion research. There are a number of mechanisms for the reduction of NO_x in oxy-fuel combustion presented in different literatures.

Bose and Wendt et al. [19] reported the slow devolatilization of the nitrogenous compound in the far post flame plays a critical role in supplying HCN, which ultimately drives reactions forming N_2 from the NO formed from the fuel nitrogen before the oxygen disappeared. They found there is an indirect heterogeneous influence on the destruction of NO in which NO is decreased using fuel as reducing agent in the fuel-rich zone. Okazaki et al. [20] observed NO reduction in oxy-fuel combustion. They reported that the reactions of NO_x with hydrocarbons are the most significant mechanism in reducing NO_x emissions, and lowers NO about 50% to 80% in oxy-fuel combustion.

Norman et al. [21] at Chalmers University studied nitrogen chemistry and NO_x reduction at high temperatures in oxy-fuel combustion. They found that at temperatures below 1400 ºC, the Zeldovich mechanism is not active, and the reburning mechanism is dominant. At higher temperatures, the reverse Zeldovich mechanism dominates the NO reduction.

High-temperature combustion only reduces NOx when the nitrogen concentration is low, as during oxygen combustion. The influence of N_2 concentration is shown in Figure 2 and Figure 3 [21]. A low equilibrium concentration is obtained at low concentrations of N_2, high oxygen purity, substoichiometric combustion zones, and low temperatures. Sufficient conversion rate by the relatively slow Zeldovich mechanism

needs longer residence time and high temperatures in the reaction zone, and the temperature profile should be decreasing along the furnace in order to lower the equilibrium concentration of NO.

1.6 Heat Transfer

The studies of oxy-coal combustion performed by the Argonne National Lab (ANL) in the 3 MW pilot-scale facility located at the Energy and Environmental Research Corporation showed that with wet recycle, an oxygen concentration of 23.8% through the burners resulted in the same overall heat transfer as air-firing. Also, it was found for an oxy-firing case with dry recycle that an overall oxygen concentration of 27% is required to obtain an equivalent overall heat transfer in both cases [1].

In addition, ANL used a two-dimensional heat transfer and combustion zone models to simulate a 50 MW power plant. This model was used to determine the effect of recycle molar ratio on the heat transfer efficiency of the boiler. The main criterion for determining the optimum recycle ratio was to achieve a similar heat efficiency with both oxy-combustion and air combustion. Their results showed that the optimum dry-recycle molar ratio was calculated to be 2.7. Similarly, the wet-recycle molar ratio was calculated to be 3.2.

In order to validate this simulation, an experiment was conducted by Energy and Environmental Research Corporation. The optimum wet-recycle molar ratio was found to be 3.25 and the optimum dry-recycle molar ratio was found to be 2.6 by comparing the overall heat transfer to both the radiative and convective heat transfer surfaces to that achieved with the baseline air-firing operation [1,16,22–25]. Buhre et al. reported that the major contributor of heat transfer from a flame is thermal radiation from water vapor,

carbon dioxide, and soot [1,16]. In oxy-fuel combustion with RFG, the concentrations of carbon dioxide and water increase tremendously, leading to a significant change in the heat of radiation.

As shown in Figure 4, Smart et al. [26] in 2010 reported that a similar adiabatic combustion temperature to conventional air-firing is obtained at a flue gas recycle ratio of 69% [26]. This value depends on the coal or fuel composition and could fluctuate within the range of 68% to 72%. The studies showed for the Russian Coal, a radiative heat flux profile similar to air-firing can be obtained for recycle ratios between 68% and 72% at 3% exit O_2 and between 68% and 75% for 6% exit O_2 [26,27].

Andersson and his colleagues [28] at Chalmers University investigated the radiative heat transfer of oxy-coal combustion in a 100 kW oxy-fuel test facility. The flue gas recycle ratio was varied, so that, in principle, the same stoichiometry was kept in all cases, whereas the oxygen fraction in the recycled flue gas mixture ranged from 25 to 29 vol.%. Radial profiles of gas concentration, temperature, and total radiation intensity in the furnace were measured and also calculated using a model developed at Chalmers University. Narrow angle radiometers were applied to measure the radiation heat flux. The model in their study is able to include all three sources of radiation (gas, soot, ash) in coal combustion. Malkmus Statistical Narrow Band Model (SNBM) was applied to model the gas radiation intensity. They found temperature, and thereby the total radiation intensity of the oxy-fuel flames, increased with decreasing flue gas recycle rate. They found that with a 25% overall oxygen concentration in the feed gas, the same radiant heat flux can be achieved (see Figure 5 and Figure 6) [28]. Their results showed particle radiation has the most dominant role in the radiation of oxy-coal flames.

In addition, they proved the increase in total gas emissivity from air to oxy-fuel operation with dry RFG only is about 5%; however, it increased more than 20% for the same case with the wet-recycling. Thus, the moisture content of the flue gas is more important than content of carbon dioxide. However, particle radiation plays the most important role in radiation [28,29].

1.7 Co-Axial Jets

Forstall [30] studied the impact of the velocity ratio on turbulent mixing in a co-axial jet containing central and annular streams. He concluded that material diffuses more rapidly than momentum; therefore, the principle independent variable determining the shape of the mixing regime is the velocity ratio. Chigier and Beer focused on the region near the nozzle in double concentric jets. They considered two streams as two different central cores and described how these two streams emerge based on their fluid entrainment due to velocity differences [31–33]. In addition, they provided plots that define the length of each stream before they emerge as a function of velocity ratio for co-axial jets. In another study, Beer [34] reported that when the secondary velocity is low and the density of the secondary fluid is considerably higher than that of the recirculating fluid, more recirculation and less secondary air is entrained in the early part of the primary jet. This means coal particles will be heated faster, and it has a significant effect on the stability of the flame. Durano [35] measured the mean velocity of a co-axial jet for three different velocity ratios. He reported co-axial jets obtain a self-preserving state faster than single round jets.

Kawn and Ko [36], in their study, divided the near field zone of double concentric jets into three zones. The nearest zone to the nozzle is called the Initial Merging Zone. The

length of the initial zone depends on the core velocity ratio. The next region is the Intermediate Zone. In this zone, the streams are still considered as potential cores. Disparaging of the central initial core is the indication of the end of this region. As shown in Figure 7, the last zone is where the two cores are fully mixed, and the jet is treated as a single jet.

Crowe et al. [37] recommended the evaluation of Stokes Number (*St*) in turbulent two-phase jets. *St* is defined as the ratio of τ_p over τ_f where τ_p is the response time of the particle and τ_f is defined as the fluid time scale, which is a function of characteristic length and velocity of the fluid. At small values of *St*, the particles follow the fluid and maintain the velocity equilibrium with the fluid. For large values of *St*, the response times of the particles are greater than the fluid response time. Thus, the particles do not follow the fluid. For the *St* in the order of one, the particles follow the fluid partially. Kennedy and Moody [38] in their research found *St* has the highest value in the near field, and it becomes much smaller downstream in the jet. Preliminary high-performance computer simulations [39] using Large Eddy Simulation (LES) suggest that coal particle ignition occurs in clusters of small particles, many of which have been transported radially outwards by large eddies. In a cold flow study, Budilarto et al. [40] used Laser Doppler Velocimetry to show that smaller particles migrated to the edge of co-axial two-phase turbulent jets. Their results showed that the dispersion of particles was enhanced with decreasing particle size and increasing the velocity ratio greater than 1.0. They found that the addition of finer particles leads to an increase in the mean velocity of the coarse particles near the pipe center and, also to a less flat radial distribution of mean velocity of the coarse particles.

1.8 Coal Chemistry

The first criterion of ignition was determined to be the amount of volatile matter; however, it was proved that a more correct way to determine the combustibility is the index of Fuel Ratio (FR), which is the ratio of fixed carbon content / volatile matter content [1,13,41]. More research showed that the fuel ratio is not always a robust index to anticipate the combustibility and ignition behavior. Oka et al. [42] studied carbon burnout in seven types of coal, and found a general trend that the higher fuel ratio coals have higher carbon burnout. However, some of the coals do not follow this trend.

Blending several types of coal is a crucial process to improve the efficiency of power plants. An optimum blend of coal based on the type of power plant can help to reduce costs, meet emission regulations, improve combustion behavior, control ash deposition, enhance fuel flexibility, and extend the acceptability of coals. Research on blending coal is categorized in different aspects. Grinding, flame stability, carbon burnout, slagging and fouling, pollutant emissions, ash disposal, and overall heat transfer and efficiency are the most important aspects of coal compositions and their blends that need to be investigated. The influence of the maceral composition of the coal on the ignition and flame stability has been pursued by Su et al. [43,44] who suggested a criterion, the maceral index, to predict burnout behavior of the coal and blends by including the effects of maceral composition such as liptinite, vitrinite, and inertinite. The burnout of coal or coal blends depends on the amount of volatile mater, physical structure of char, and the diffusion rate of char burning. This relation fundamentally depends on the maceral composition of the coal or blend. Liptinite has the highest hydrogen content and volatile matter, and liptinite is associated with ignitibility and flame stability [45]. In addition, Su

et al. [43] defined an expression for the maceral index (MI) to predict burnout in two different pilot-scale facilities at Australian Coal Industry Research Laboratory (ACIRL) and Energy and Environmental Engineering Research Corporation (EER).

$$MI = \frac{L + \frac{V}{R^2}}{I^{1.25}} \left(\frac{HV}{30}\right)^{2.5} \quad (1)$$

where L is liptinite volume percent, V is the volume percent of vitrinite, and I stands for the volume percent of inertinite. All of these indices are measured free-mineral based. R represents the mean maximum reflectance and HV is the heating value of the coal. RF presents the reactivity of coal or blend. It was found that MI correlates with the burnout, and can potentially be used to predict ignitability as well.

Based on very simple models, in order to obtain a stable flame, coal particles need be heated to temperatures where the heat generation is balanced with the heat loss. The rate of consumption and production are respectively a function of velocity and coal composition. Also, it is found that coals with the same proximate analysis may not have the same ignition and flame stability characteristics. This is because the ignition and flame stability are the results of fast heat release, not only the amount of volatile matter.

Hallate et al. [46] researched the dependency of coal oxidation on coal particle size using thermo-gravimetric analysis (TGA). He found the oxidation rate of vitrinite increases with decreasing particle size while oxidation of inertinite is independent from the particle size. It is important to note that all of these studies were conducted in the air atmosphere; therefore, the behavior of coal ignition in an O_2/CO_2 environment based on its composition and chemistry is not yet well understood.

1.9 Previous Work at the University of Utah

This work builds on a previous study at the University of Utah, performed by Zhang et al. [47,48]. That study focused on the effects of the following on coal particle ignition and flame stability:

1. The effect of partial pressure of oxygen in the primary stream
2. The effect of partial pressure of oxygen in the secondary stream
3. The effect of preheat temperature of the secondary stream
4. The effect of transport medium

Zhang et al. [47] proved that by increasing the partial pressure of oxygen in the primary stream, flame stability increases. The total amount of oxygen in this test was kept constant, and the oxygen was transported consequently from the secondary stream to the primary stream such that partial pressure of oxygen in the primary stream changed from 0.0% to 20.9% in five different cases. It is important to note that the preheat temperature was maintained at T= 489 K. Also, the velocities of both streams were kept constant in order to minimize the effect of jet aerodynamics as much as possible. In order to investigate the effect of preheat temperature, the previous test was repeated; however, the preheat temperature of the secondary steam was changed to T=544 K. The results of this new test and the previous test showed that by changing the secondary stream preheat temperature, the flame stability increases such that even at low oxygen concentration in the primary stream, coal ignition occurs earlier, leading to a more stable flame.

In addition, the effect of an increase of oxygen in the secondary stream was explored by increasing the total amount of oxygen in the secondary stream. It is important to note that no oxygen was fed into the primary stream to observe the contrasting effects

of the presence of oxygen in the secondary stream. The results of this research showed that the increase of oxygen in the secondary stream facilitates coal particle ignition and results in a shorter flame stand-off distance which provides more flame stability.

Furthermore, a study was performed on the impact of the transport medium or combustion environment. Two sets of experiments were executed. One was performed in an O_2/CO_2 environment and the other one was in O_2/N_2. This experiment was very similar to the first experiment explained above, but in a different environment. The results of this study proved that the ignition of coal particles start at earlier stages in O_2/N_2, leading to more stable flames with short stand-off distances. It was explained that the concentration of O_2 at the surface of the coal particle plays a key role in particle ignition and, due to higher molecular diffusion of O_2 in N_2 compared to O_2 in CO_2, the concentration of oxygen increases earlier, causing a faster ignition and resulting in a more stable flame. The results of these experiments were consistent with the results that Shaddix and his colleagues found parallel to this research [4,11].

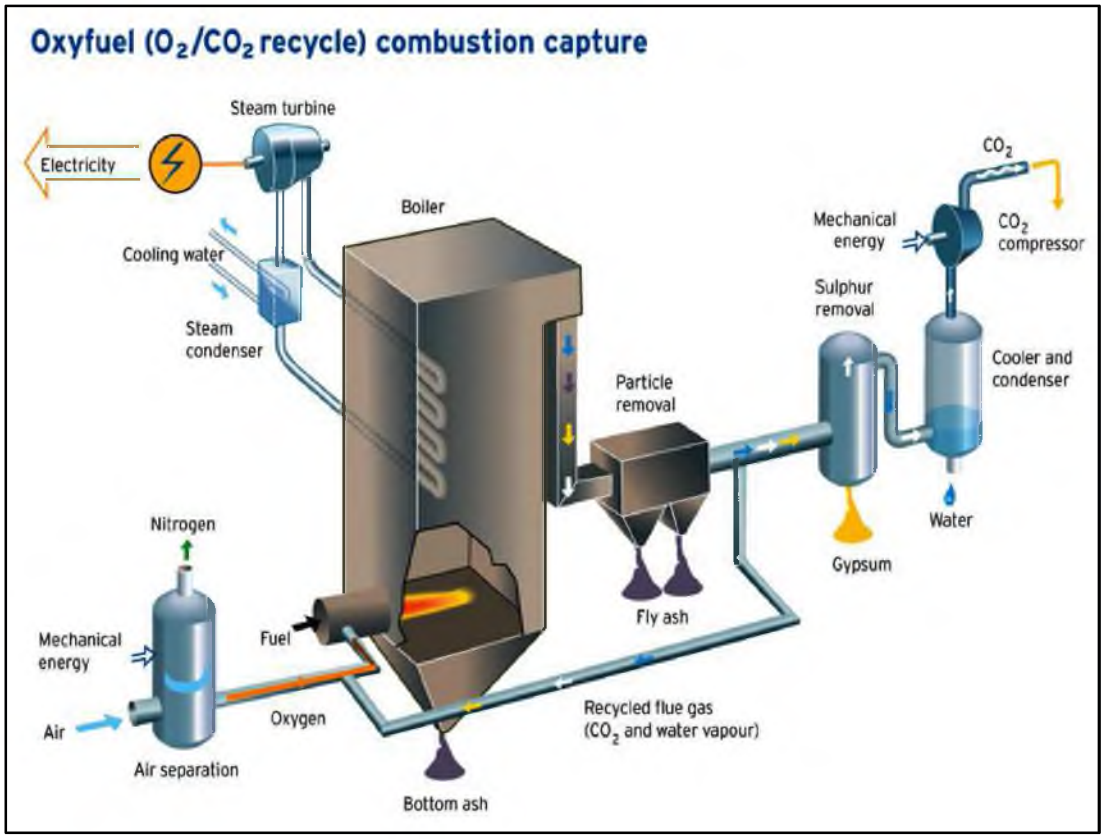

Figure 1. Oxy-Fuel Combustion Schematic

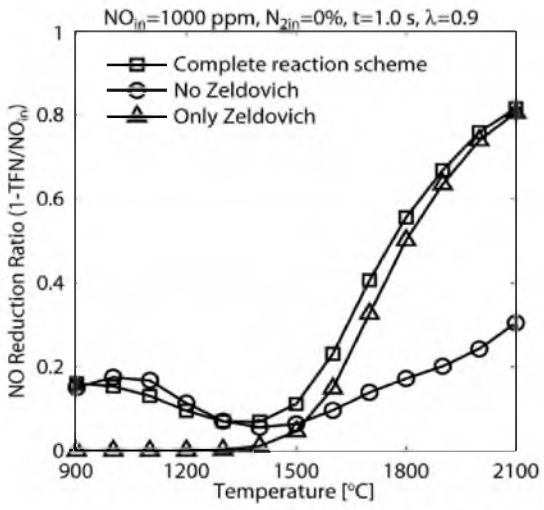

Figure 2. NO reduction ratio for various combinations of N_2 and NO

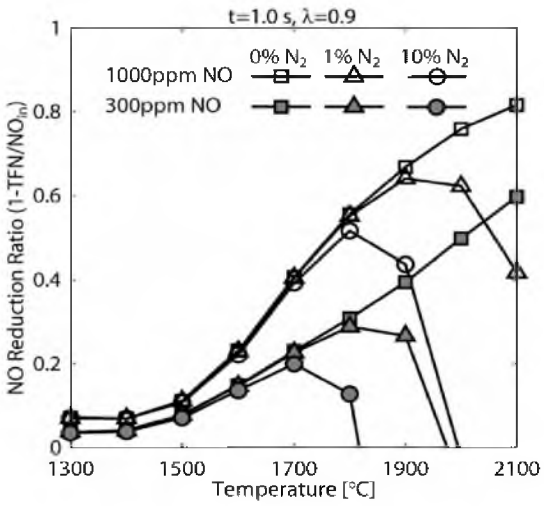

Figure 3. NO reduction ratio for isolated reduction

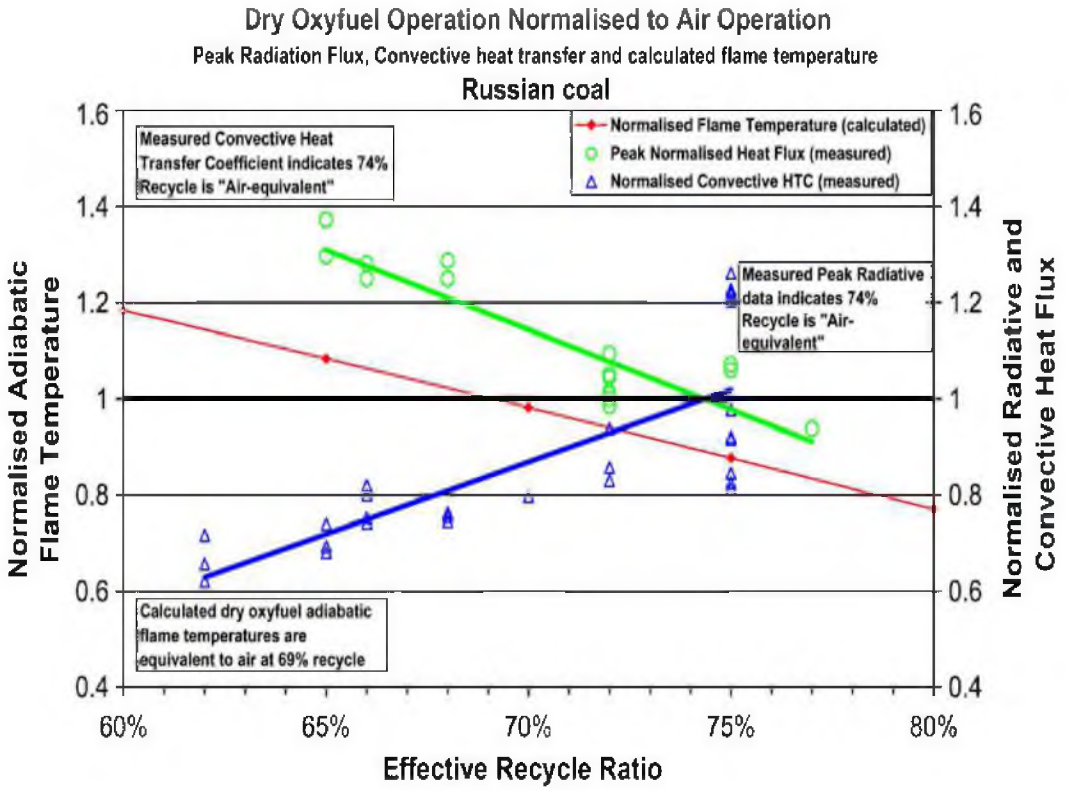

Figure 4. Effect of flue gas recycle ratio on flame temperature and radiative heat flux

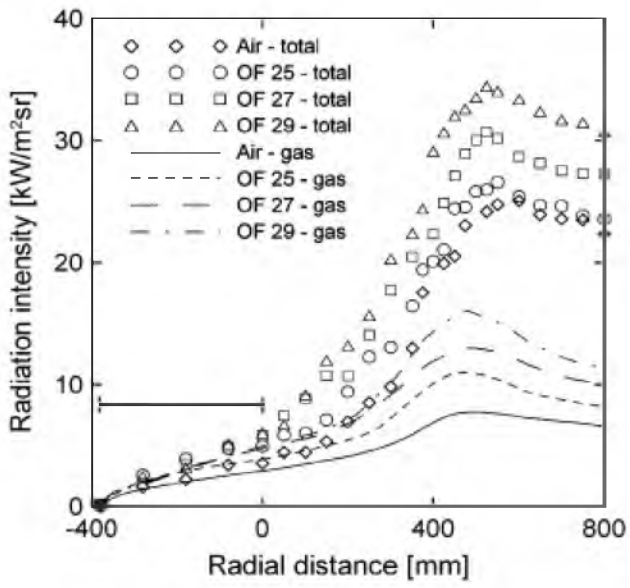

Figure 5. Comparison of radiation intensity in air and oxy-firing

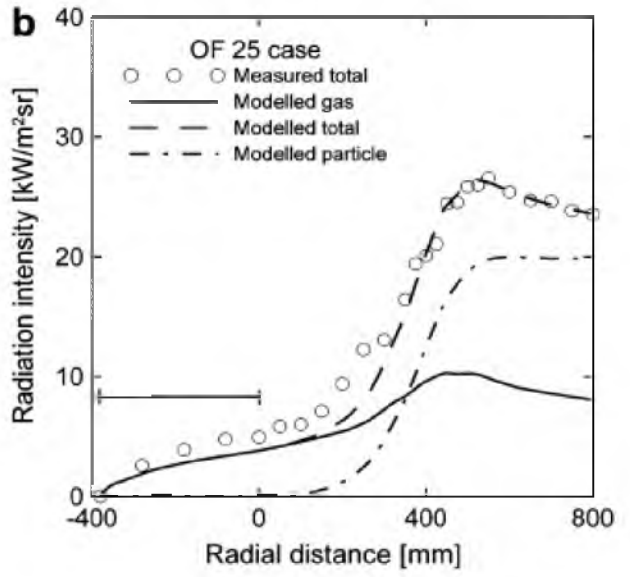

Figure 6. Comparison of radiant intensity measurements and gas radiation modeling at 384mm from the burner inlet in the Chalmers furnace. The furnace walls are located at radial distances of 800mm

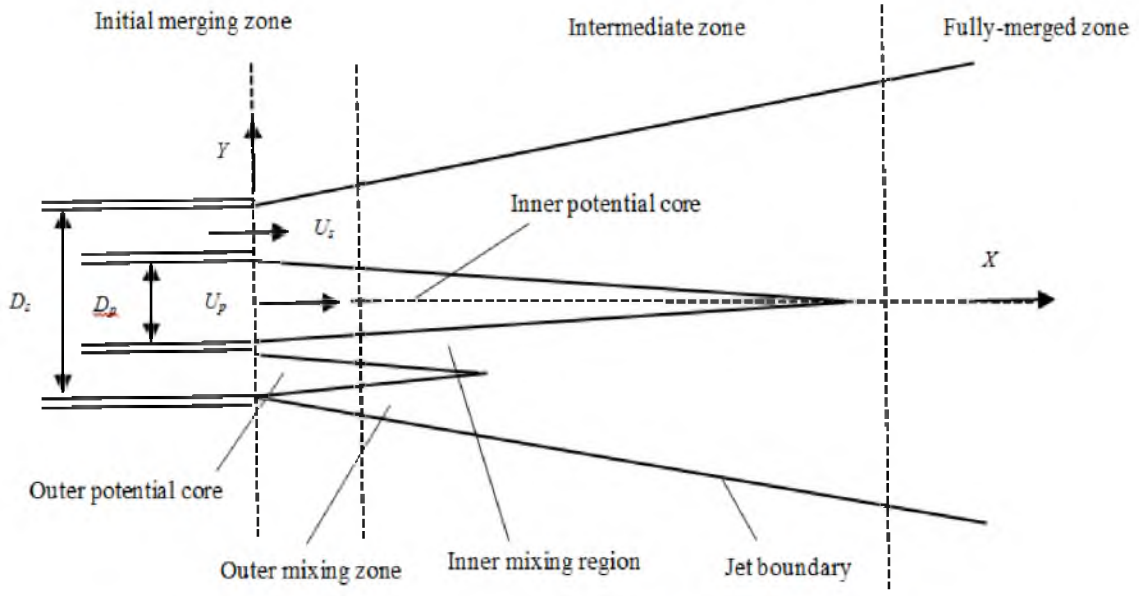

Figure 7. Near field zones of double concentric jets

2. RESEARCH OBJECTIVES, MOTIVATION, AND ORGANIZATION OF THIS DISSERTATION

One of the advantages of oxy-coal combustion is having the oxygen concentration and injection configuration as a crucial variable compared to air combustion. In oxy-coal combustion, especially in simple burners such as IFRF type-0 burners, two streams, namely, the primary stream and secondary stream, exist. The primary stream is utilized to transport pulverized coal using a carrier gas, and the secondary stream is applied as an oxidant stream containing oxygen and carbon dioxide from the recycle line. As mentioned before, coal combustion flames are less stable at 21% oxygen in a CO_2 environment as compared to an N_2 environment (air combustion). Therefore, it is very important to research the most suitable percentage and configuration of oxygen in order to find the most optimum flame. Previous research has elucidated this aspect of oxy-combustion; however, the impact of the injection of pure oxygen as a segregated stream is not well understood. In this research, the following items are determined to be the main objectives:

1. To extend the results of Zhang et al. [49] with a view to understanding the effects of coal composition on axial flame attachment and detachment under oxy-coal combustion conditions
2. To understand how advanced O_2 distribution strategies for co-axial burners in the University of Utah, 100 kW Oxy-Fuel Combustor (OFC) might affect flame

stand-off distances and flame stability, using as examples two configurations : namely, one with pure oxygen in an inner annulus and the other with pure oxygen in a central pipe.

3. To determine the effects of these oxygen input strategies not only on flame stability, but also on flame length, heat flux, and NO_x formation.
4. To determine the consequences on flame stability, flame length, heat flux, and NO_x formation of segregating all the input oxygen into one stream composed of 100% oxygen, using the co-axial burner configuration detailed above.
5. To determine the effects of minimizing the amount of recirculated flue gas on flame stability, flame length, heat flux, and NO_x formation, using the co-axial burner configuration detailed above.
6. To contribute to the validation, with uncertainty quantification, of coal jet ignition submodels of the co-axial burner configurations referred to above.
7. To interpret the data obtained using simple mechanistic concepts in order to understand why certain configurations resulted in observed changes in the flame near field aerodynamics, such as stand-off and flame stability, in contrast to simulations, which are outside the scope of this project.

This dissertation is organized as follows: first, the experimental equipment used is described in Chapter 3. This is followed by a detailed description of the methodology used to extract quantitative PDFs describing stand-off distances and flame length from photo images obtained.

Chapter 5 is based on a paper suitable for publication and entitled, "THE EFFECT OF COAL COMPOSITION ON IGNTION AND FLAME STABILITY IN CO-AXIAL

TURBULENT DIFFUSION FLAMES." This portion of the research deals with extending Zhang's work to different coals, and has been extracted from a manuscript with the same title, ready for submittal for publication in Energy and Fuels. It contains its own self-contained conclusions.

Chapter 6 is based on another suitable paper for publication, entitled "NEAR FIELD AERODYNAMIC EFFECTS OF PURE O_2 INJECTION IN CO-AXIAL OXY-COAL TURBULENT DIFFUSION FLAMES." It contains material taken from a second manuscript that is also ready for submittal for publication in Energy and Fuels. This chapter, therefore, also contains its own conclusion.

Chapter 8 contains results from the third phase of this work and focuses on heat flux measurements from systems with minimum flue gas recycle, and for consistency with the preceding chapters, also contains its own conclusions. This chapter is followed by a discussion of future work in Chapter 9.

3. EXPERIMENTAL

3.1 Oxy-Fuel Combustor (OFC)

The combustion furnace employed in this research is a nominally 100 kW combustor with the capability for both oxy- and air-firing at the University of Utah. This combustor was initially constructed by Zhang [49] and modified for flue gas recycle by Morris [50]. It was then further modified in this work, to accommodate multiple inlet streams of various compositions into the burner, and to allow possible cooling in the upper combustion chamber. As shown in Figure 8, Figure 9, and Figure 10, the oxy-fuel combustor (OFC) is equipped with a recycle system to provide similar oxy-operating conditions as industrial oxy-coal combustors. As presented in Figure 8, OFC is a down-fired flame combustor. The top section of the furnace is called the burner zone. The position of the burner is on top of this section, and during the combustion process, the flame is located mainly in this part of the furnace. Because this research explores the aerodynamics and radiation of the flame in various conditions, most of the experiments are focused on this zone. The second part of the OFC following the burner zone is the radiant zone. The third part located horizontally in the bottom of the furnace is the convective zone. This section is equipped with water heat exchangers to simulate an environment similar to industrial pulverized coal boilers. There are 26 circular ports along the furnace symmetrically that are applied as probe inputs. K-Type thermocouples are installed along the furnace to measure the temperature of combustion.

gaseous products. It is important to note that in this research, the recycle system was not applied. Therefore, instead of recycled flue gas (RFG), pure CO_2 was fed from a tank. The qualitative diagram and the details of the piping system used in this study are illustrated in Figure 11. The first valves used in each pipe line are ball valves to stop possible hazard caused by gas leak manually. The second valves are solenoid valves controlled electronically, allowing them to be connected to a central control system. In addition, the flow is measured using a mass flow controller. The mass flow controllers are calibrated separately for each gas. Solenoid valves and mass flow controllers communicate with each other to maintain the

desired flow. This control is managed by a control system program called OPTO22 that will be explained in this chapter. A picture of a part of the pipe lines equipped with the valves and mass flow controllers especially for CO_2 and O_2 is shown in Figure 12.

3.2 Burner Zone

The burner zone of the OFC is where the flame is located. Since this study mostly focuses on flame aerodynamics and near burner zone combustion, it was critical to equip the burner zone section with instruments to obtain information about the flame under desired combustion operating conditions with the highest possible control. The burner zone contains four windows located in its quadrants allowing optical access to the flame and the chamber of combustion. Photo images of the flame are captured from these windows. These images potentially provide information regarding the flame stability using the photo-imaging technique that will be discussed later. In addition, having the windows in four quadrants permits applying other techniques such as Particle Image Velocimetry (PIV) or Particle Shadow Velocimetry (PSV).

Details of the design of these windows are provided in Figure 13. The burner zone is a part of the furnace that has the highest temperature. To prevent heat loss from this section, 3 inches of fiber board 2600 is employed. The fiber board insulation is formed from a special blend of regular Fiberfrax alumina-silica fibers and is able to tolerate temperatures up to 2600 °F.

In order to have a control on the furnace wall temperature in the burner zone, ceramic heaters are applied. These ceramic plates are 6 inches wide, 10 inches long, and have the thickness of ½ inch. In order to cover the surface of the chamber for the purpose of managing the wall temperature uniformly at desired values, 24 ceramic plate heaters supplied with 840 W of power are embedded into the inside surface of the chamber. The heaters are composed of mainly 38% Al_2O_3 and 60% SiO_2. The ceramic plate heaters are purchased from the company Thermcraft. The thermal conductivity of the heaters is 0.22 W/m.K. K-Type thermocouples are attached to the back of the heaters that allow setting the temperature of the wall heaters to desired temperatures using the OPTO22 control system.

Six circular ports benefit the burner zone for the purpose of collecting several data of the flame. For instance, radiometer probes have been employed to measure the heat of radiation of the flame in the OFC. The principles of the probes and results of this study are discussed later in this chapter.

3.3 Convection Zone

As shown in Figure 11, the convection zone of the OFC consists of four main sections, and each section contains two heat exchangers. A picture of one of these sections is provided in Figure 14. The two heat exchangers shown in this picture are equipped with

two K-Type thermocouples in their water outlet stream. The thermocouples are very important for safety. In order to measure the flue gas temperature, one K-Type thermocouple is installed on each section.

The convective zone of the OFC is located in the lowest part of the furnace; therefore, ash buildup caused by combustion happens mostly in this area. The cleaning of this zone of the furnace after ten days of experimentation is suggested. The ash buildup causes pressure buildup in the furnace that can potentially create serious hazards.

3.4 Gas Heater

As shown in Figure 11, a gas heater is installed in the line of the secondary stream in order to increase the secondary stream gas temperature to desired values. The power of this gas heater is 2 kW. The power of the gas heater was determined after calculating the amount of heat required to heat up a mixture of flue gas containing O_2 and CO_2 to a temperature of 520 °F. Figure 15 shows an inside view of the heater. The heater consists of an electric element and a K-Type thermocouple. The electric element is located in a metal shell, and the gas enters from the left side of the element and exists from the right. The shell is insulated using insulation blankets and an aluminum shield. The picture of the insulated gas heater is represented in Figure 16.

3.5 Wide Angle and Narrow Angle Radiometers

One narrow angle (NA) and three wide angle (WA) radiometers were applied to measure the radiant heat flux of the flame in various combustion operating conditions (see Figure 20 and Figure 21). The design of the wide angle radiometers was dedicated by Praxair, and was built at the University of Utah. The WA probes measure the total radiation coming to the location of measurement, and the NA probe measures the

radiation being emitted from a location in the small view of the probe. The WA probe has nearly a full hemispheric view. The view of the wide angle radiometers is discussed in this chapter. This is limited slightly by imperfections in the machining at the inlet orifice for the elliptical element. In addition, the reflectance of the gold coated surface of the ellipsoidal cavity has a great impact on the efficient view angle of the WA radiometers. The narrow angle radiometer view is a small angle of about 5 to 6 degrees that can collect the emitted radiation of radiant subjects in that path. The typical locations of these radiometers are provided in Figure 17 and Figure 18. It is important to note that the location of the probes might change based on the type of experiment. The details of radiometer construction will be discussed further in later chapters.

3.6 Wide Angle Radiometer

The WA radiometer measures the total radiation coming to the measurement location from subjects seen in the view zone. Due to the ability of a wide angle radiometer to have a nearly hemispheric view, radiation from the flame and wall can be captured using the WA radiometer (see Figure 20). The schematic of the principle of the wide angle radiometer is shown in Figure 19. A copper ellipsoidal element is located in the front of the probe that collects all the radiation in the radiometer view to the orifice [51]. The orifice is located at the front of the ellipsoidal cavity that collects the radiation from the furnace and flame.

The material of the cavity in this probe is from copper, and the inside surface of the cavity is gold coated. The gold coated surface amplifies the collection and reflection of all radiation received in the cavity to the thermopile. In theory, the ellipsoidal cavity can capture all the radiation in an imaginary hemisphere view located at the front of the

probe; however, due to the possible roughness of the surface of the cavity, the angle of the view becomes smaller, implying the radiometer can capture only a portion of the radiation in the aforementioned hemisphere. A calibration was performed to obtain the view angles of the radiometers. The detail of the calibration is explained in this chapter. All the radiation coming inside the cavity is focused onto a stainless steel thermopile at the opposite focal point. The thermopile consists of a hemispherical pellet and a cylinder that is connected to the pellet and a cooled mass. All three parts are made of stainless steel. The surface of the pellet is blackened and oxidized in order to absorb nearly 95% to 98% of the radiation. The metal mass is kept cool by the cooling water. There are two constantan wires; one is connected to the pellet (high temperature segment), while the other is connected to the metal mass (low temperature segment). This temperature gradient generates a current in the wires that is proportional to the energy received by the pellet. A picture of one of the wide angle radiometers used in this research is provided in Figure 20. The pipe around the probe plays the role of a water cooling jacket heat exchanger. Water enters the inner side of the jacketed heat exchanger and exits from the outer shell. This configuration lowers the temperature of the cavity as much as possible, minimizing errors associated with radiation from the inner surface of the ellipsoidal cavity. Changes in the flow rate of water do not have a significant effect on the calibration of the radiometer; however, the water flow rate should be high enough to adequately lower the temperature of the cavity. A 2.0 gpm rotameter is installed to measure the water flow rate. The water flow rate is kept constant at 1.25 gpm in this study. In order to prevent ash buildup in the ellipsoidal cavity, CO_2 needs to be purged into the bottom of the cavity, carrying the ash out through the orifice. The purged gas circulates inside the cavity and cleans the inner surface. The presence of any ash on the

inner surface of the cavity can have a tremendous impact on the reflectance of the cavity, resulting in significant errors in the readings of the radiometers. The amount of purged CO_2 has a considerable effect on the calibration of the radiometer due to the high emissivity of CO_2 and its participation in radiation. The amount of CO_2 purged in the system was kept constant at 20 standard cubic feet per hour (scfh). This value needs to be maintained constant in all the experiments after the calibration. The exit velocity of CO_2 from the orifice is calculated to be about 4.1 (ft/s). A 22 (scfh) rotameter was applied in the system to control the amount of CO_2.

3.7 Narrow Angle Radiometer

The NA radiometer measures radiation being emitted from a location (see Figure 21). In this study, the location was 175 mm below the burner tip. The investigation of the radiation of this region provides a better insight regarding flame stability. The schematic of the narrow angle radiometer is shown in Figure 22. First, the radiation enters the pipe and, after passing through, sees a focusing lens. Radiant light after passing through the lens is focused on a thermistor, inducing a change in resistance as the thermistor temperature changes. Another thermistor is placed next to the other thermistor in order to capture the ambient effects. The combination of the two thermistors creates a Wheatstone bridge circuit. The difference between the two thermistors generates a voltage across the Wheatstone bridge circuit, corresponding to the radiant heat received by the radiometer from a location. In the same manner as the wide angle radiometer, a water heat exchanger is required to lower the temperature of the probe; however, changes in the flow rate of water do not have remarkable effects on the calibration of the radiometer. A 3.5 gpm rotameter was installed to measure the water flow rate, which was kept constant

at 1.25 gpm. The purpose of purging CO_2 is to prevent any particles or contaminants (condensing ash, tars, etc.) from entering the probes. Therefore, especially in wide angle radiometers, the amount of purging cannot be too low. At 20 scfh, as it was mentioned, the exit velocities for wide angle radiometers are 4.1 ft/s. This value for the same amount of CO_2 in a narrow angle radiometer was calculated to be 1.7 ft/s. The amount of purged CO_2 in the NA radiometer is not as critical as in the wide angle radiometer, for any particles covering the inner surface of the cavity can create errors in the performance of the WA radiometers.

3.8 Calibration of Radiometers

3.8.1 Thermal Response of Radiometers

The calibration of the radiometers is critical, and is required before measurements can be taken. Despite the fact that CO_2 is being purged into the system, there is a chance that a small amount of particles can enter the ellipsoidal cavity and settle especially on the edge of the orifice, inner surface of the cavity, or even on the pellet, lowering the reflection efficiency of the radiation considerably. Additionally, due to the heat of the furnace, there is always a chance of physical shocks to the thermopile that can damage the reception of radiation by the thermopile. The same issue may present itself in the orifice and should be taken into consideration.

In order to calibrate the radiometers, a blackbody radiator was employed. The blackbody radiator is a thermally insulated and electrically heated graphite tube cavity. The image of the blackbody radiator used in this calibration is shown in Figure 23. The blackbody radiator contains a thermocouple that can regulate the temperature of the enclosure to any desired value. In order to calibrate the radiometer, it should be subjected

to radiation from a blackbody radiator set to different temperatures. The results of the calibrations are presented in a linear graph showing voltage signals (mV) as a function of received radiant energy from the blackbody radiator. The energy from the blackbody radiator is only a radiant energy that can be controlled based on the set temperatures of the blackbody radiator. Limitations such as overheating the thermopile, or lack of capability of the blackbody to reach to high temperatures (above 2000 ºF), need to be taken into consideration in the calibration process.

Figure 24 and Figure 25 show calibrations of both wide and narrow angle radiometers performed on 05-09-2011. As shown, the radiant power is plotted as a function of the voltage received by the radiometers. The amount of radiant power corresponds to the temperature of the blackbody ($Q = \sigma T^4$). Also, it is important to note that the response time of the wide angle radiometers is of the order of nearly one minute, not allowing monitoring of the radiation instantaneously.

However, the narrow angle thermistor is more sensitive to temperature differences due to radiation, and the values might change in the order of one second. Therefore, the voltage reported is an average over the time the measurements have been performed.

3.8.2 Angular Response of WA Radiometers

The main purpose of this experiment was to find the angular response of the WA radiometers. Additionally, by this test, the field of view of the radiometers was obtained [52]. For this experiment, each radiometer was positioned in front of the blackbody radiator with the radiometer axis parallel to the axial axis of the radiating aperture of the blackbody. The radiometer axis was aligned with the blackbody axis using a protractor. Several angles of 0°, ±15°, ±30°, ±45°, ±60°, ±75°, and ±90° were chosen for the

measurements. At each angle, the radiometers were aligned in front of the blackbody radiometer for 10 minutes, and the average of the signals (mV) was counted as the response signal of the radiometer at that specific angle. The results for the three radiometers are presented in Figure 26, Figure 27, and Figure 28. As shown in the figures, the response of the radiometers is normalized based on their highest value, occurring when the radiometers are completely facing the blackbody radiator aperture. Theoretically, the field of view of the WA radiometers is a hemisphere. This assumption is true if the inner surfaces of the radiometers are extremely polished such that all the radiation going inside the cavity reflects onto the thermopile. However, according to the test results, in reality, the optimum field of view of the radiometers is a cone with the angle of 120°. Additionally, one can assume that the cone is a right circular cone due to the symmetry of the angular response of the radiometers. Based on the angular response calibration, the field of view of the radiometers was determined. Figure 29 shows the view fields in the OFC.

More experiments were conducted to explore the effect of water flow rate of the radiometers on the response values. The results showed that the water flow rate does not have a considerable effect on the radiometers' performance. However, the flow rate should be set to a minimum value that can keep the ellipsoidal cavity around room temperature.

3.9 Burner Design

3.9.1 Design of Double Concentric Burner

Many studies have been performed on double concentric burners [31–34]. A typical double concentric burner contains two streams with the coal carrier stream usually situated in the center of the jet. A double concentric burner consisting of two streams

named: 1) Primary stream; 2) Secondary stream, was employed in this study. The primary stream is located in the center of the burner. A carrier gas transports the coal into the chamber from the primary stream. The carrier gas in this study is either CO_2 or a mixture of O_2 and CO_2. The secondary stream contains a mixture of O_2 and CO_2 and flows around the primary jet.

Achieving a stable flame in oxy-combustion is a crucial issue. Coal particles exiting the burner require to be mixed with O_2 in the secondary stream. Meanwhile, it is important for coal particles to have enough residence time in order to reach high temperatures for devolatilization. Thus, it is important to note that in the design of burners, the momentum of the primary stream should be less than the secondary stream. Additionally, a secondary stream with a higher momentum will create recirculation around the jet, assisting the mixing and stability of the flame.

In another study, Villermaux and Rehab et al. [53] studied water jets and showed that the potential core length is proportional to the velocity ratio. Also, they recommended that the effects of variable density jets could be accounted for by substituting velocity ratio with the square root of the momentum flux ratio. Work by Favre-Marient and Schetti et al. [54] showed that the core length is proportional to the ratio of the square root of ρU^2 for variable density nonreacting jets up to a momentum flux ratio of approximately 50 where recirculation in the inner jet stream starts. The ratio of $\sqrt{\frac{\rho_1}{\rho_2}}$ for the gases in this study is nearly one; therefore, it was decided to only focus on the velocity ratio instead of the momentum ratio.

In addition, in this scale, it is not possible to conduct the experiments by keeping the momentum ratios constant. In order to minimize the aerodynamic impacts as one of

the strong factors of mixing to be able to explore the mixing phenomena, it was decided to maintain the velocity ratios constant. The sketch of the double concentric burner employed in this research is presented in Figure 30. The size of the pipes is chosen in such a way that the velocity ratio of the secondary stream to the primary stream is nearly 2.5.

This type of burner was the only type applied in the previous study performed by Zhang in which the focus was mostly on the effect of the mole fraction of oxygen in the primary and secondary streams on flame stability. The results and details of this study are provided elsewhere [49].

3.9.2 Triple Co-centric Annulus Burner Configuration A: Burners with Oxygen Stream in Middle Annular Stream

In order to investigate the effects of directed pure oxygen injection, a pure oxygen stream was dedicated to the previous type of burner. This stream might contain a specific fraction or 100% of all the oxygen required for combustion for the combustion operating condition. The primary stream is a transport medium carrying pulverized coal particles in the chamber and, for the experiments in this design, contained only CO_2, with no oxygen. Directed oxygen and transport streams were maintained at room temperature. The secondary stream is a mixture of O_2 and CO_2, and plays a significant role in moderating the combustion temperature as well as entrainment of the flame jet. In order to explore the effects of directed injection of O_2, two possible important impacts of O_2 have been investigated. The first parameter is the fraction of the total amount of oxygen that could be situated either in the pure oxygen stream or in the secondary stream. The orientation or configuration of the O_2 stream can have significant effects on combustion, such as flame

stability as well as heat transfer and NO_x formation. O_2 stream configuration was the second aspect to be explored. It is inevitable that the aerodynamic conditions of a flame jet has big impacts on the flame property; therefore, it was decided to maintain the velocity ratios of all the streams constant in all the operating conditions by changing the streams' pipe diameter. Several burners were built and employed to allow the stream velocities to remain constant. The typical schematic of these burners is shown in Figure 31. As shown in Table 1, as case number increases, O_2 is added from the secondary stream to the pure oxygen stream while the overall O_2 is maintained constant.

It is important to note that in burner number 6, all of the oxygen required is being introduced in the pure directed oxygen stream. The primary stream (Coal + CO_2) is located in the center of the burner. The annulus around the primary stream is the directed oxygen stream, and the furthest outer annulus contains the secondary stream. The velocity of the pure oxygen stream and the primary stream are kept approximately equal in order to delay mixing, leading to potentially longer flames with a more uniform heat distribution. The secondary stream velocity is 2.5 times higher than that of the other two streams, creating external recirculation in the upper chamber and maintaining jet entrainment (IFRF Type-0 flame).

Multiple burners with various appropriate dimensions allowed the stream velocities to be maintained constant such that aerodynamic mixing effects were unchanged as much as possible, as shown in Table 1. An image of one of the configuration A burners is presented in Figure 32.

3.9.3 Triple Co-centric Annulus Burner Configuration B: Burners with Oxygen Stream in Centrally Located Pipe

For Configuration B, the burners are also triple concentric burners but now with a pure oxygen stream located in the center pipe. The primary stream that carries the coal particles is located in the inner (middle) annulus. The primary stream contains only CO_2 and coal. The outer annulus is the secondary stream. The secondary stream carries O_2 and CO_2 to the combustion chamber. As for Configuration A, several cases cover different fractions of total oxygen in the oxygen stream located in the center from 0% to 100%. In the very last case, all the oxygen is once again in one segregated stream (now at the center). The typical schematic of Configuration B burners is provided in Figure 33. The velocity ratios of the streams are similar to Configuration A to minimize the aerodynamic differences as shown Table 2. Keeping the velocities similar for all the cases allows the experimental data to be comparable, especially the results obtained from Configurations A and B. An image of Configuration B burners is presented in Figure 34.

3.10 Coal Sample and Analysis

Two types of coal were used in this research: Utah Skyline Bituminous and Illinois #6 Bituminous. Illinois #6 was applied in all the studies of this research; however, in order to investigate the effect of coal composition, Utah Skyline Bituminous was utilized in this research as well. The ultimate, proximate, and ash analyses of the coals are provided in Table 3, Table 4, and Table 5. It is important to note that these data are reported based on As Received (AR). Both coals were pulverized and prepared for steady feeding to the combustor. Since the size of the coal particle is one of the indices of coal ignition, both coals were prepared with similar particle size distribution. The particle

size distribution was calculated and is summarized in Figure 36. According to the data shown in Figure 36, the mass average diameters of both coals were calculated to be 62 μm and 68.5 μm, respectively, for the Utah Skyline and Illinois #6 coal particles.

3.11 Gas Analyzers

In order to collect samples for the gas analyzers, a flue gas probe is located at the end of the convective zone of the OFC. This probe contains a baghouse that allows for the capture of ash particles in the first step. The gas goes through a modified refrigerator with a vacuum pump that condenses the moisture of the flue gas. Moisture can cause damage to analyzers. The gas once again goes through three more layers of filters and another condenser in order to be prepared for gas analyzers. Six types of gas analyzers were employed in this study to permit the measurement of oxygen, carbon dioxide, NO_x, and SO_x during the combustion process. Figure 37 shows the array of analyzers in the control room of the University of Utah combustion lab. The analyzers applied were the following:

- Yokogawa - Zirconia oxygen analyzer ZA8
- Horiba- Paramagnetic oxygen analyzer
- California Analytical Instrument - Infrared CO and CO_2 gas analyzer: ZRH
- California Analytical Instrument - Infrared CO and CO_2 gas analyzer: ZRE
- Thermal Environmental Instrument – Chemiluminescense NOx analyzer
- Horiba - Chemiluminescense NOx analyzer CLA-510SS

It is important to note that the lack of filters in the line can cause serious damages to the analyzers. In the same manner, the moisture needs to be removed from the gas sample for the safety of the analyzers.

3.12 O_2 and CO_2 Delivery

As mentioned before, the OFC at the University of Utah is equipped with a recycled flue gas system; however, required O_2 and CO_2 in this study were provided from tanks. The opportunity to have O_2 and CO_2 allowed for better control of the gas flow rates, leading to more accurate measurements. O_2 and CO_2 gas supply was delivered from tanks donated by Praxair to the University of Utah combustion research lab. The O_2 tank has a capacity of 6000 gallons, and the CO_2 tank can store up to 400 gallons of carbon dioxide. The O_2 tank contains liquid oxygen, and a vaporizer is equipped in the line to convert the liquid oxygen to its gaseous state. Additionally, it is important to note that the O_2 tank was installed professionally by Praxair, and the handling of oxygen to the furnace must follow the safety requirements. Pictures of the CO_2 and O_2 tanks are presented in Figure 38 and Figure 39.

3.13 U-Shaped Tube Water Cooling Heat Exchanger

It is important to note that u-shaped heat exchanger tubes were designed only to be applied in the experiment of the reduction of CO_2 (minimization of recycled flue gas). As discussed, the OFC is a combustor with the capacity of 100 kW. U-shaped heat exchanger tubes were designed with the aim of performing the experiment at higher coal feeding rates. However, in order to be able to have a correct comparison between data sets, the decision was to conduct the test at the same heating rates as before. Therefore, the heat exchanger tube was never employed in this study. However, for higher heating rates, especially to study the effects of CO_2 reduction, lowering the amount of CO_2 will increases the temperature of combustion such that it could damage the refractory and the

insulation of the furnace. Therefore, it is recommended to employ a cooling heat exchanger to prevent any possible damage under these conditions. These tubes also simulate a furnace similar to industrial boilers. There are several types of heat exchanger, such as water cooling jacketed heat exchangers, that could be installed either on the furnace wall facing flame or underneath the insulation. However, In order to have a heat exchanger that does not block the windows of the OFC, and compatible with the current design of the furnace, it was decided to choose U-shape heat exchangers. In this work, the heat exchanger consisted of 4 U-shape stainless steel pipes being hung from the top plate of the burner zone. The size of the pipes used in this heat exchanger is ¾", Sch 40. New plumbing was required to supply water to these heat exchangers. The new plumbing system transports the required water stream from the cooling tower to the top of the furnace to provide water for U-shape heat exchangers. The manifold shown in Figure 40 divides the water pipe into four different streams at the end of each pipe. Each water stream enters into one heat exchanger. Also, four flow meters are provided in the line to measure the flow rate of water. The other manifold on the left-hand side collects the water from the heat exchangers. This water stream flows back to the cooling tower to be cooled. As shown in Figure 41, it was decided to employ hoses to connect the heat exchangers to the manifolds. Also, four 6" long K-Type thermocouples were installed to measure the exit water temperature from each heat exchanger. By knowing the temperature difference and the flow rate, we were able to have a better understanding of the heat transfer to the heat exchangers. The Solidworks drawings and an image of the heat exchanger are provided in Figure 42 and Figure 43. The size annotations in the drawing are reported in inches.

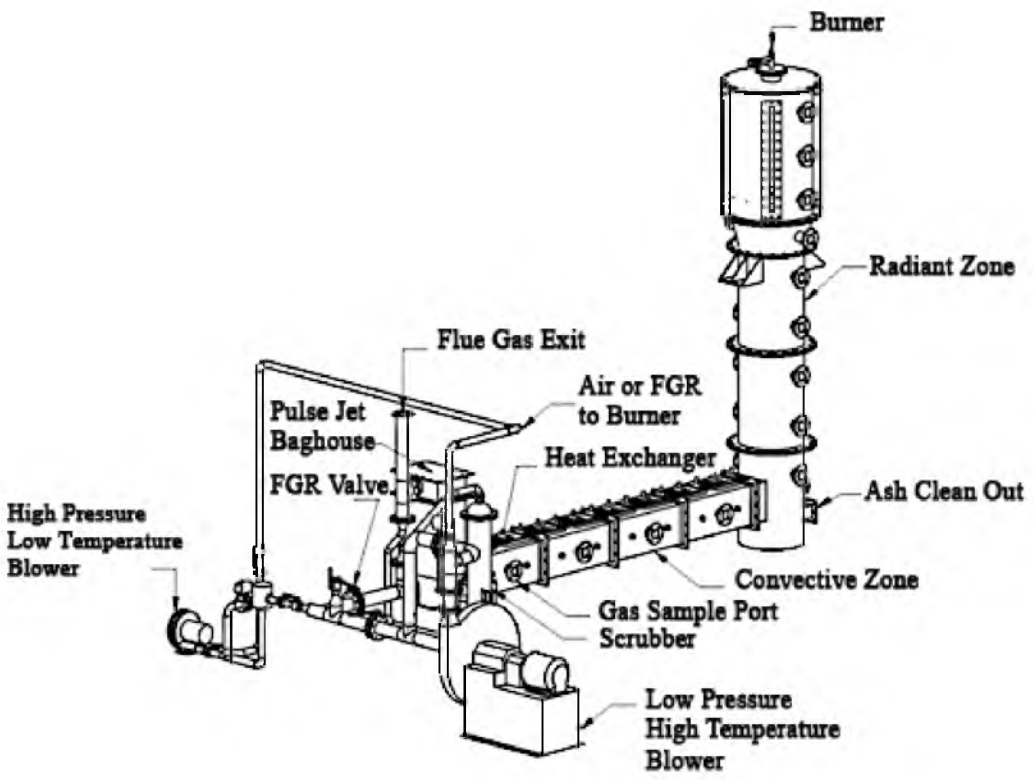

Figure 8. Oxy-Fuel Combustor (OFC) at the University of Utah

Figure 9. Recycle Flue Gas system of OFC at University of Utah

Figure 10. OFC at the University of Utah

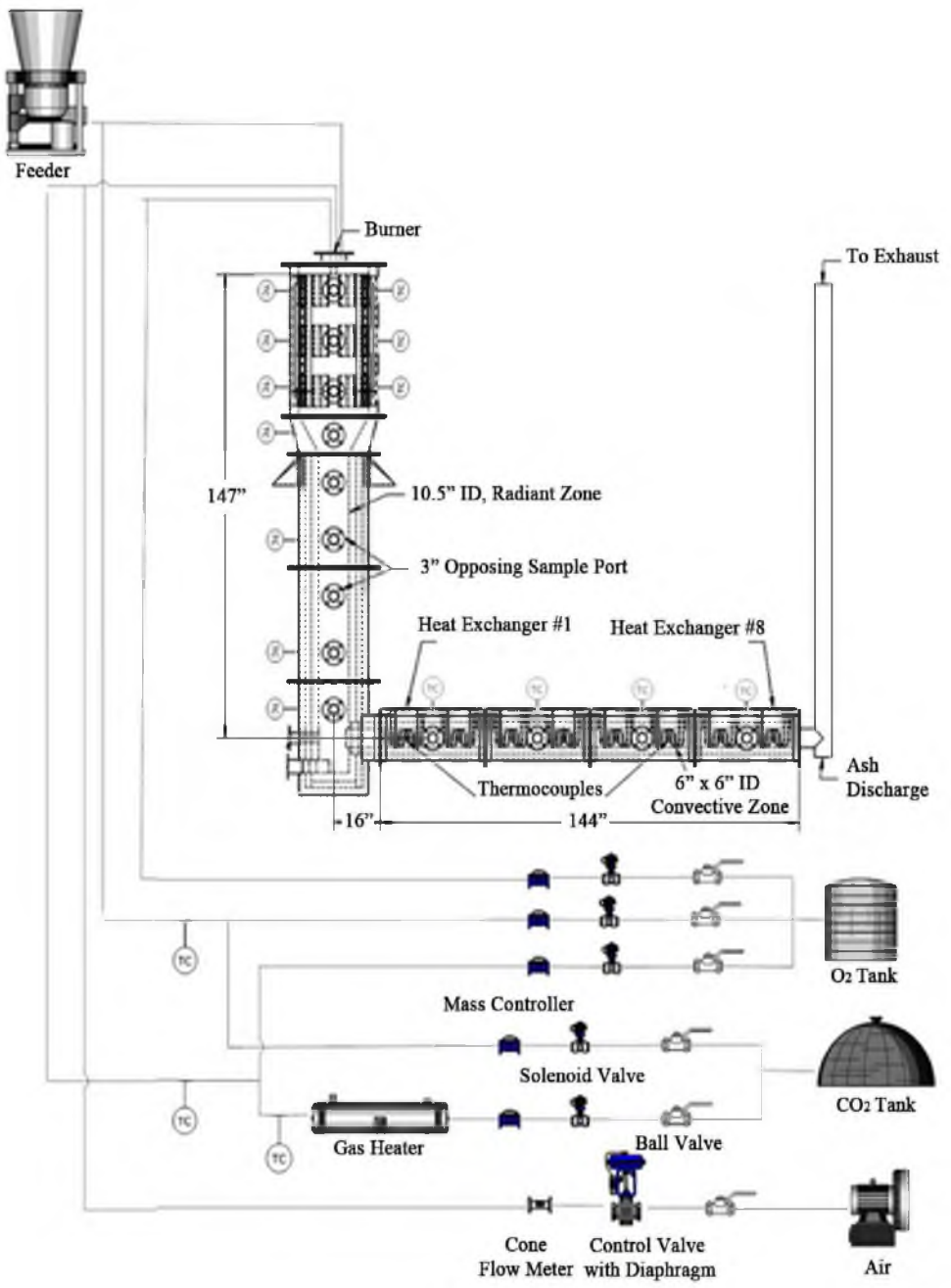

Figure 11. Flow diagram of OFC

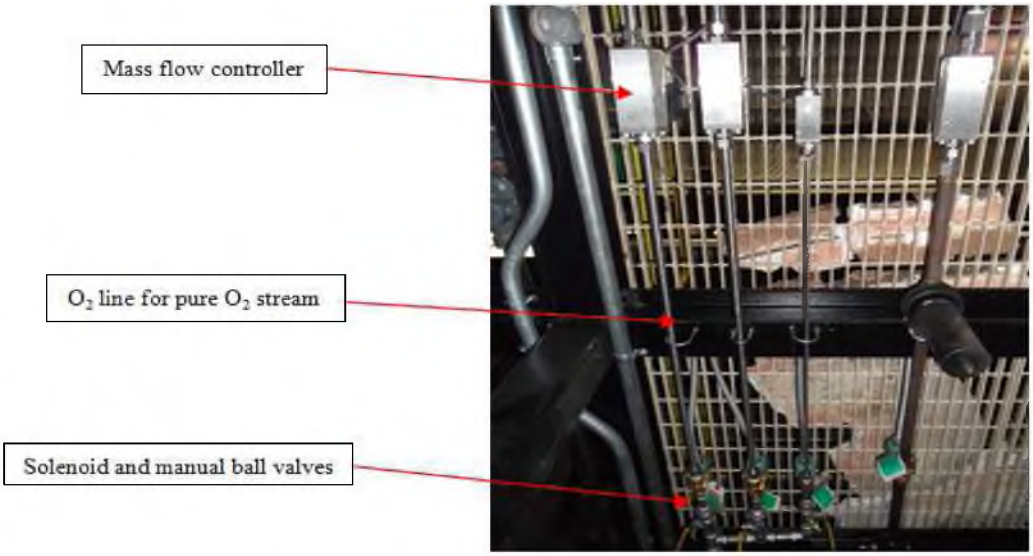

Figure 12. O_2 and CO_2 lines equipped with solenoid valve and mass flow controller

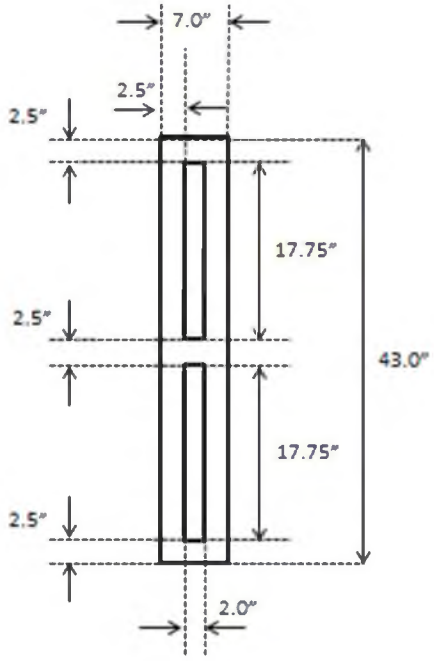

Figure 13. Drawing of windows

Figure 14. Heat exchanger of convective zone of OFC

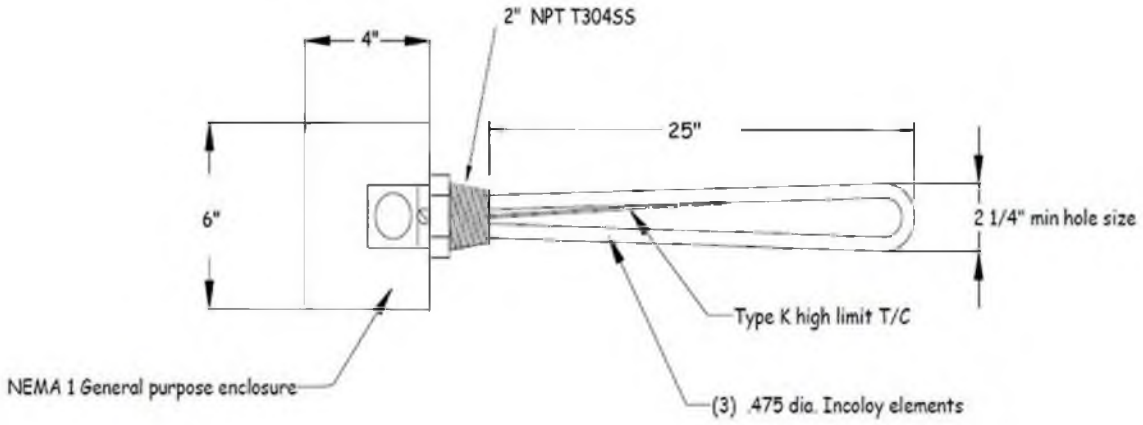

Figure 15. Sketch of gas heater electric element

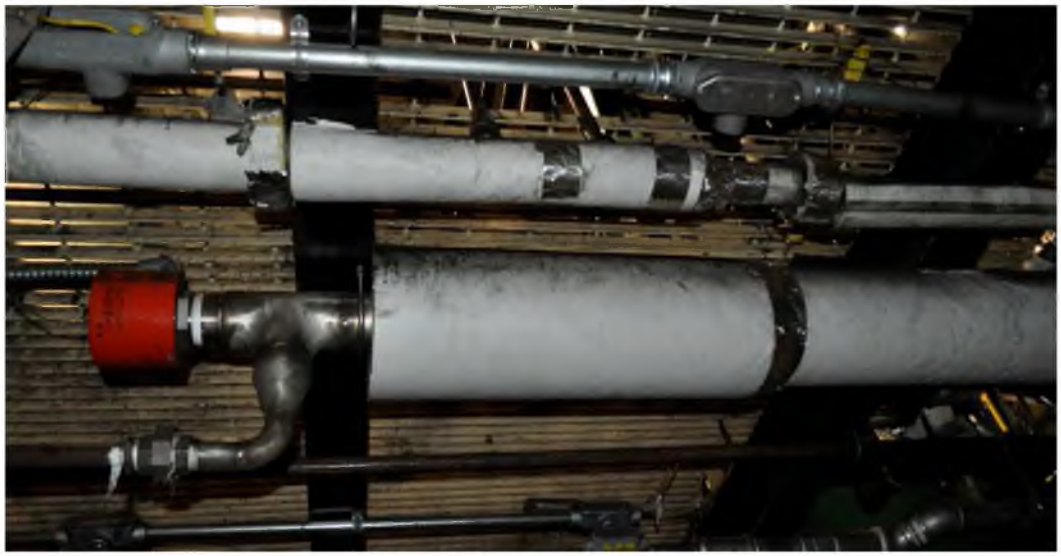

Figure 16. Gas heater installed in line

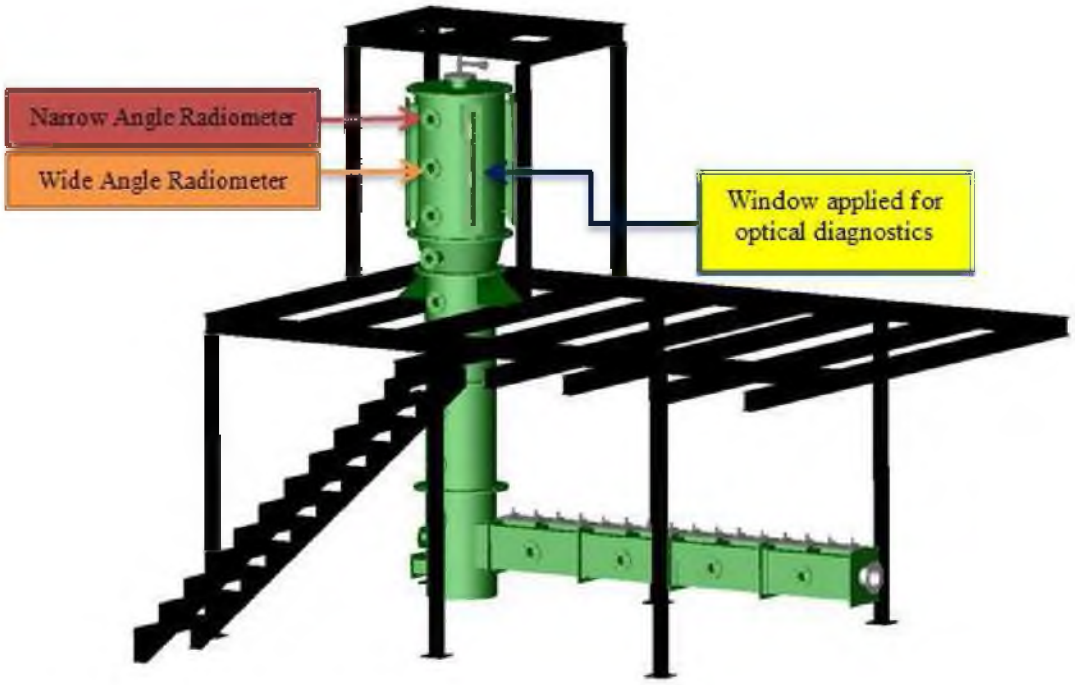

Figure 17. Schematic of OFC

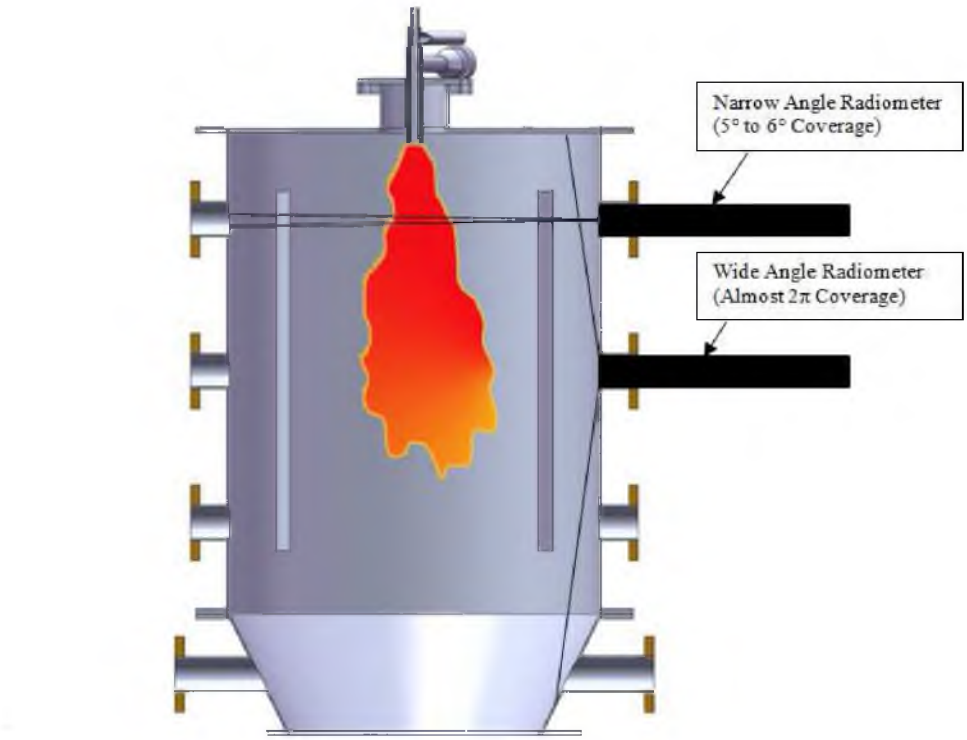

Figure 18. Schematic of location of radiometers in OFC.

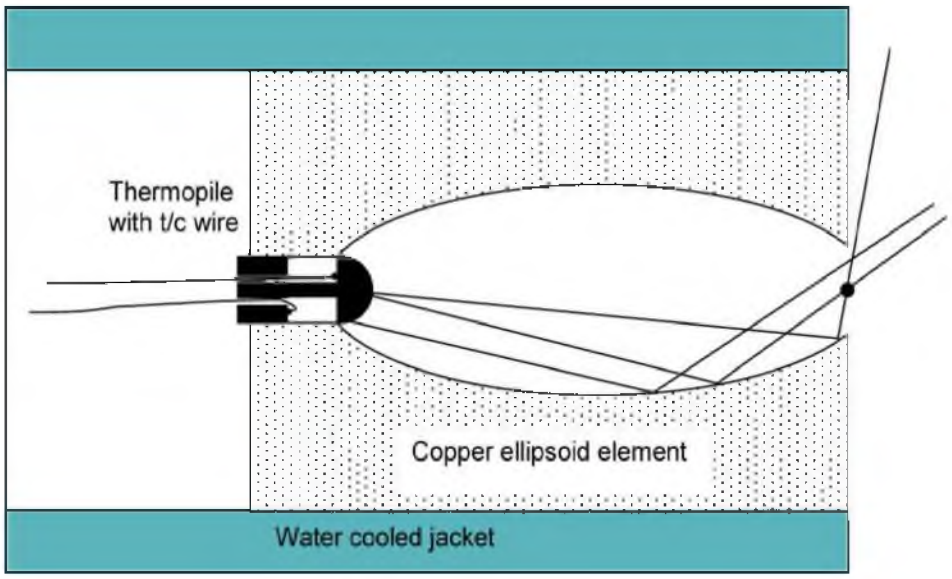

Figure 19. Schematic of principle of wide angle radiometer

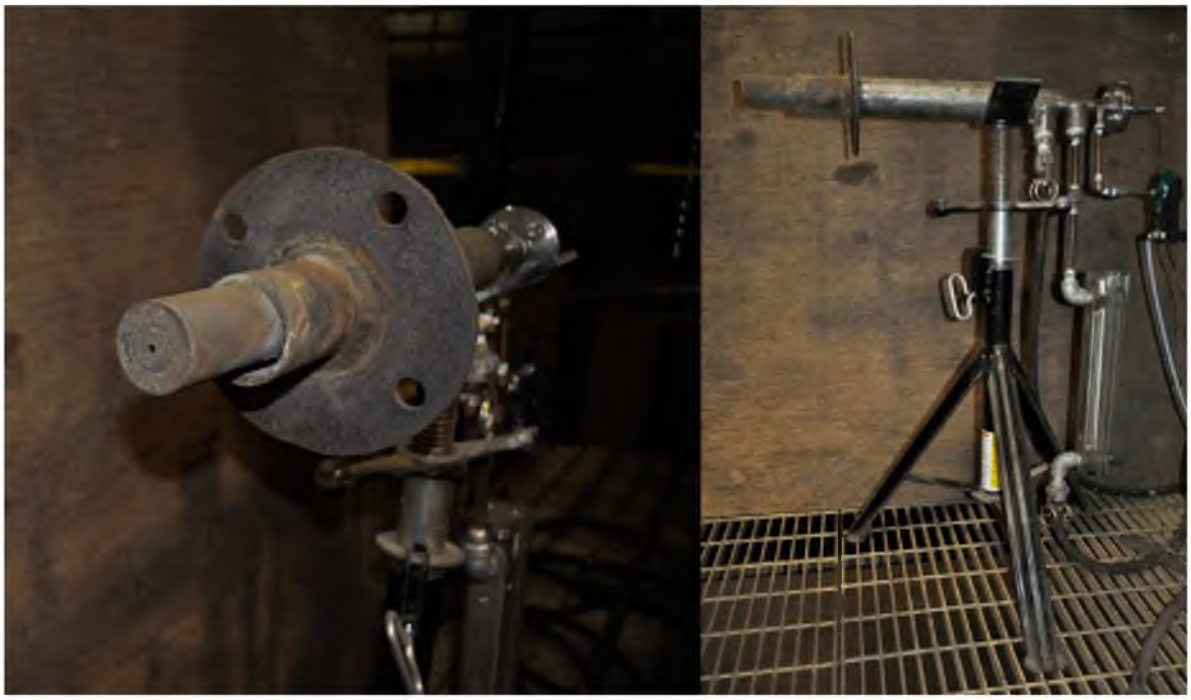

Figure 20. Pictures of wide angle radiometer

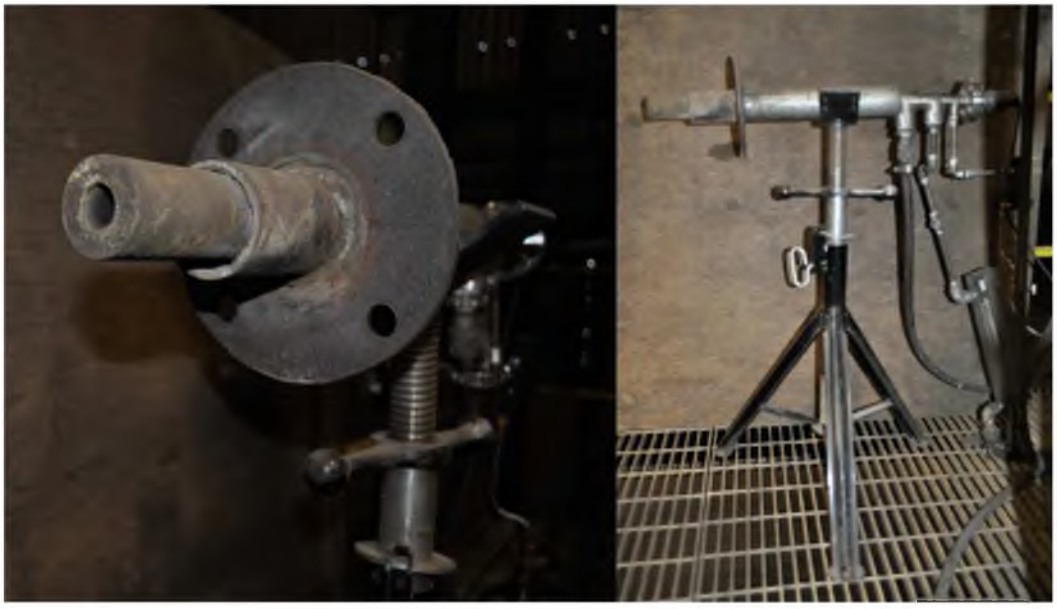

Figure 21. Pictures of narrow angle radiometer

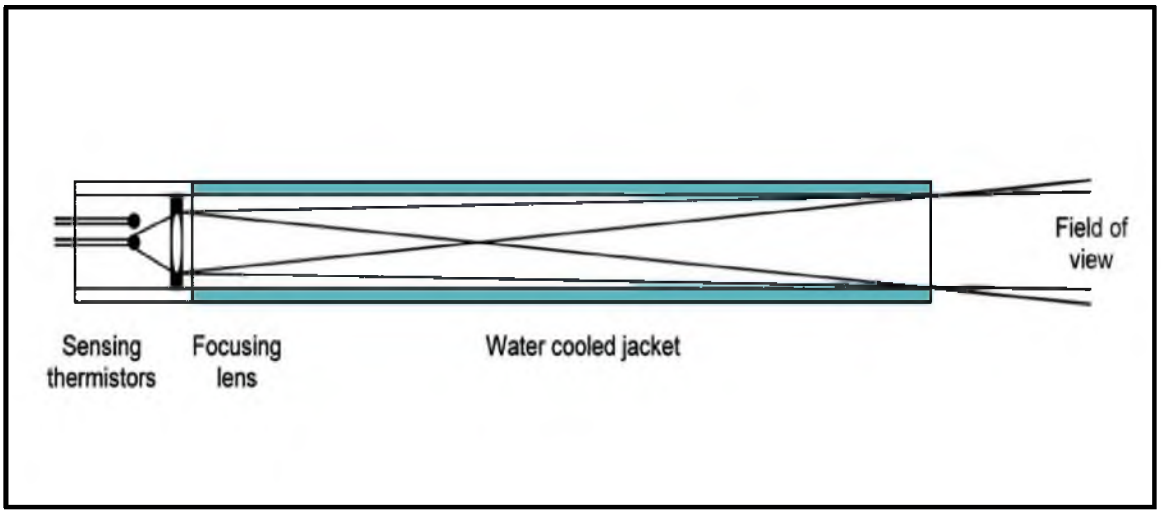

Figure 22. Schematic of narrow angle radiometer

Figure 23. Blackbody radiator

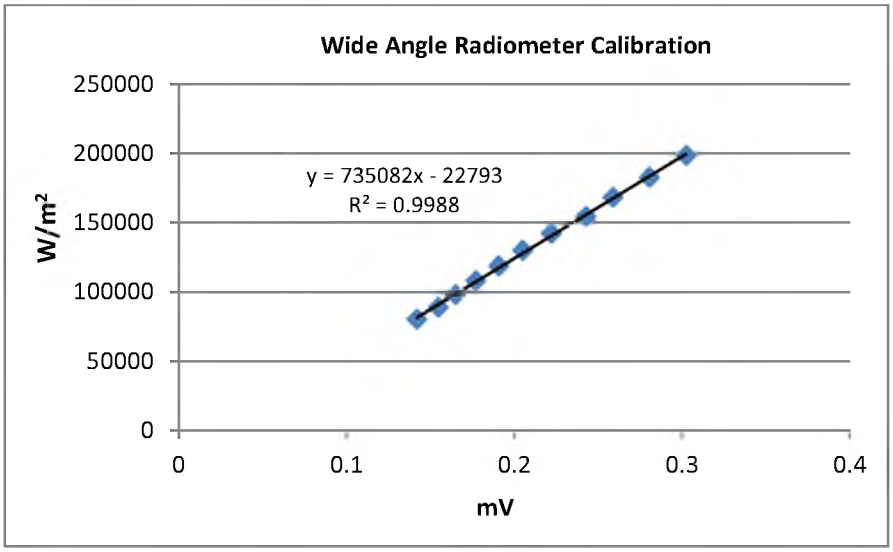

Figure 24. Wide angle radiometer calibration on 05-09-2011

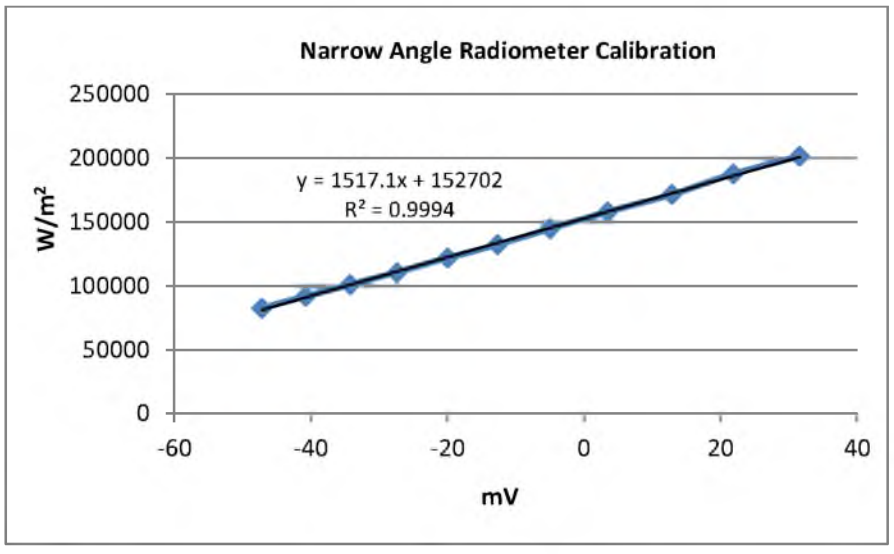

Figure 25. Narrow angle radiometer calibration on 05-09-2011

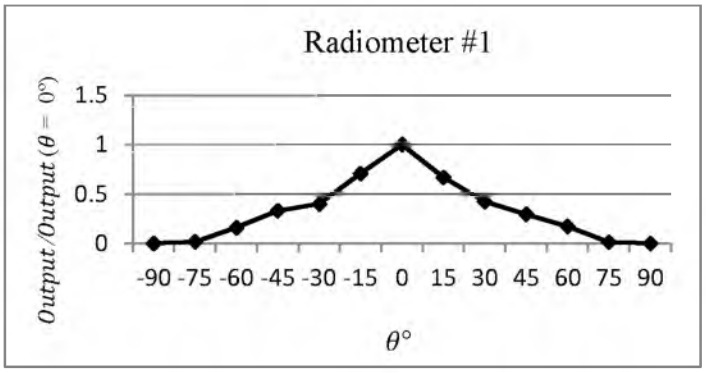

Figure 26. Angular response of Radiometer #1 (top port)

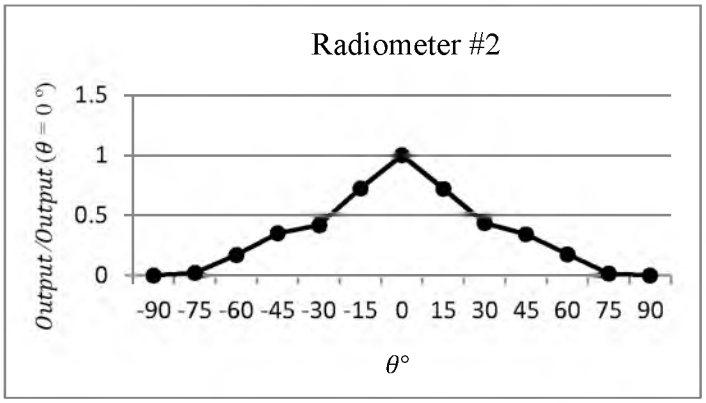

Figure 27. Angular response of Radiometer #2 (middle port)

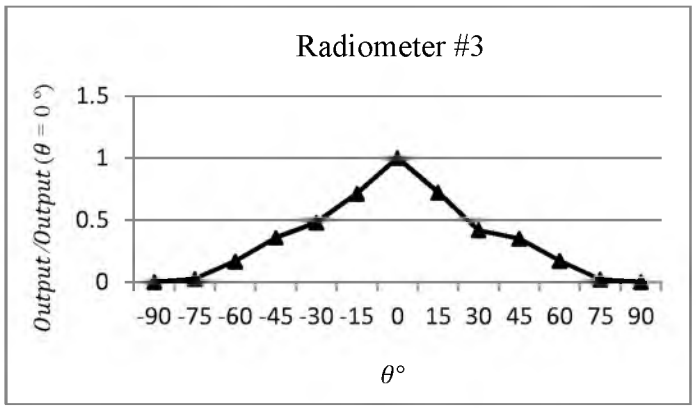

Figure 28. Angular response of Radiometer #3 (bottom port)

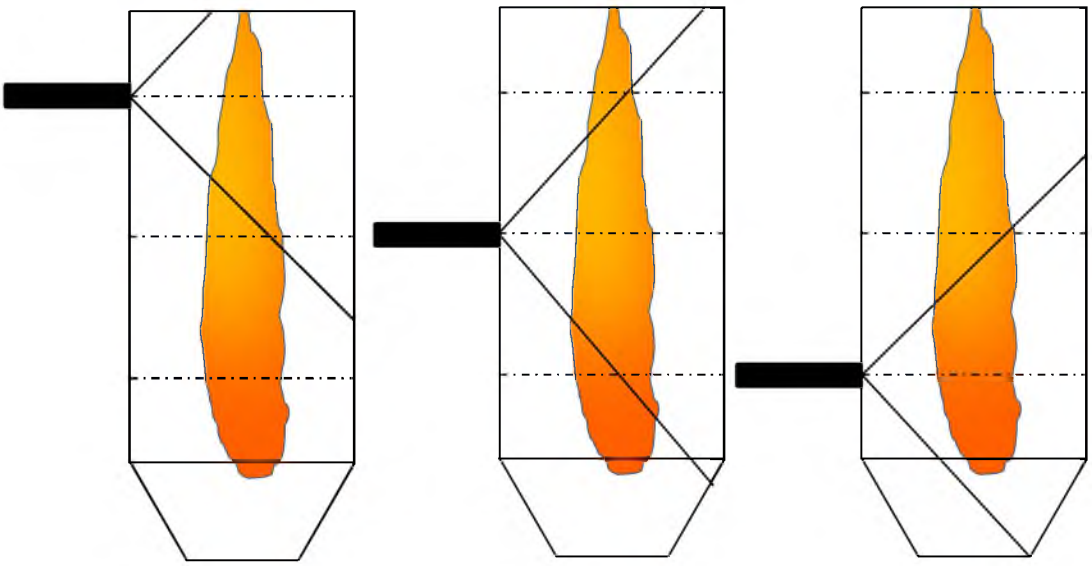

Figure 29. Field of view of wide angle radiometers in OFC

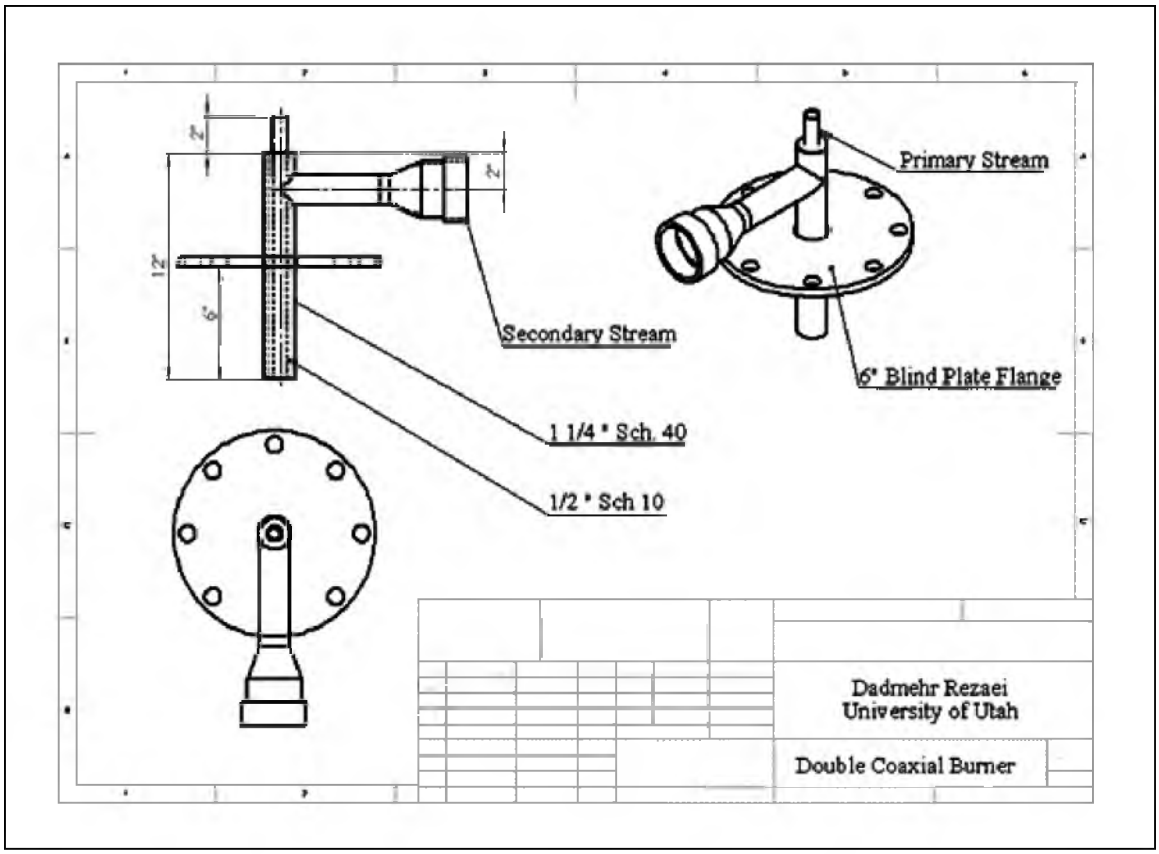

Figure 30. Sketch of double coaxial burner

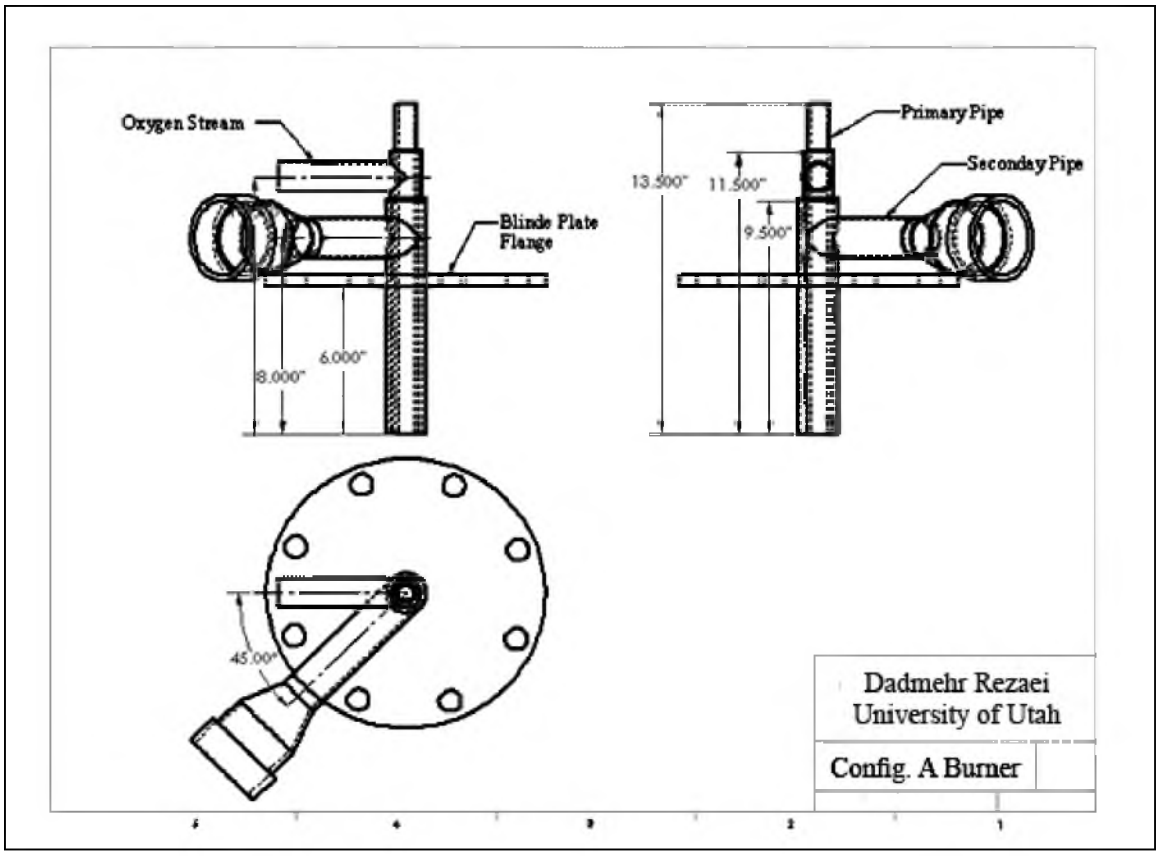

Figure 31. Schematic of Configuration A burners

Figure 32. Configuration A Burner

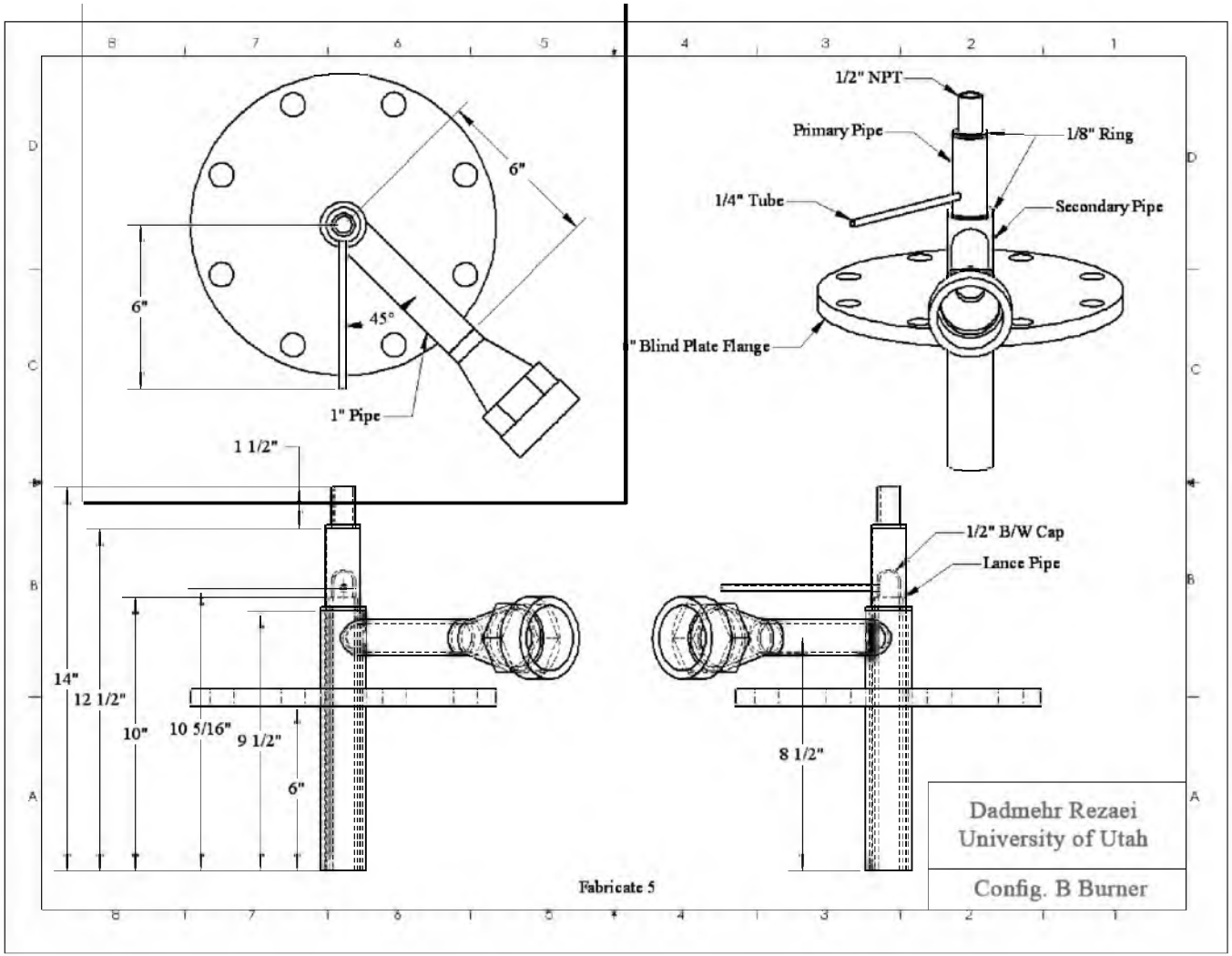

Figure 33. Schematic of Configuration B burners

Figure 34. Configuration B burners used in this study

Figure 35. Configuration B burner

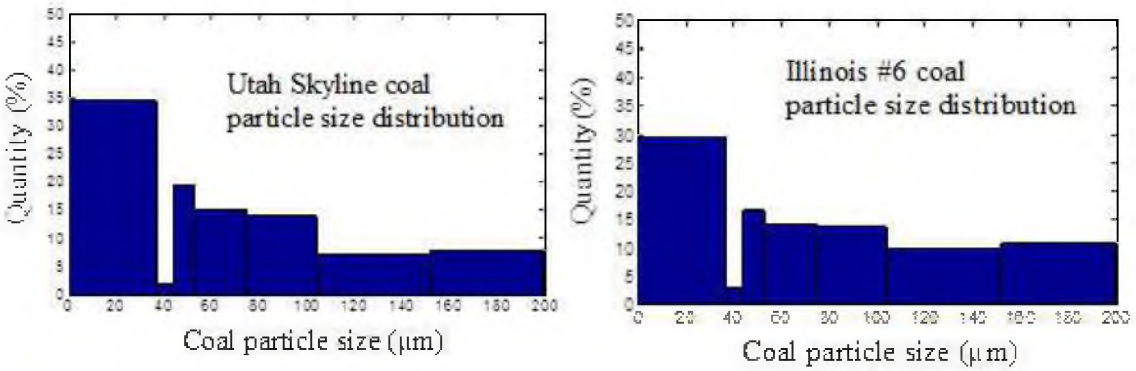

Figure 36. Particle size distribution of Utah Skyline and Illinois #6 coals

Figure 37. Gas analyzers at the University of Utah combustion research lab

Figure 38. Carbon dioxide tank

Figure 39. Oxygen tank

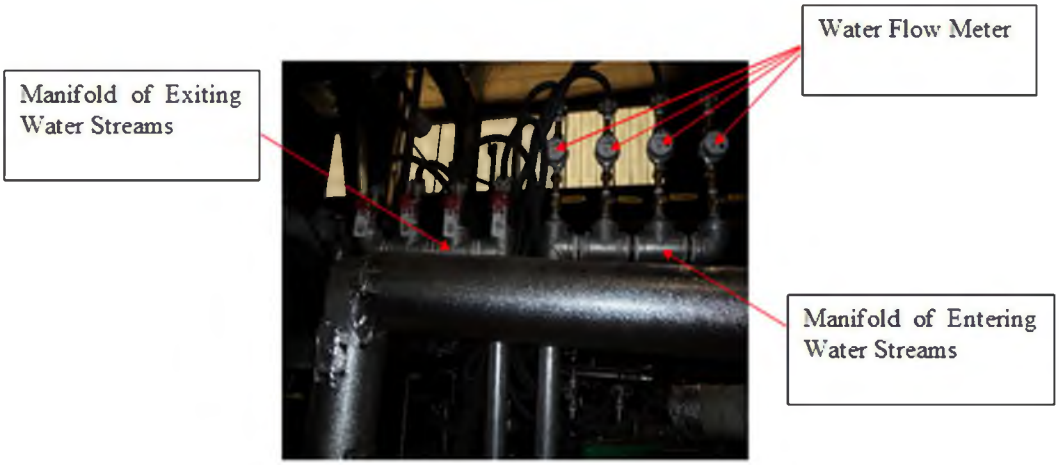

Figure 40. Manifolds equipped with flow meters and valves

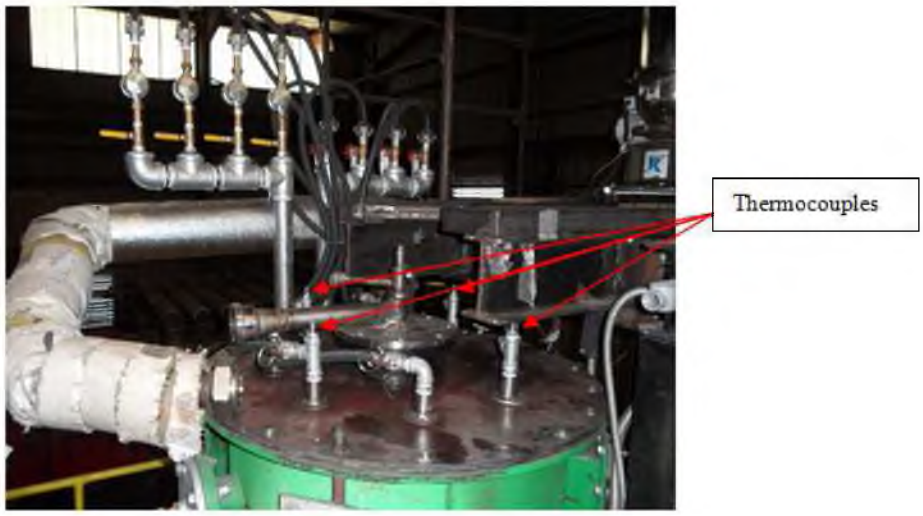

Figure 41. Position of thermocouples on top plate

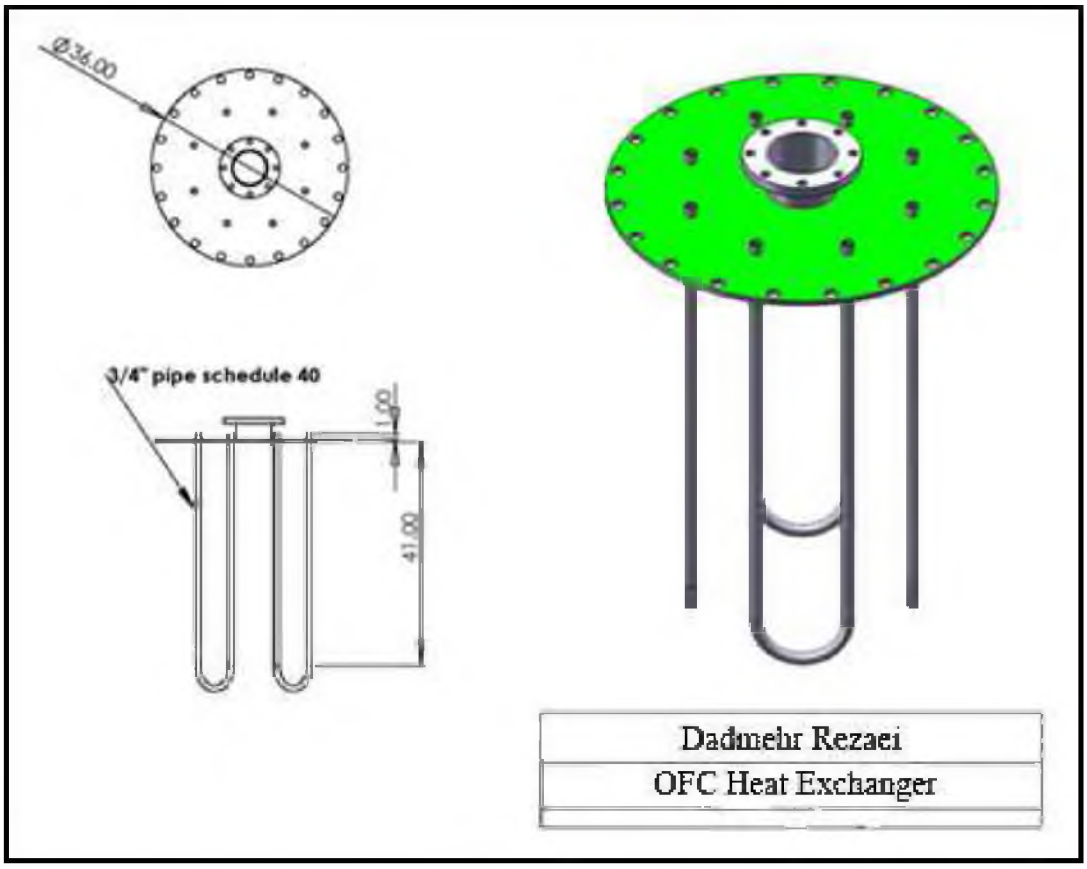

Figure 42. Schematic of cooling heat exchanger

Figure 43. U-shape water cooling heat exchanger

Table 1. Flame aerodynamic conditions for burners with inner annular oxygen stream (Configuration A)

Case	F_{O2} inner O_2 annulus	Prim. Vel. (m/s)	O_2 stream Vel. (m/s)	Second. Vel. (m/s)	Prim. A_S (cm^2)	O_2 Stream A_S (cm^2)	Second. A_S (cm^2)
1	0.0%	6.37	0.0	14.9	1.9604		6.0744
2	23.0%	6.37	6.10	15.8	1.9604	1.0653	5.0665
3	55.0%	6.34	6.40	15.8	1.9604	2.3788	3.9442
4	75.0%	6.38	6.10	14.6	1.9478	3.2475	3.9515
5	85.0%	6.38	6.70	14.6	1.9478	3.5059	3.6361
6	100.0%	6.38	6.50	15.0	1.9478	4.2651	3.0994

Table 2. Flame aerodynamic conditions for burners with central oxygen stream (Configuration B)

Case	F_{O2} center O_2 stream	Prim. Vel. (m/s)	O_2 stream Vel. (m/s)	Second. Vel. (m/s)	Prim. A_S (cm^2)	O_2 Stream A_S (cm^2)	Second. A_S (cm^2)
1	0.0%	6.37	0.0	14.9	1.9604		6.0744
2	21.0%	6.40	6.28	16.43	1.9801	0.9066	4.9498
3	44.0%	6.32	6.22	16.27	2.0005	1.9604	4.3723
4	64.0%	6.00	6.26	15.8	1.9883	2.9267	3.9442
5	80.0%	6.26	6.27	16.21	1.9883	3.5244	3.4077
6	100.0%	6.30	6.26	16.17	1.9883	4.3825	2.8689

Table 3. Coals proximate analysis

Proximate Analysis (As Received Basis)				
Coal	Moisture wt%	Ash wt%	Volatile Matter wt%	Fixed carbon wt%
Utah Skyline	3.10 ± 0.07	10.27 ± 1.44	38.70 ± 0.10	47.91 ±1.47
Illinois #6	9.65	7.99	36.78	45.58

Table 4. Coals ultimate analysis

	Ultimate Analysis (As Received Basis)				
	C	H	O	N	S
Coal	wt%	wt%	wt%	wt%	wt%
Utah Skyline	68.44 ±	4.85 ± 0.56	13.14 ±	1.32 ± 0.09	0.45 ± 0.07
Illinois #6	64.67	4.51	8.07	1.12	3.98

Table 5. Coals elemental analysis

	Elemental Analysis										
	Al	Ca	Fe	Mg	Mn	P	K	Si	Na	S	Ti
Element	Al_2O_3	Cao	Fe_2O_3	MgO	MnO	P_2O_5	K_2O	SiO_2	Na_2O	SO_3	TiO2
Utah	13.30	11.57	5.06	2.88	0.05	0.30	1.49	52.37	1.44	2.44	0.65
Ill #6	17.66	1.87	14.57	0.98	0.02	0.11	2.26	49.28	1.51	2.22	0.85

4. METHODOLOGY OF MEASURMENT OF STAND-OFF AND LENGTH OF FLAME

In this research, the flame stability is determined based on the flame stand-off distance concept. Flame stand-off distance is defined as the distance between the tip of the burner and the visible part of the flame. The methodology of defining stand-off distance and flame stability using image processing was developed by Zhang et al. at the University of Utah [49]. This method was applied for the purpose of this study to measure the flame length. In order to measure the stand-off distance, a high-speed camera was used to capture the flame images. This camera is an EPIX CMOS camera SV5C10 with XCAP software, providing a friendly interface. During the test, the lens was adjusted such that the camera could capture the entire length of the windows. This setup allowed for measuring both flame length and stand-off distance simultaneously for each image.

It is obvious that because of the turbulent nature of co-axial flames, the presence of fluctuations was witnessed. However, the purpose of this technique was not to capture the flame turbulence fluctuations, but to find the flame envelope leading to the measurement of the flame length and stand-off distance. The camera operating conditions chosen for this set of experiments are an 8.3 millisecond (ms) exposure time and 30 frames per second (fps). For every combustion condition, 6000 images were taken. For this exposure time, it was discovered that there are stand-off distance and

flame length fluctuations that need to be considered when using this method. It was suggested to include all the fluctuations in the flame images by the Probability Density Function (PDF).

In order to define the flame envelope, it is required to define a luminosity intensity threshold. The first step that needs to be considered is that the goal is not to capture the details of the flame structure. However, the purpose is to understand what the envelope of the flame is and where it exists. Therefore, it was decided to set up the camera such that smeared images can be produced. This methodology is applicable for smeared images.

As a summary to elucidate the methodology for the flame length and stand-off distance measurement, the following procedures were applied:

1. Convert the original images to gray scale
2. Use the Sobel operator for edge detection. The Sobel operator finds the zones where the intensity gradient of the luminosity has the highest value. The Sobel operator of MatLab has been applied to evaluate the intensity gradient of each pixel of the images based on the brightness and darkness of the pixels. The maximum gradients can define that flame envelope. The intensity values at the maximum gradients were calculated, and their average was determined as the threshold for the whole image. It is important to note that every image has its own threshold.
3. Convert the images to black and white images using the threshold obtained from the previous step. If the luminosity intensity of a pixel has a value smaller than the threshold, the pixel will be assumed to be a black pixel, and if the pixel

luminosity intensity is more than the threshold, that pixel is considered to be a white pixel.

4. Measure the stand-off distance, which is the distance from the tip of the burner to where the flame starts. The point that the flame starts is defined as explained above, and it is where the first white pixel is calculated.
5. Calculate the flame length in a similar manner. The flame length is defined as the distance from where the flame starts to where the flame ends.
6. Measures the PDF of the stand-off distance fraction of occurrences (out of 6000 frames) of the "ignition zone" lying between two specified distances.

Figure 45 shows examples of flame stand-off distance, and Figure 46 provides flame length reported in PDF form. Flame stability provides results that can be applied in understanding flame ignition and near burner zone mixing. In addition, these data permit the exploration of the effects of different important parameters of combustion such as O2 concentration, wall temperature, preheating temperature, and flame aerodynamics changes on the stability and ignition of coal particles. Furthermore, data obtained from flame length elucidate mixing in co-axial turbulent diffusion flames. In addition, flame length provides information regarding the heat distribution of the flame.

The results of these experiments will be contributed to the validation, with uncertainty quantification, of coal jet ignition submodels that can be used in simulations of practical axial coal flames.

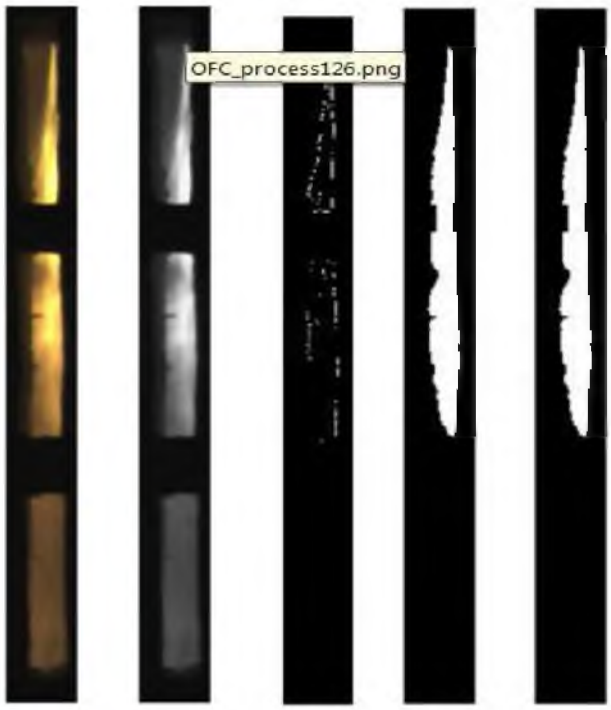

Figure 44. Procedure of optical methodology to measure flame stand-off distance

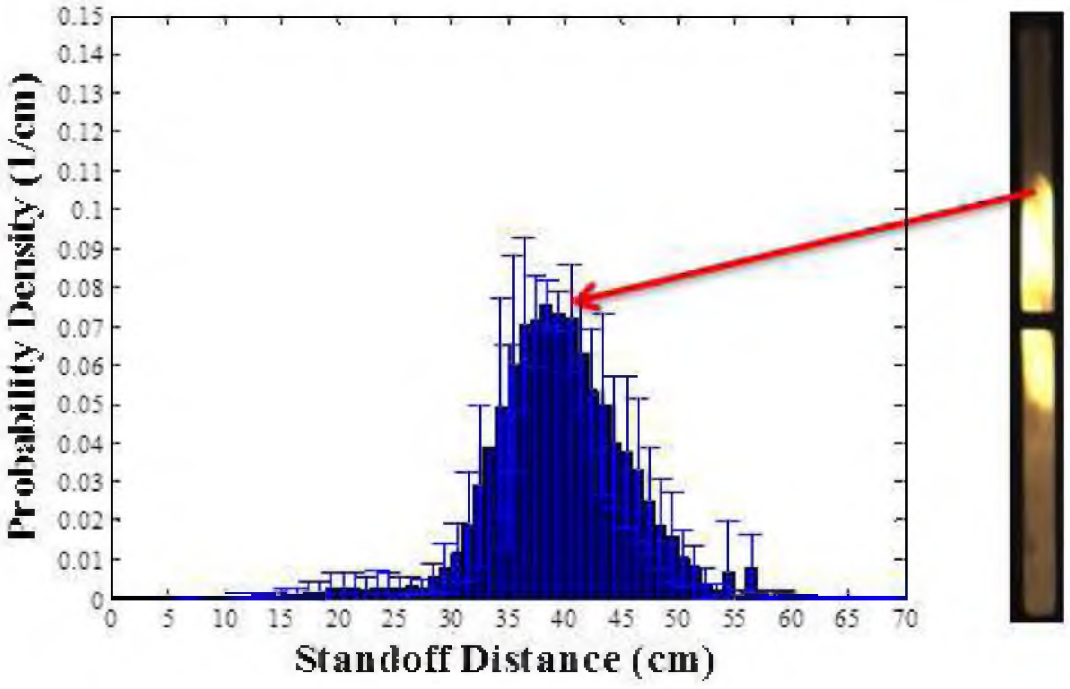

Figure 45. Flame stand-off distance in PDF form

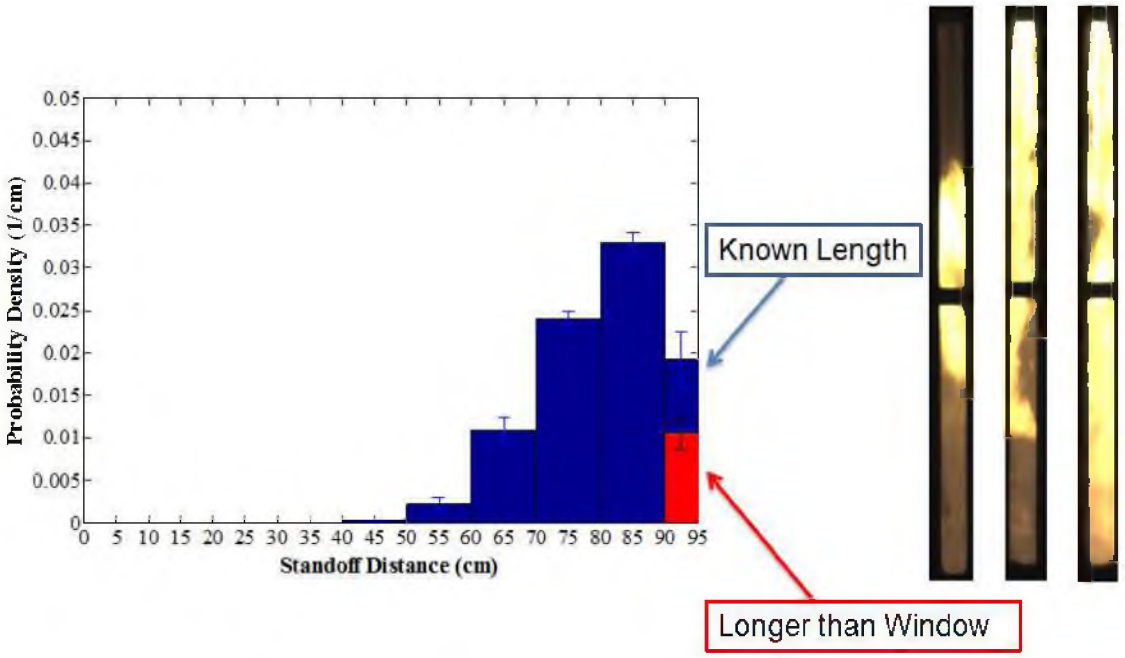

Figure 46. Flame length distance in PDF form

5. THE EFFECT OF COAL COMPOSITION ON IGNITION AND FLAME STABILITY IN CO-AXIAL TURBULENT DIFFUSION FLAMES

Dadmehr Rezaei*, Yuegui Zhou, Jingwei Zhang, Kerry E. Kelly, Eric G. Eddings, Ronald J. Pugmire, Mark S. Solum, Jost O.L. Wendt

*Corresponding author.

Institute for Clean and Secure Energy, Department of Chemical Engineering, University of Utah, 155 South 1452 East, Room 350, Salt Lake City, UT, 84112, USA

5.1 Abstract

Past research at the University of Utah on flame stability and stand-off distance was performed for one specific coal, namely a Utah Bituminous Coal. The experiments were carried out in a 100kW pulverized coal test rig with a co-axial turbulent diffusion burner. The purpose of the research described in this paper is to extend the previous work and to explore how coal composition changes affect the following dependencies that control flame stand-off distance and flame ignition, namely (1) the effect of partial pressure of oxygen (P_{O2}) in the primary stream with differing preheat temperatures in the secondary stream and (2) the effect of P_{O2} in the secondary stream with zero O_2 in the primary stream. The results of this new study were designed to extend previously obtained knowledge on the effects of secondary preheat temperature, turbulent mixing,

and P_{O2} in various streams, from one single coal to other coals of differing compositions. This paper, therefore, explores the effects of coal composition on ignition in oxy-coal, coaxial, turbulent diffusion flames. In this research, the stability and stand-off distance of the flame were studied for the following two types of coal: Utah Skyline Bituminous, Illinois #6 Bituminous. To this end we investigated: 1) the effect of P_{O2} in the primary stream, 2) the effect of P_{O2} in the secondary stream, and 3) the effect of preheat temperature in the secondary stream, on flame stand-off distance, using the same photo-imaging methodology described elsewhere. The results of the ignition and flame stability analysis for these two coals under oxy-firing conditions are compared, and the effects of coal composition are elucidated. At 420°C preheat temperature, Illinois coal showed a more stable flame. Flame stability of Illinois coal did not change at 520°C preheat temperature; however, Utah Skyline flame stability increased significantly. Data obtained from TGA analysis and solid state ^{13}C NMR data provide further insight regarding the structural variation in these two coals as well as their pyrolysis behavior. These data justified the difference in the flame behaviors of two coals with similar coal composition in a pilot-scale oxy-fuel combustor.

5.2 Introduction

The increase of greenhouse gases, and particularly carbon dioxide, for energy production has resulted in new technologies with lower emissions of NO_x, and SO_x. These techniques are capable of complying with carbon dioxide capture and sequestration. Oxy-Fuel Combustion technology has been suggested as the most promising strategy for the conventional coal power plants to generate electric power [4]. In oxy-coal combustion, coal burns with pure oxygen instead of air, and the combustion

gases are diluted using the recycled flue gas (RFG), which essentially contains CO_2 and H_2O. The gas mixture has higher emissivity and subsequently greater heat transfer while at the same time a lower volume. By recycling the flue gas, a gas consisting mainly of CO_2 and water is produced, ready for CO_2 capture and sequestration [1]. One of the difficulties associated with oxy-fuel combustion is delayed ignition. Several studies have shown the effect of the burner aerodynamics and higher momentum flux of primary stream on the flame stability and delayed ignition [13,55]. Other research groups have investigated the impact of the CO_2 atmosphere on coal ignition. Yu Qiao and his colleagues claimed that thermal conductivity of the gas atmosphere surrounding the particle could significantly affect the observed particle ignition [10]. Another study showed that the use of CO_2 as diluents will retard devolatilization due to the lower mass diffusion of fuel volatiles in CO_2 compared to a nitrogen atmosphere [4]. The fuel ratio, defined as fixed carbon content / volatile matter content, is believed to provide an index to predict the combustibility, but it does not always anticipate the real ignition behavior [42,56]. The influence of the maceral composition of the coal on the ignition and flame stability has been pursued by Su who suggested a criterion, the maceral index, which predicts burnout behavior of the coal and blends by including the effects of maceral composition such as liptinite, vitrinite, and inertinite [57]. However, these studies were conducted in an air atmosphere and, hence, the behavior change of coal ignition in an O_2/CO_2 is not yet well understood.

Previous work by Zhang [49] on Utah Skyline Bituminous in the 100 kW vertical oxy-fuel combustor at the University of Utah explained the effects of PO_2 in the primary stream on ignition and flame stability at different preheat temperature in the secondary

stream. In addition, this work provided information in connection with ignition and flame stand-off distance by increasing PO_2 in the secondary stream without O_2 in the primary stream. However, the influence of coal composition, which is one of the key criteria of combustibility in this set of experiments, is not well known. The present study was conducted to compare the ignition behavior, under similar oxy-fuel operating conditions, of two coals with remarkably similar rank and elemental analysis composition in a 100 kW pilot-scale combustor with a co-axial turbulent diffusion burner operated in a O_2/CO_2 environment. The results of this study will contribute to the validation, with uncertainty quantification, of coal jet ignition submodels for simulations of axial coal flames.

5.3 Coal Selection and Sample Preparation

Two coals of similar rank and elemental composition, except for sulfur content (Utah Skyline HVB and Illinois #6), were chosen in this study. The ultimate, proximate, and ash analyses of the coals are provided in Table 3 and Table 4.

Both coals were pulverized and prepared for a steady feeding to the combustor. Since the size of the coal particles is one of the indices of coal ignition, both coals were prepared in a manner to have a similar particle size distribution. The maximum size of the coal particles is 150 μm. The particle size distribution has been calculated and is summarized in Figure 36. According to data shown in Figure 36, the mass average diameters were calculated to be 62 μm and 68.5 μm for Utah Skyline and Illinois #6 coal particles, respectively. Hence, this study could be focused only on the differing effects of coal composition/structure.

5.4 Oxy-Coal Combustor

The Oxy-Fuel Combustor (OFC) consists of three sections, namely 1) Burner zone or the main chamber; 2) Radiant zone, which is located in the bottom of the main chamber; 3) Convective zone, which benefits from the heat exchangers to resemble the industrial furnace conditions (see Figure 47).

The dimension of the burner zone is 0.61m I.D, 0.91m O.D. and, 1.22m as the height of the burner zone. The chamber is insulated by 76 mm thick Fiberboards that tolerate high temperatures up to 1700 K. The temperature of the furnace can be monitored by three high-temperature-resistant K-Type thermocouples that are located along the height of the chamber.

Also, to have an optical access to the flame regarding optical diagnostic, four quartz windows have been provided on the quadrants of the cylindrical chamber. The chamber of the OFC is equipped with 24 ceramic electric heaters that have been arranged in three rows. The 840 watt heaters permit control of the wall temperature of the chamber in an accurate way. Wall temperature has an important role on ignitibility of coal. Therefore, in this study, the wall temperature for all studies was kept at 1850 °F.

5.5 Gas Analyzers

The flue gas probe is located at the end of convection zone of the OFC. This probe is used to monitor the exhaust gas composition during the combustion process using oxygen, carbon dioxide, NO_x, and SO_x analyzers.

The furnace is controlled and monitored by the OPTO22 control system. All the data from the furnace and analyzers have been plotted, and saved on charts during the experiment. This system provided extensive control on the OFC.

5.6 Burner and Feeder

The schematic of the burner drawn in Solidworks is shown in Figure 48. The burner consists of: 1) Primary stream; 2) Secondary stream. The primary line is located in the center of the burner. A carrier gas transports the coal into the chamber from the primary stream. The carrier gas in this study is either CO_2 or a mixture of O_2 and CO_2. The secondary stream contains a mixture of O_2 and CO_2 and flows around the primary jet. A heat exchanger is installed in the secondary stream, which provides the ability to preheat the secondary flow up to 700 K. The flow and temperature of both streams are accurately automated and under control using the OPTO22 control system.

Having a steady coal feeding system is one of the most effective indices of flame stability. In this study, it was decided to use a twin-screw coal feeder with a solid conveying eductor. In the eductor system, the primary stream gases get mixed with coal fed by the screw feeder. The eductor provides a steady stream of pulverized coal feeding through the burner.

5.7 Methodology of Flame Stability Measurement

Flame stability is determined based on the flame stand-off distance concept. Flame stand-off distance is defined as the distance between the tip of the burner and visible part of the flame. In order to measure stand-off distance, a high-speed camera was used to capture the flame images. The methodology for quantification of flame stability was developed in the University of Utah combustion laboratory [47]. Due to the turbulent nature of the flame, existence of fluctuations in the flame properties is obvious. The camera operating conditions chosen in this set of experiments are 8.3 ms exposure time and 30 fps. For every combustion condition, 6000 images were taken. Since flame

attachment is defined by human eye vision, the operating conditions of the camera are set to simulate the detection capabilities of the human eye instead of capturing all the turbulent fluctuation. For this exposure time, all stand-off distance fluctuations are required to be considered. The method suggests including all the fluctuations in the flame images by the Probability Density Function (PDF).

5.8 Combustion Operating Conditions

The experiment operating conditions and the burner jet aerodynamic parameters are shown in Table 6 and Table 7. In order to have a robust comparison to investigate the effect of coal composition on ignition and flame stability, the operating conditions were kept constant for each type of coal. However, to maintain the total Stoichiometric Ratio (SR) of the combustion process, it was necessary to change the coal feeding rate based on the SR (see Table 8).

In this study, there are three sets of experiments. The experiments of set A and B were designed to research the effect of oxygen in the primary stream. The second objective of this experiment was to investigate the role of turbulent diffusion mixing in the burner jet by increasing the oxygen in the primary stream. The overall oxygen concentration is kept at 40%; however, in each case, the amount of oxygen is deducted from the secondary stream, and added to the primary stream. The flow rates in both the experiments of set A and B are identical. In order to evaluate the effect of secondary stream preheat temperature on the combustibility of the coals, two temperatures were determined. For the experiments of set A, the secondary stream preheat temperature was kept at 489 K, and for the experiments of set B, the temperature was maintained at 544 K.

The experiments of set C were devised to look at the importance of overall

oxygen concentration in the furnace. In this case, the primary stream oxygen concentration is zero; however, the amount of oxygen in the secondary stream increases. The overall oxygen increases until the attached flame is obtained. The secondary stream temperature in the experiments of set C was kept at 489 K.

5.9 TGA and NMR Experiments

Thermo-gravimetric Analysis (TGA) data were obtained in both oxygen and nitrogen environments. The temperature ramp of the TGA was 20 K/min. The same pulverized coal that was used in combustion was applied for the TGA analysis. As it was mentioned, the diameters of the coal particles were 62 μm and 68.5 μm, respectively, for the Utah Skyline and Illinois #6 coals. At the beginning of each experiment, 25 mg of the coal sample was loaded into the pan in the furnace of the TGA. The amount of the purge gas was 100 ml/min for both N2 and Air environments [44]. Each sample was heated from 30°C to 1000°C. The solid-state 13C NMR experiments were conducted as previously described [58]. The coal structural data are given in Table 9, which also contains the lattice structural parameters of the two coals as defined in reference [59].

5.10 Results

5.10.1 Combustion of Utah Skyline and Illinois #6 Coals at 489 K Preheat Secondary Stream Temperature and Overall 40% Oxygen Concentration

The results of the experiments in set A are shown in the PDF plots for Illinois #6 and Utah Skyline coals. It is noted that at these conditions, attached flame was obtained from Illinois #6 coal at P_{O2}=0.144 in the primary stream. However, for Utah Skyline coal,

the attached flame was obtained at P_{O2}=0.207 in the primary stream. Results are presented in Figure 49.

5.10.2 Combustion of Utah Skyline and Illinois #6 coals at 544 K Preheat Secondary Stream Temperature and Overall 40% Oxygen Concentration

This set of experiments was selected to evaluate the effect of secondary stream temperature on the combustibility of the coals. The temperature of the secondary stream was kept at 544 K during the experiment. The results of this set are provided in Figure 50. According to the results for Utah Skyline, a semi-attached flame was obtained at P_{O2}=0.054 and it was fully attached at P_{O2}=0.099 in the primary stream. However, Illinois #6 coal had an attached flame at P_{O2}=0.144. Also, it is noticeable that the results of the Illinois #6 coal at 544 K preheat temperature did not change considerably compared to the results at 489 K of the secondary stream preheat temperature.

5.10.3 Combustion of Utah Skyline and Illinois #6 Coals at 489 K Secondary Stream Temperature with Increasing of Overall Oxygen Concentration in the Secondary Stream

In this set of experiments, the secondary stream preheat temperature was kept at 489 K. However, to see the effect of overall oxygen on combustion, the amount of oxygen in the secondary stream was increased. It is important to note that in this test, attempts were made to keep the primary stream's aerodynamics constant. This operating condition only permits the study of the influence of overall oxygen concentration on

frame stability. Therefore, the amount of oxygen in the primary stream was zero. The results of this test are shown in Figure 51 in PDF form.

5.11 TGA Analysis

TGA provides information regarding the devolatilization of both coals and possible relationships to the fundamental structural features of these coals. TA Q500 TGA was applied for this test. Nitrogen and air were chosen as the environmental gases for this experiment. In the nitrogen environment, the weight loss of the coal due to drying and devolatilization in an inert gas is presented in Figure 52. In Figure 53, devolatilization in an air environment presents a more complex picture of the differences in the pyrolysis/combustion behavior of the two coals, indicating that the fundamental structural differences of two coals of a similar rank can be manifested in their reaction/oxidation processes. The temperature ramp for both coals was 20 °C/min and the samples were heated to 1000 °C.

5.12 Discussion

According to the results in Figure 49, by increasing the oxygen in the primary stream from the secondary stream, flame stability increases. Better flame stability implies better ignition. The first criterion of ignition is the amount of volatile matter; however, it is believed the more correct way to determine the combustibility is the Fuel Ratio index (FR) which is the ratio of fixed carbon / volatile matter content [1,13,55]. A general trend is observed that the higher fuel ratio corresponds with less carbon burnout. However, this reasoning is not always reliable [42]. The PDF data for set A agree with the fuel ratio indices; however, it is not consistent with the data from the experiments in set B. In

addition, the difference between the fuel ratios is not significant enough to allow for sole reliance on this ignition index. Therefore, in order to justify the results, it was decided to use TGA tests. The TGA plots and data are presented in Figure 52 and Figure 53. The fuel ratios of Utah Skyline and Illinois #6 are provided in Table 10.

The TGA plots in Figure 52 provide the weight loss of both Utah Skyline and Illinois #6 coals in a nitrogen environment. The first peak in each coal trace indicates the moisture lost, and the subsequent peaks manifest the devolatilization processes of both coals. The pyrolysis pattern of the Illinois #6 coal in a nitrogen environment begins at a lower temperature than that of the Skyline coal but the differential weight loss curves are quite similar. The TGA experiment was also carried out in an air environment and the results are shown in Figure 53.

In the air environment, significant differences are noted in the differential weight loss of the two coals. The first peak in both traces (~79°C) corresponds with moisture loss. Four additional inflection points are identified (251, 350, 452, and 610°C) in the differential weight loss of Illinois #6 while only 3 inflection points (296, 450 and 640°C) are evident in the Utah Skyline coal. The differences noted in the pyrolysis behavior can be traced to the fundamental differences in the chemical structure of the two coals, as reported earlier [60–63]. Detailed studies of combustion devolatilization data have been compared on Illinois #6, Montana Rosebud sub-bituminous, and North Dakota Beulah Zap Lignite [61], while comparisons of matched tar-char pairs in rapid pyrolysis of Illinois #6 and Beulah Zap Lignite are described in reference [62]. The details of the differences in the chemical structures are quite similar in a ^{13}C NMR standard cross-polarization magic angle spinning experiment, as one can observe in Figure 54. NMR

Spectra acquired by means of dipolar dephasing begin to illustrate major differences in the structure of these two coals (see Figure 55). The details of the structural parameters (referred to as lattice parameters) of the two coals can be obtained as described in reference [44] and these data are presented in Table 9.

For purposes of discussion, the critical lattice parameters are the average number of aromatic carbons in the aromatic clusters (C), the coordination number or number of attachments or cross links per cluster (σ+1) that consist of either side chains (S.C.), bridges and loops (B.L.), or bi-aryl linkeages to adjacent clusters in the lattice. The molecular weight of an averaged cluster (M.W.) and the average mass of the aliphatic attachments to the aromatic clusters or half of the mass of the cross links between aromatic clusters is represented by M_δ. The number of cross links (σ+1) per cluster in Illinois #6 suggest that the pyrolysis/oxidation processes would begin liberating light gases prior to the release of comparable amounts of aliphatic-derived components in Utah Skyline coal. The release of aliphatic chain ends is more energetically favored than the breakage of fairly stable aliphatic bridges and loops between aliphatic structure [63].

This early release is noted at approximately 250°C for Illinois #6 while the first major release of light gases is at approximately 300°C in Utah Skyline. Once the lattice begins to break down, a broad range of volatile material is released, including aromatic as well as aliphatic components, and this process appears to start at approximately 350°C in the Illinois #6 and reach a maximum differential weight loss near 450°C. A similar secondary release is not present in the Utah Skyline coal but at 450°C, one would expect the onset of lattice break up for both coals and oxidation of the remaining aromatic structures, which continues from 450°C to approximately 700°C. Hence, the lattice

structure data seem to predict the general pyrolysis data in these two coals of similar rank and elemental content.

The TGA data are reliable evidences for the combustion behavior in the two types of coal utilized in Experiments A and B. Illinois #6 pyrolysis occurs at lower temperatures than Utah Skyline; therefore, it is seen that in Experiment A, carried out at 489 K secondary stream preheat temperature, flame stability of Illinois #6 develops by increasing the primary stream oxygen concentration. However, this effect is not significant for Utah Skyline coal.

Experiment B was performed at 544 K secondary stream preheat temperature. It is notable that only a 55 K increase of temperature in the secondary stream stimulates the devolatilization of Utah Skyline. Comparing Figure 49 and Figure 50, it is shown that Utah coal flame stability increases significantly. However, Illinois #6 is already able to be pyrolyzed at lower temperatures, and increasing the temperature will not have a more considerable influence on the ignitibility of the Illinois #6 coal. As it is shown in Figure 49 and Figure 50, PDF plots of Experiments B-4 and A-4 appear to be quite similar.

In Experiment C, the amount of overall oxygen was increased until an attached flame was observed. The amount of oxygen in the secondary stream was increased in each case of Experiment C; however, the concentration of oxygen in the primary stream was kept at zero. Figure 51 shows the influence of increasing overall oxygen is more important for Utah Skyline than Illinois #6. The Utah coal flame has some indication of an attached flame at 42% overall O_2 concentration, and it is fully attached at 44% overall concentration of O_2. However, there was not any indication of an attached flame for the Illinois #6 coal until the concentration of O_2 was increased to 48% and even at 52% of

overall O_2, a fully attached flame was not witnessed. According to the proximate analysis of both types of coal, the moisture content of Utah Skyline is 3.03% and for Illinois coal is more than three times greater (9.65%). It is important to note that when the overall oxygen concentration increases, the velocity of the burner jet in the secondary stream increases as well; therefore, the residence time decreases. The values of both velocity and residence time for each case of Experiment C has been calculated and tabulated in Table 7. The lack of sufficient residence time for the high moisture content coal retards the rate of both heat transfer and mass transfer for drying and devolatilization of the coal particles. Therefore, the flame stability of Illinois #6 coal lowers compared to Utah Skyline coal, even though O_2 concentration was increased.

5.13 Conclusion

The studies carried out in the pilot scale oxy-fuel combustor, and TGA analysis on two types of coals of similar rank and elemental composition but different structural composition, reveal the important role of moisture content as well as key structural components that contribute to the nature and release of volatile matter on the ignition of the coal particles. The existence of moisture in the coal particle retards the heat transfer and mass transfer for the devolatilization; therefore, the ignition of the particles decreases. Higher residence time for high moisture content coals must be considered in burner design. The fuel ratio is a widely used index to estimate the combustibility of the coal; however, it is not an accurate way to anticipate the combustibility of coals. It is important to note that coal structure can have a significant effect on the ignition of the coal particle in the oxy-coal combustion. The details of the chemical structure of two coals from the Argonne Premium Coal Sample Bank (Blind Canyon, and Illinois #6),

which are similar to the two coals used in this study (Utah Skyline, and Illinois #6), suggest that the differences in the chemical structures of these coals could be the source of the variability in the pyrolysis/combustion properties of these coals [59]. In the case of the two coals studied, TGA analysis seems to be a suitable method to investigate the devolatilization of the coal for the prediction of the combustion behavior.

Secondary stream preheat temperature has an important influence on the flame stability of the coals. However, it should be noted that increasing the preheat temperature higher than the required temperature for the devolatilization of the coal particle will not considerably enhance the ignitability of the coal.

5.14 Acknowledgments

This material is based upon work supported by the Department of Energy under Award Number DE-NT0005015. Special thanks for advice from Prof. Terry Ring. Assistance in running the experiment, and preparing the data were provided by Ryan Okerlund, Colby Ashcraft, and Charles German

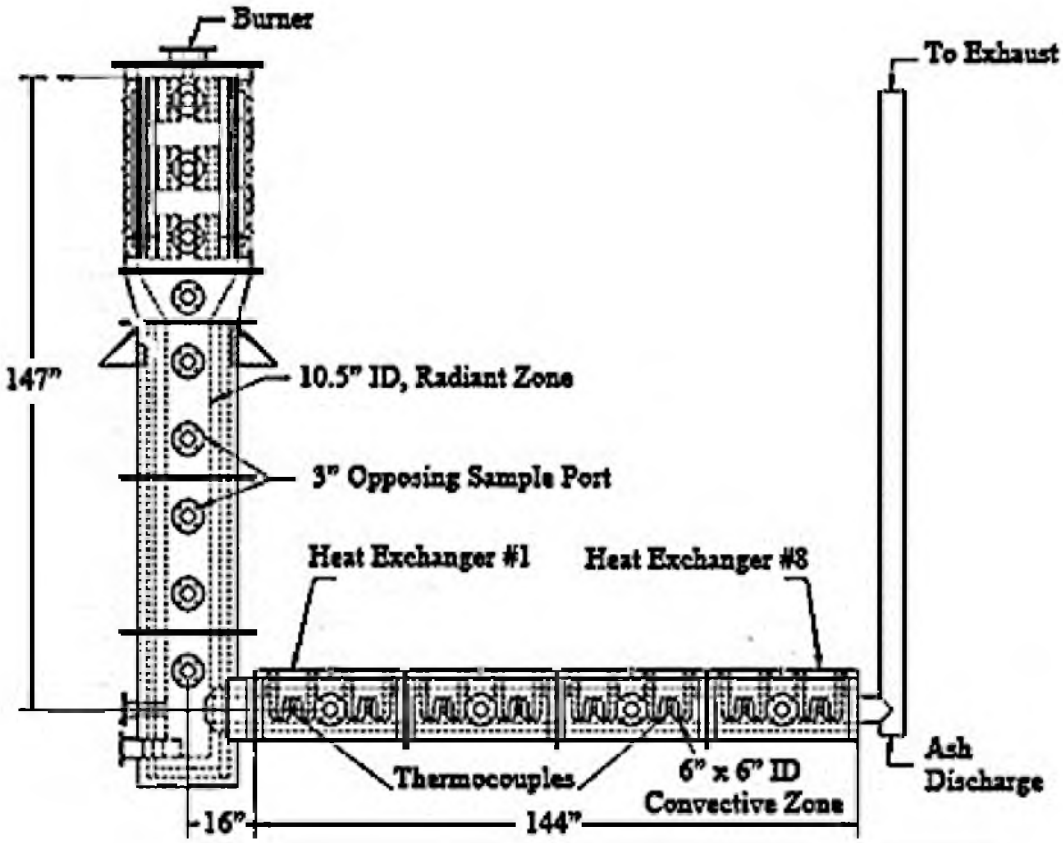

Figure 47. Schematic of OFC (side view with no recycle)

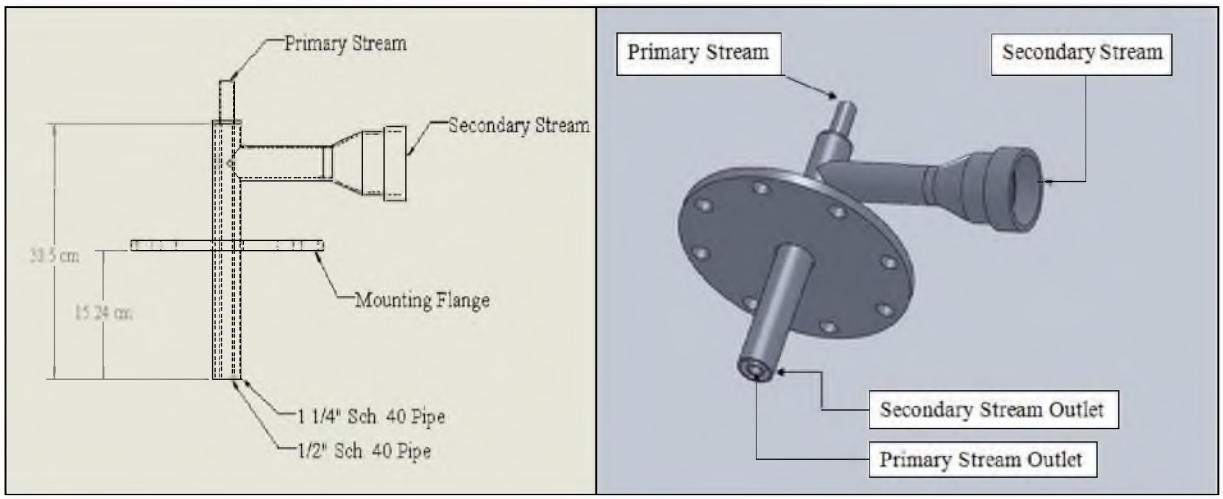

Figure 48. Design and drawing of burner

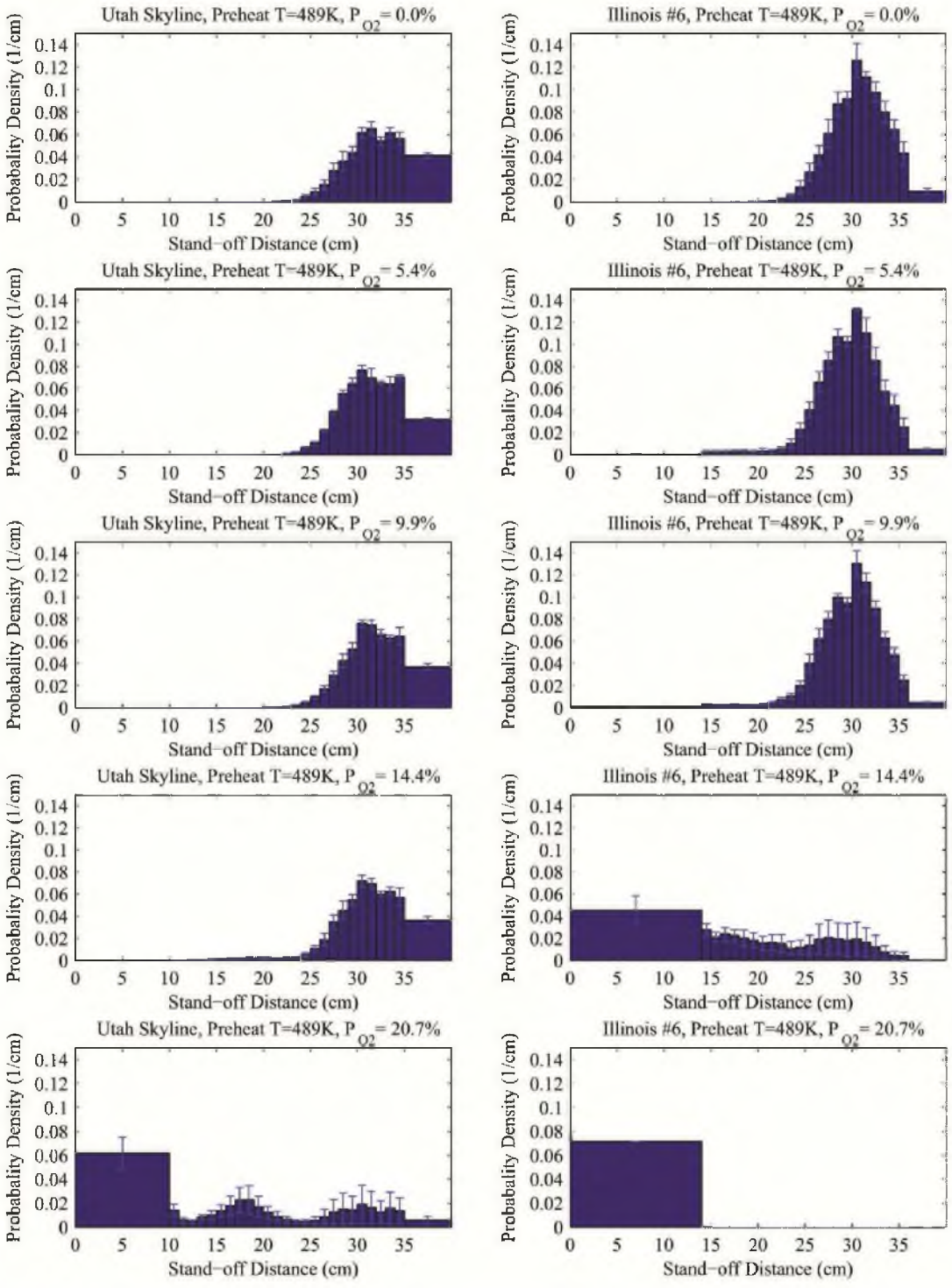

Figure 49. Comparison of PDF of stand-off distance for Utah Skyline (Left column) and Illinois #6 (Right column) coals at 489°K preheat temperature

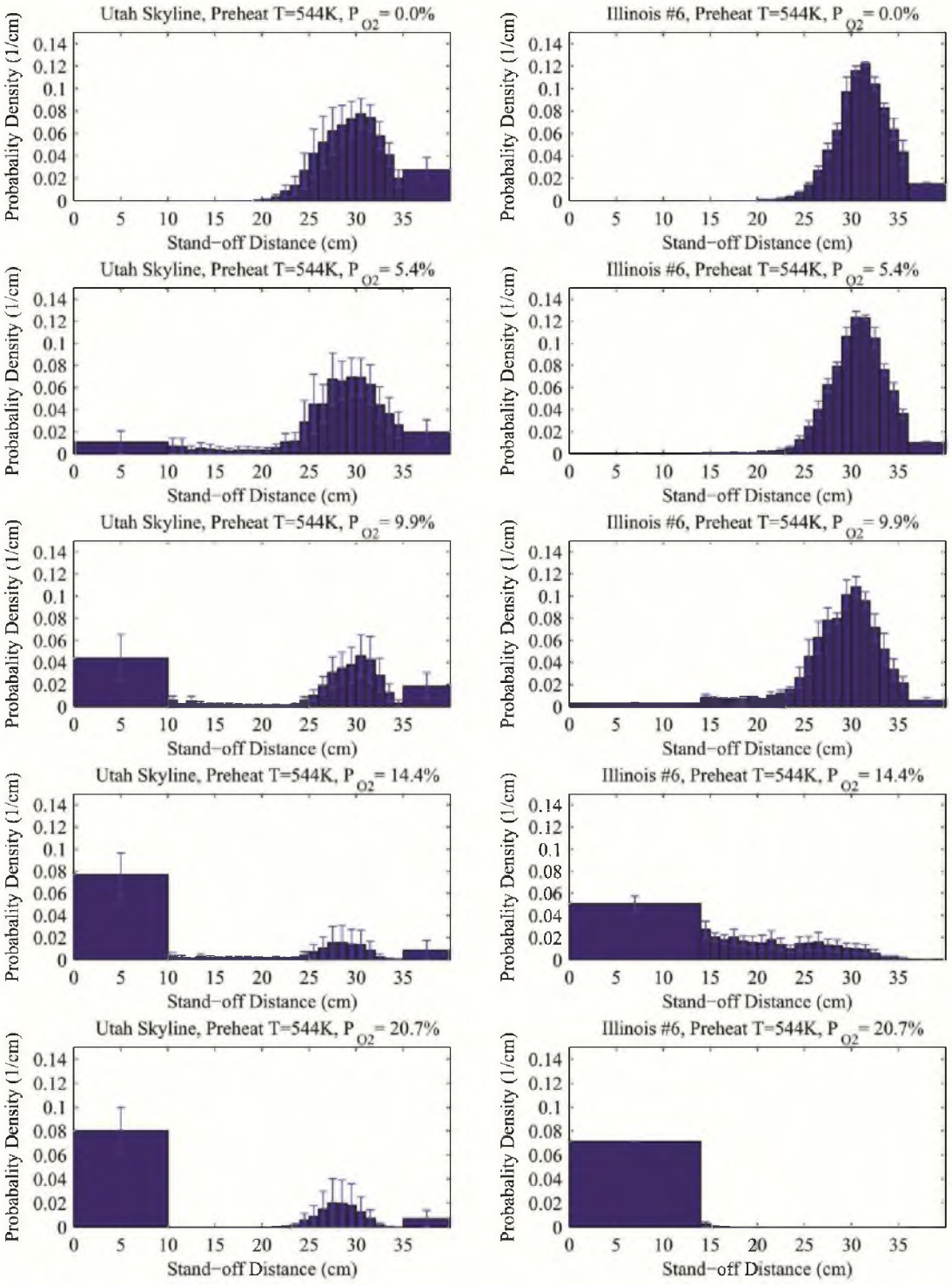

Figure 50. Comparison of PDF of stand-off distance for Utah Skyline (Left column) and Illinois #6 (Right column) coals at 544°K preheat temperature

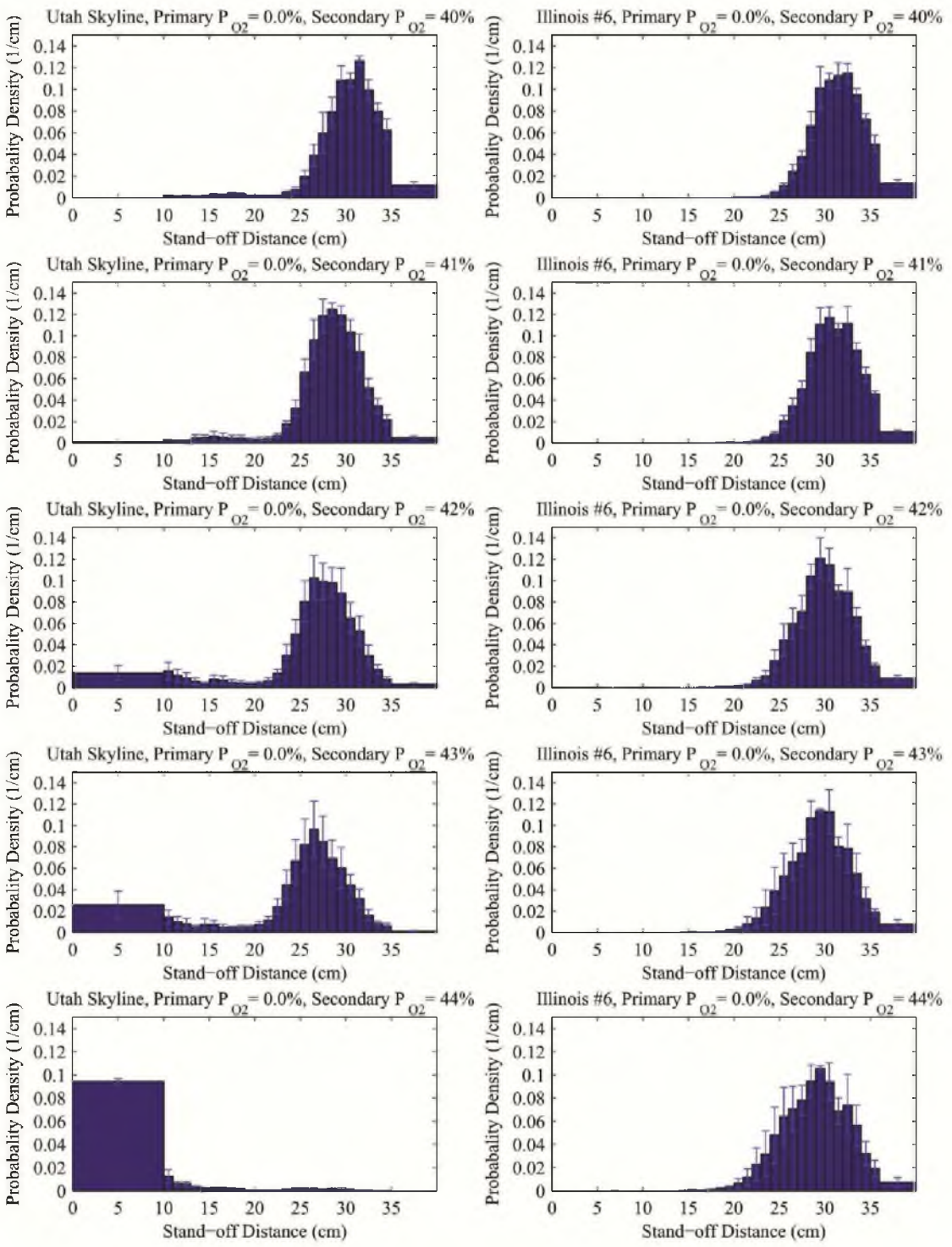

Figure 51. Comparison of PDF of stand-off distance for Utah Skyline (Left column) and Illinois #6 (Right column) coals at 489°K preheat secondary temperature with increasing of overall oxygen concentration

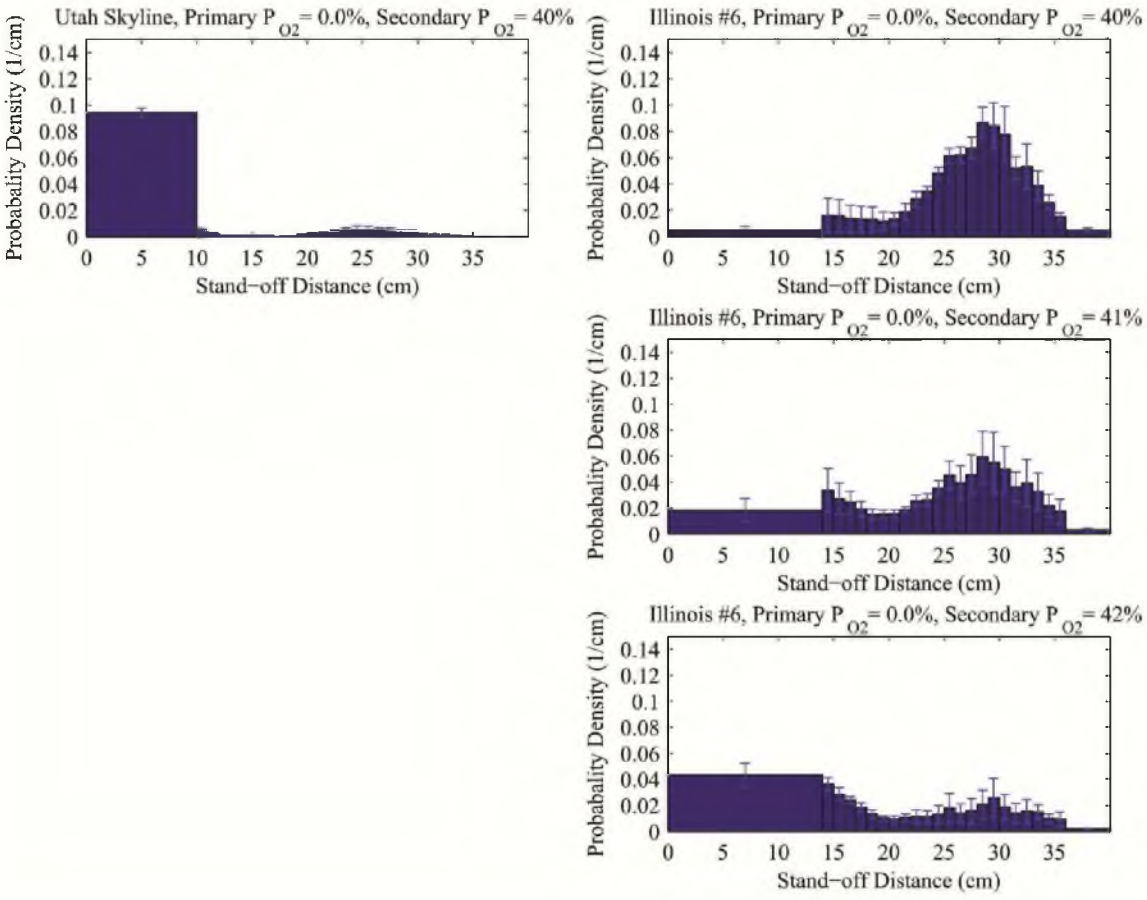

Figure 51. Continued

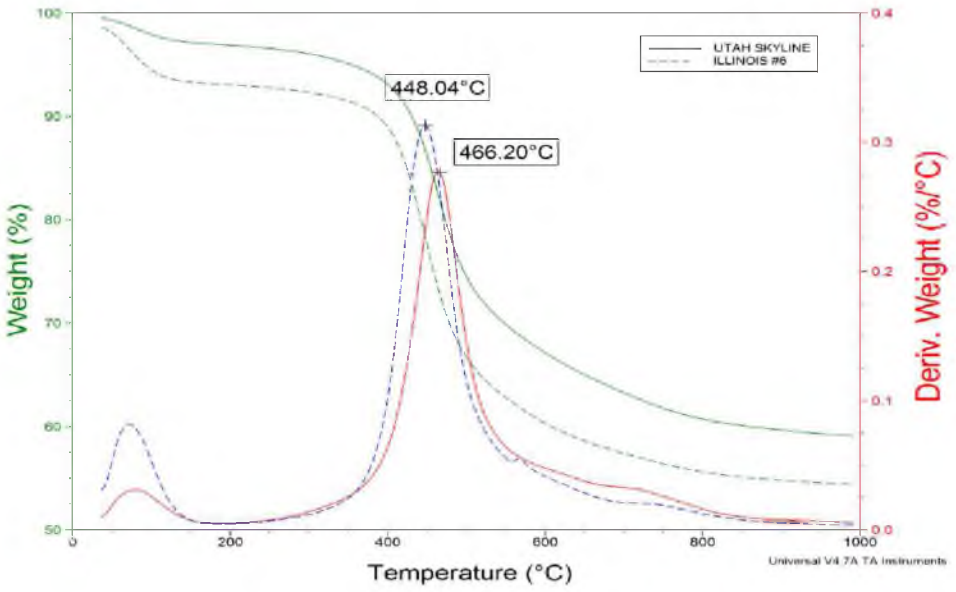

Figure 52. TGA analysis for Utah Skyline and Illinois #6 coal in Nitrogen environment

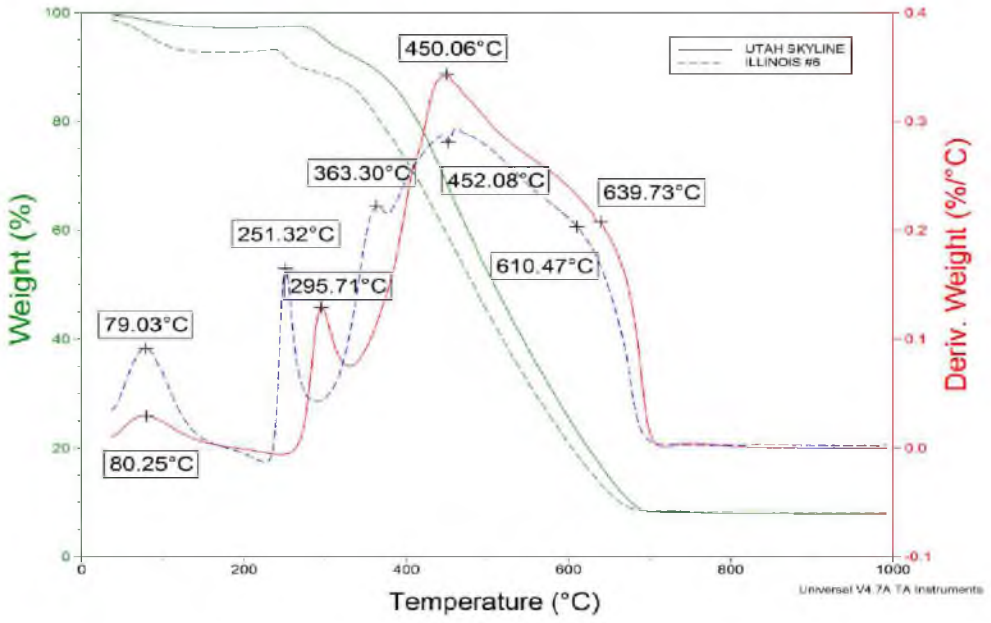

Figure 53. TGA analysis of the Utah Skyline and Illinois #6 coal in Air environment

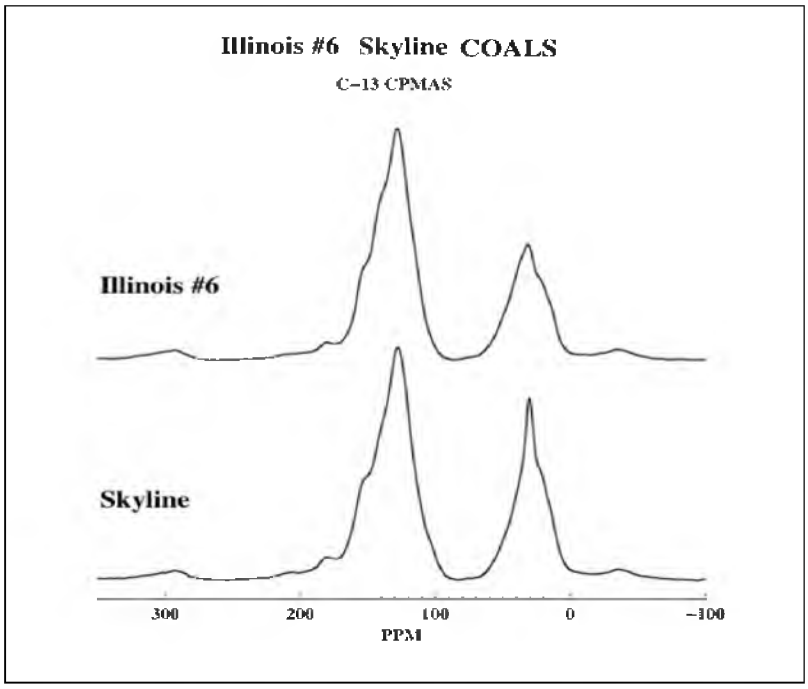

Figure 54. ^{13}C CPMAS spectra of the two coals taken with a 1 s pulse delay and a 2 ms contact time. All carbon types are seen in these spectra.

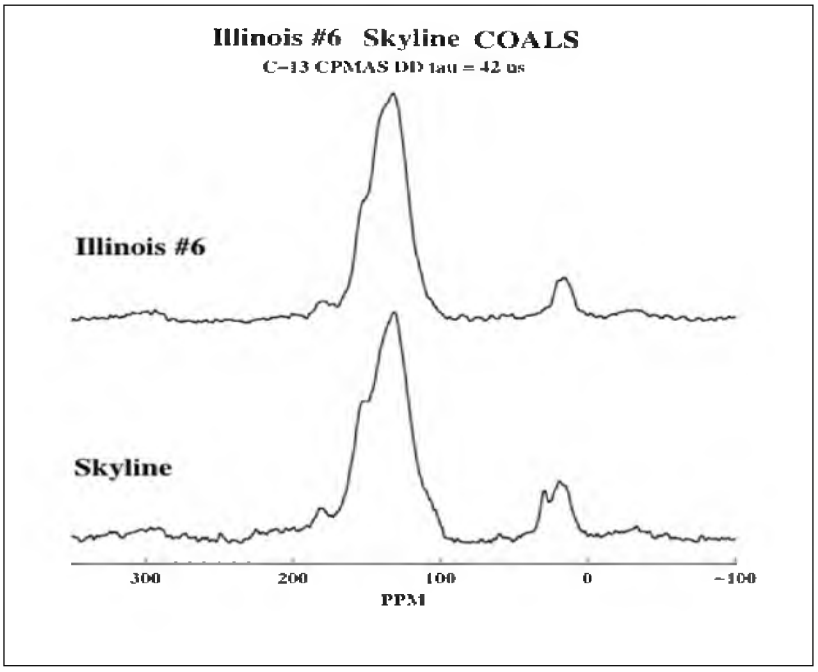

Figure 55. ^{13}C CPMAS dipolar dephased spectra of the two coals taken with a 1 s pulse delay, a 2 ms contact time, and a dipolar dephasing time of 42 μs. These spectra show nonprotonated carbons, methyl groups, and protonated carbons subject to a large degree of molecular motion.

Table 6 Constant key parameters

Constant Parameters	Quantity
Total stoichiometric ratio	1.15
Primary stream temperature	305 K
Primary stream velocity	6.3 (m/s)
Secondary stream velocity & temperature	Refer to Table 7
Wall temperature	1283 K
Overall O_2 volume fraction	40%

Table 7. Combustion aerodynamic operating conditions for both Utah Skyline and Illinois #6 coal

Exp.	Pri.[a] P_{O2} M.F.[e]	Pri. Vel.[b] m/s	Sec.[c] Vel. m/s	Sec.T[d] K	Pri. O_2 Kg/hr	Pri. CO_2 Kg/hr	Sec. O2 Kg/hr	Sec. CO_2 Kg/hr	Residence time ms
A.1	0.000	6.3	14.9	489	0.00	6.84	11.05	15.91	91
A.2	0.055	6.4	14.9	489	0.27	6.48	10.80	16.27	91
A.3	0.101	6.3	14.9	489	0.50	6.16	10.58	16.60	91
A.4	0.146	6.4	14.9	489	0.73	5.87	10.33	16.92	91
A.5	0.210	6.3	14.9	489	1.04	5.40	10.01	17.35	90
B.1	0.000	6.3	16.6	544	0.00	6.84	11.05	15.91	83
B.2	0.055	6.4	16.6	544	0.27	6.48	10.80	16.27	82
B.3	0.101	6.3	16.6	544	0.50	6.16	10.58	16.60	82
B.4	0.146	6.4	16.6	544	0.73	5.87	10.33	16.92	82
B.5	0.210	6.3	16.6	544	1.04	5.40	10.01	17.35	82
C.1	0	6.3	14.9	489	0.00	6.84	11.05	15.98	91
C.2	0	6.3	15.3	489	0.00	6.84	11.52	15.98	89
C.3	0	6.3	15.6	489	0.00	6.84	12.02	15.98	87
C.4	0	6.3	15.9	489	0.00	6.84	12.53	15.98	85
C.5	0	6.3	16.3	489	0.00	6.84	13.03	15.98	84
C.6	0	6.3	17.8	489	0.00	6.84	15.34	15.98	76
C.7	0	6.3	18.6	489	0.00	6.85	16.60	15.97	73
C.8	0	6.3	19.5	489	0.00	6.85	17.96	15.97	69

[a] Primary stream
[b] Velocity
[c] Secondary stream
[d] Temperature
[e] Mole fraction

Table 8. Coal feeding rate based on SR

Coal type	Feeding rate based on SR. (Kg/hr)	Ratio of Coal weigh/ Carrier Gas volume (Kg/m3)
Utah Skyline	4.8	1.26
Illinois # 6	5.2	1.35

Table 9. Structural and lattice parameters of coals

Structural Parameters														
Compound	f_a	f_a^c	f_a^o	f_a^{oo}	f_a	f_a^H	f_a^N	f_a^P	f_a^S	f_a^E	f_{aa}	f_{aa}^H	f_{aa}^c	f_{aa}^o
Illinois #6	0.69	0.03	0.01	0.02	0.66	0.25	0.41	0.07	0.18	0.16	0.31	0.26	0.05	0.01
Skyline	0.65	0.04	0.01	0.03	0.61	0.21	0.40	0.08	0.15	0.17	0.35	0.26	0.09	0.00

Lattice Parameters								
Compound	χ_b	C	$\sigma+1$	P_0	$B.L.$	$S.C.$	$M.W.$	M_β
Illinois #6	0.242	11.6	4.4	0.80	3.5	0.9	269	29
Skyline	0.279	13.4	5.0	0.61	3.1	1.9	329	33

Illinois#6 $C_{100}H_{93}N_{1.5}S_{2.5}O_9$

Skyline $C_{100}H_{88}N_{1.7}S_{0.5}O_{11}$

Table 10. Fuel ratio of coals

Coal type	Fuel ratio
Utah Skyline Bituminous	1.20
Illinois #6 Bituminous	1.23

6. NEAR FIELD AERODYNAMICS EFFECTS OF PURE O_2 INJECTION IN CO-AXIAL OXY-COAL TURBULENT DIFFUSION FLAMES

Dadmehr Rezaei*, Eric G. Eddings, Kerry E. Kelly, Jost O.L. Wendt

*Corresponding author.

Institute for Clean and Secure Energy, Department of Chemical Engineering, University of Utah, 155 South 1452 East, Room 350, Salt Lake City, UT, 84112, USA

6.1 Abstract

Oxy-coal combustion allows the concentration of oxygen in each burner stream to be controlled as an independent variable. Input concentrations of oxygen and the way it is injected can have significant impacts on the turbulent mixing and flame stability in coaxial turbulent jets. Whereas previous studies have quantified the effects on flame stability of partial pressure of oxygen in primary and secondary streams in coaxial oxy-coal burners, this research focuses on triple concentric coaxial oxy-coal burners, with a view to determining flame stability effects of adding as much oxygen as possible in a pure oxygen stream, located either in the middle annulus, with coal/CO_2 in the center and O_2/CO_2 in the outside, or in the center tube, surrounded by annular coal/CO_2, and O_2/CO_2 streams. Flame stability was quantified by flame probability density functions (PDF) of

the stand-off distance, which were determined using photo-imaging techniques developed in previous work. PDFs of flame length were also obtained. Experiments were conducted in a systematic way so that differences caused by stream composition changes alone could be explored, keeping velocities constant. The PDFs obtained from these simplified prototype configurations can be used for simulation validations, and also lead to physical insight into flame stabilization mechanisms. For example, flame stand-off distances for flames with pure oxygen in the center annulus are more attached than those with oxygen in the center pipe. This result is consistent with a physical picture of coal jet attachment mechanisms in which fine particles that are the key to ignition are transported radially outward by large turbulent eddies, passing through the pure oxygen stream when that is in the middle annular position, but away from the pure oxygen stream when that is at the center pipe.

6.2 Introduction

Oxy-coal combustion, in which coal is burned with oxygen rather than air with flue gas recycle to modulate flame temperatures, has the potential for producing concentrated CO_2 flue gas streams suitable for compression and sequestration. Combustion of pulverized coal in mixtures of oxygen and recycled flue gas is different from that in air, since under oxy-coal conditions, the input oxygen concentration can be varied independently. Also, oxygen need not be distributed evenly across all input streams, but can be introduced in at different concentrations in each stream. There are practical and safety advantages in adding the oxygen to as few input streams as possible, with special safety benefits accrued from having all the oxygen required in a single pure oxygen stream. Zhang [47] quantified flame stand-off distance in co-axial pulverized coal

turbulent diffusion flames as a function of partial pressure of oxygen in the primary jet. He also showed that at high enough P_{O2} in the secondary jet, it was possible to stabilize those flames with zero oxygen in the primary jet. The present paper builds on this previous work, but now focuses on the near field aerodynamic impacts of *directed pure* oxygen in a *segregated* stream. As in previous work [1], this study focuses on *interactions* between coal particle ignition and turbulent mixing in co-axial jets, rather than on ignition chemistry or turbulent mixing by themselves. The directed pure oxygen in this study is contained either

1. In an annulus located between a central coal/CO_2 circular jet and an outer O_2/CO_2 secondary oxidant stream annulus (Configuration A), or
2. In a central pipe surrounded by a coal/CO_2 middle annulus, surrounded again by an O_2/CO_2 secondary oxidant stream annulus (Configuration B).

Shaddix and Molina [4] claimed the presence of CO_2 retards single particle coal ignition. Particle devolatilization proceeds faster with higher O_2 concentration, and decreases with the use of CO_2 because of the influence of these two species on the mass diffusion of O_2 and volatiles. Qiao [10] and his colleagues proved the impact of thermal conductivity of CO_2 as another factor for the lower ignition of coal in O_2/CO_2 environments. Wall and Buhre [1], in their review, present the impact of CO_2 on coal ignition retardation as well as improvement of flame stability due to pure O_2 injection. Molina [11] found oxygen concentration decreases ignition delay in a meaning that could be used to counteract the retardant effect of CO_2. Kimura [12] showed that the flame propagation speed is much smaller in O_2/CO_2 atmosphere than in O_2/N_2 and O_2/Ar, and that in O_2/Ar was the highest. The propagation speed increases as the oxygen

concentration increases in all cases, as expected. Nozaki injected 15% to 20% of the total oxygen into the furnace directly [13]. His group at IHI found HCN formation in near burner zone increases in O_2/CO_2 with oxygen injection, and he claimed devolatilization becomes more active at high gas temperature realized near the burner by oxygen injection.

Forstall [30] studied the impact of velocity ratio on the turbulent mixing in a coaxial jet containing central and annular streams. He concluded material diffuses more rapidly than momentum and that the principle independent variable determining the shape of the mixing regime is the velocity ratio. Chigier and Beer focused on the region near the nozzle in double concentric jets. They considered two streams as two different central cores and described how two streams emerge based on their fluid entrainment due to velocity difference [31–33]. In addition, they provided plots that define the length of each stream before they emerge as a function of velocity ratio for co-axial jets. In another study, Beer [34] reported when the secondary velocity is low and the density of the secondary fluid is considerably higher than that of the recirculating fluid, more recirculation and less secondary air is entrained in the early part of the primary jet. This means coal particles will be heated faster, and it has a large effect on the stability of the flame. Durano [35] measured mean velocity of a co-axial jet for three different velocity ratios. He reported co-axial jets obtain a self-preserving state faster than single round jets. The current work builds upon these pioneering contributions on coal ignition and coaxial jet structure referenced above, but with the special focus on how *directed* pure oxygen, according to Configuration A and Configuration B above, affects flame stand-off distance and flame length.

6.3 Experimental

6.3.1 Coal Selection and Sample Preparation

The coal applied for this study was Illinois #6 Bituminous coal. The ultimate and proximate analysis of the coal as received (AR) is provided in Table 3, Table 4, and Table 5. According to particle size distribution calculation of the coal used in this experiment, maximum particle size was in the range of 150μm to 200μm, and the mass average diameter was 62μm.

6.3.2 Oxy-Coal Combustion Furnace

The Oxy-Fuel Combustor (OFC) at the University of Utah is a 100kW down-fired furnace [1] with the capability of both air and oxy-combustion with either once through CO_2 or recycled flue gas ongoing various flue gas cleaning options. For the present study only, once through, pure CO_2 from a tank was used. The OFC consists of a near field aerodynamic (burner zone) or the main chamber followed by a radiant zone located below the main chamber; burner zone dimensions are 0.61m I.D, 0.91m O.D. with 1.22m as the height. In order to reduce the heat lost, the burner zone is insulated by 76mm thick Fiberboards that tolerate high temperatures up to 1700K. In addition, twenty-four 840W electric heaters embedded in fiberboard allow us to control the wall temperature at any desired temperature up to 1111K. In this study, the wall temperature was kept at 1283K. There are K-Type thermocouples all along the furnace to monitor the temperature. In order to have an optical access to the flame regarding optical diagnostic, four quartz windows have been provided on the quadrants of the cylindrical chamber. Additional details regarding the OFC is provided elsewhere [47].

6.3.3 Methodology of Flame Stability Measurement

Flame stability measurement employed similar methods as those used in reference [47]. Stand-off distance and flame length are defined by the position of the luminous zone, as observed by the human eye, but recorded on 6000 photo images at 30fps with an exposure of 8.3ms. Each run had up to 5 replicates taken. Therefore, flame stand-off distance is defined as the distance starting from the tip of the burner to the luminous and visible part of the flame, and it is described in detail elsewhere [47].

6.3.4 Burners and Combustion Operating Conditions

In the previous studies, coaxial double annulus burners with only two streams have been used [47]. However, in this research, a pure oxygen stream was dedicated to the burner in order to investigate the effects of directed pure oxygen injection. This stream might contain a specific fraction or 100% of all the oxygen required for combustion for the combustion operating condition. The primary stream is a transport medium carrying pulverized coal particles in the chamber and for the experiments here contained only CO2, with no oxygen. Directed oxygen and transport streams were at room temperature. The secondary stream is a mixture of O2 and CO2, and plays a significant role on the combustion temperature as well as entrainment of the flame jet. Secondary stream temperature is controlled at 489K by a gas preheater. Coal feed rate, primary stream CO_2 (30% of the total CO_2 required), overall volume fraction O_2 (40%), stoichiometric ratio (1.15), and wall temperature (1283K) were all kept constant. These and other variables are shown in Table 11.

6.3.5 Experimental Methodology for Configuration A: Burners with Oxygen Stream in Middle Annular Stream

In this set, six burners were used to allow stream velocities to remain constant, as shown in Table 12. As case numbers increase, O_2 is added from the secondary stream to the pure oxygen stream while the overall O_2 is maintained constant. It is important to notice that in burner number 6, all of the oxygen required is being introduced in the pure directed oxygen stream. The primary stream (Coal + CO_2) is located in the center of the burner. The annulus around the primary stream is the directed oxygen stream, and the furthest outer annulus contains the secondary stream (see Figure 31). The velocity of the pure oxygen stream and the primary stream are kept approximately equal in order to delay mixing, leading potentially to longer flames with a more uniform heat distribution. The secondary stream velocity is 2.5 times higher than that of the other two streams, creating external recirculation in the upper chamber and maintaining jet entrainment (IFRF Type-0 flame). Multiple burners with various appropriate dimensions allowed the stream velocities to be maintained constant such that aerodynamics mixing effects were unchanged as much as possible, as shown in Table 12.

6.3.6 Experimental Methodology for Configuration B: Burners with Oxygen Stream in Centrally Located Pipe

For Configuration B, burners are also triple concentric burners but now with a pure oxygen stream that is located in the center pipe. The primary stream that carries the coal particles is located in the inner (middle) annulus, and the outer annulus is the secondary (O_2/CO_2) stream (see Figure 33). As for Configuration A, six cases cover different fractions of total oxygen in the oxygen stream located in the center from 0% to

100%. In the very last case, all the oxygen is once again in one segregated stream (now at the center). Velocity ratios of the stream are similar as for Configuration A, to minimize the aerodynamic differences as shown in Table 13.

6.4 Results

Figure 56 shows the PDF of flame stand-off distance and also that for the flame length for Configuration A with no directed oxygen in the middle annulus, and all the oxygen required for combustion mixed in with the secondary CO_2 in the outer annulus (Case 1 in Table 12). F_{O2} is the fraction of the total oxygen entering as the directed pure oxygen stream, with (1- F_{O2}) being the fraction mixed in with secondary CO_2 in the outer annulus. These data can be used to validate simulations of a limiting case with no directed oxygen injection, but with the appropriate hardware in place.

The plot on the left of Figure 56 represents the probability of the distance from the tip of the burner until the luminous part of the flame. As mentioned before in the image processing technique section, 3 to 5 replicates have been performed. Error bars represent the standard deviation of the replicates. The plot on the right shows the PDF of flame length. In this paper, the flame length is measured in number of (calibrated) pixels from the point where the luminous part of the flame starts to the point it ends. A PDF of flame length can then be created for each operating condition

Two main effects of oxygen configuration and oxygen fraction on flame stability were investigated in this study. The contribution of oxygen stream configuration to flame stability was explored by situating the oxygen stream in different locations, namely Configuration A and Configuration B. Ultimately, the effects of injection of all the oxygen in a segregated stream were studied.

Figure 56 shows the flame stability results for the both oxygen Configurations A (left) and B (right) at different fractions (F_{O2}) of the total inlet of O_2 being placed in the directed pure oxygen stream. In both configurations, placing increased amounts of the total oxygen in the directed pure oxygen stream amplifies the stability of the flame; however, this effect is considerably more significant when oxygen is located in the middle annular stream (Configuration A), rather than in the central pipe (Configuration B). For Configuration A (Left side), the stand-off distance of the flame does not change appreciably until $F_{O2} = 64\%$. At $F_{O2} = 75\%$, the first indications of a stable attached flame can be appear. The flame attachment is in a transient status at this point. However, at higher fractions of oxygen 85% and 100%, extremely stable and attached flames were generated. It is important to note that in the last condition, *all* the oxygen was located in a single stream.

The PDF plots on the right of the Figure 57 present the data for Configuration B. As with Configuration A, flame stand-off distance diminishes with increasing F_{O2} in the central oxygen stream. However, the flame never became fully attached even when $F_{O2} = 100\%$. These data show that injection of oxygen in the inner annulus creates more flame stability that when it is injected in the center of the burner.

Figure 58 shows results depicting flame length, defined by the length of the luminous zone. The PDFs on the left present the data of Configuration A and the PDFs on the right provide flame length data of the Configuration B. In both types of configurations, flame length increased as the fraction of total oxygen placed in the directed pure oxygen stream increased. This increase of flame length was more significant with burners containing directed oxygen injection in the inner annulus

(Configuration A). The red bar in the plots represents the probability of the flames that were longer than the length of the window, and they were not possible to be measured. It was found that although the stand-off distance PDFs of the cases F_{O2} = 85% and F_{O2} = 100% do not manifest a difference, the flame length PDFs show significant changes in the flame length of these two cases. By increasing oxygen fraction, the probability of the flames with a length longer than the window increased.

6.5 Discussion and Conclusions

The study was carried out to help understand the effects of directed pure oxygen and the manner in which it is injected on the length and stability of pulverized oxy-coal flames stabilized on triple concentric co-axial burners with no swirl. Two configurations of burners were used in this research: Configuration A with directed pure O_2 in a middle annulus and Configuration B with directed pure O_2 in the center pipe. In both types, an increase of F_{O2}, the fraction of total oxygen in the directed oxygen stream, increased the stability of the flame; however, it was more significant in Configuration A burners containing the pure oxygen stream in the inner annulus such that fully attached and stable flames were obtained at F_{O2} = 85% and higher. In Configuration B burners, even at F_{O2} = 100% the flame was detached and unstable.

In order to explain the mechanism of observation of flame stability in Configuration A compared to Configuration B, two hypotheses were proposed that might account for the fact that the directed oxygen in the middle annulus is more effective in attaching Type 0 oxy-coal flames than directed oxygen in the center pipe. There are two justifications for the flame behavior.

The first is concerned with coal particle dispersion effects on flame stability.

Budilarto [40] used Laser Doppler Velocimetry to show that smaller particles migrated to the edges of co-axial two-phase turbulent jets. Preliminary high-performance computer simulations [39] using Large Eddy Simulation (LES) suggest that coal particle ignition occurs at clusters of small particles, many of which have been transported by large eddies radially outwards. The experimental results of Zhang et al. [48] suggest that coal jet ignition in coaxial oxy-coal flames similar to those investigated here is determined by a mechanism through which large eddies project clusters of particles and their surrounding fluid radially outwards. The new results on flame attachment for the two configurations are consistent with these mechanisms. With directed oxygen in an annulus surrounding the coal jet (Configuration A), (smaller) coal particles migrate from the center *towards and through* the pure oxygen stream, thus providing a suitable environment for early ignition and flame attachment. With directed oxygen in the center (Configuration B), the (smaller) coal particles are now directed *away* from the high oxygen concentration regions, thus delaying ignition and consequent flame attachment. Crowe et al. recommended that the evaluation of Stokes Number [37] in turbulent two phase jets be:

$$St = \frac{\tau_p}{\tau_f} \tag{2}$$

Stokes number (St) is a dimensionless number corresponding to the behavior of particles suspended in a flow field. If the value of St < 1, the particles will respond to the fluctuation of the turbulence and they will follow the eddies. However, if the St > 1, the particles will not respond to the turbulence fluctuations and they will penetrate through turbulent eddies due to their own inertia. τ_p is particle aerodynamics response time, which is a measure of responsiveness of a particle to a change in fluid velocity. This number is

defined as:

$$\tau_p = \frac{\rho_p d_p^2}{18\mu_f} \tag{3}$$

where $d_p$is the coal particle diameter, μ_f is the viscosity of the fluid, and ρ_p is the solid density of the coal particle. The solid density of Illinois #6 is reported to be about 1450 (kg/m^3) [64]. Viscosity of the fluid (CO_2) at the nozzle is calculated to be 1.48×10^{-6}. τ_f is a measure of the time available for the interaction between the fluid and particle [37,38,65,66]. According to previous research [67,68], the value of τ_f can be calculated using the average velocity of the jet in the axial direction:

$$\tau_f = \left|\frac{d\bar{u}_f}{dx_1}\right|^{-1} \tag{4}$$

Kennedy et al. measured the mean velocity of the jet in the axial direction using hot wire anemometry. The derivative of the mean velocity with respect to the axial direction value gave the values of τ_f for different locations. They found this scale is the smallest near the nozzle exit, and it increases monotonically as the jet develops ($L/D \geq 40$). Therefore, if one can find a value of particle diameter that follows the flow at the nozzle exit, it can be proven that all the particles with that certain size will follow the streamlines of the jet anywhere downstream of the jet. Additionally, in this study, it was our goal to investigate the diffusion direction of the coal particles in the near burner zone. Therefore, to find the critical particle size, the Stokes numbers of all the coal particles with different sizes were calculated at the nozzle exit (see Figure 59). Assuming an upper bound for the turbulent eddy velocity to be of order *u* (jet exist velocity), leads to a value of τ_f that is given by:

$$\tau_f = \frac{L}{u} \tag{5}$$

where u is the upper bound of a turbulent eddy velocity and L is the characteristic size of the largest eddies and is given by the inner diameter of the primary stream.

As shown in Figure 59, the critical particle size for the system in this study was calculated to be 66μm. Therefore, according to our model, particles smaller than 66μm will follow the flow streamlines and the particles larger than 66 μm will not follow the flow and will drop down due to gravity. More information regarding the coal particle size distribution of Illinois #6 applied in this study is provided in Figure 60.

The second hypothesis to explain why Configuration A was more stable than Configuration B is related to heat transfer effects on coal ignition and is related to shielding of wall radiation to the oxygen/coal free shear layer interface by the coal stream in Configuration B.

6.6 Acknowledgments

This material is based upon work supported by the Department of Energy under award number DE-NT0005015. Assistance in running the experiment and preparing the data were provided by David Wagner, Ryan Okerlund, Taylor Geisler, Charles German, Michael Newton, and Travis LeGrande.

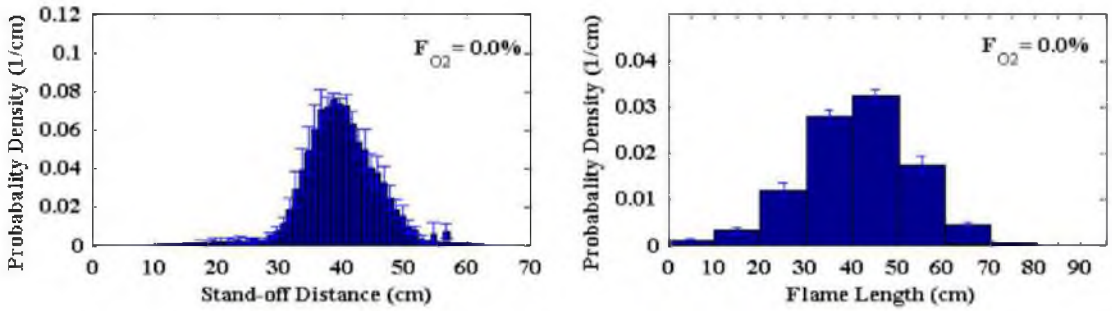

Figure 56. Stand-off distance and length of the flame for zero oxygen in the directed O_2 stream for Configuration A, Case 1, Table 12

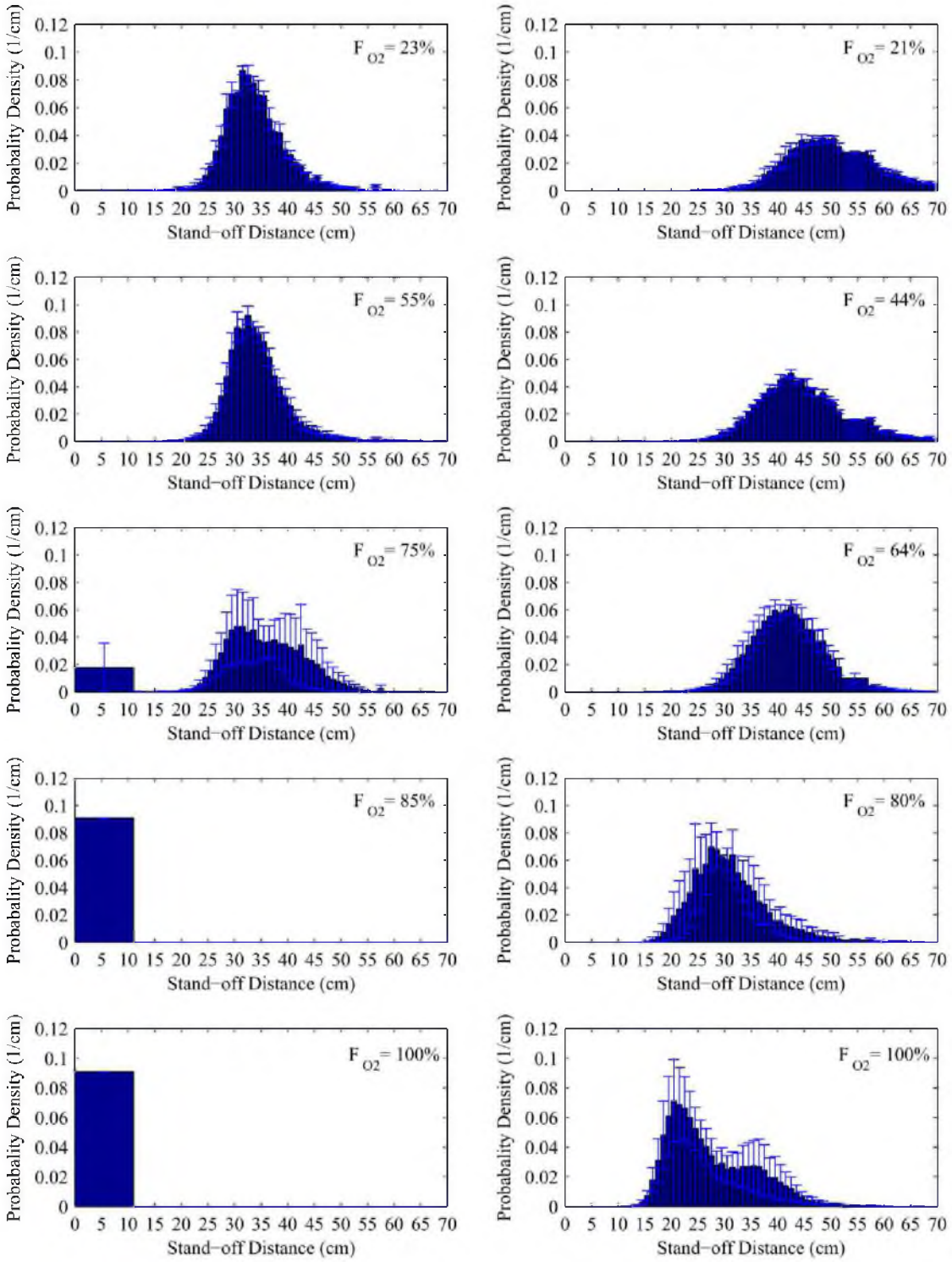

Figure 57. Flame stand-off distance PDFs. Left: Configuration A, Right: Configuration B

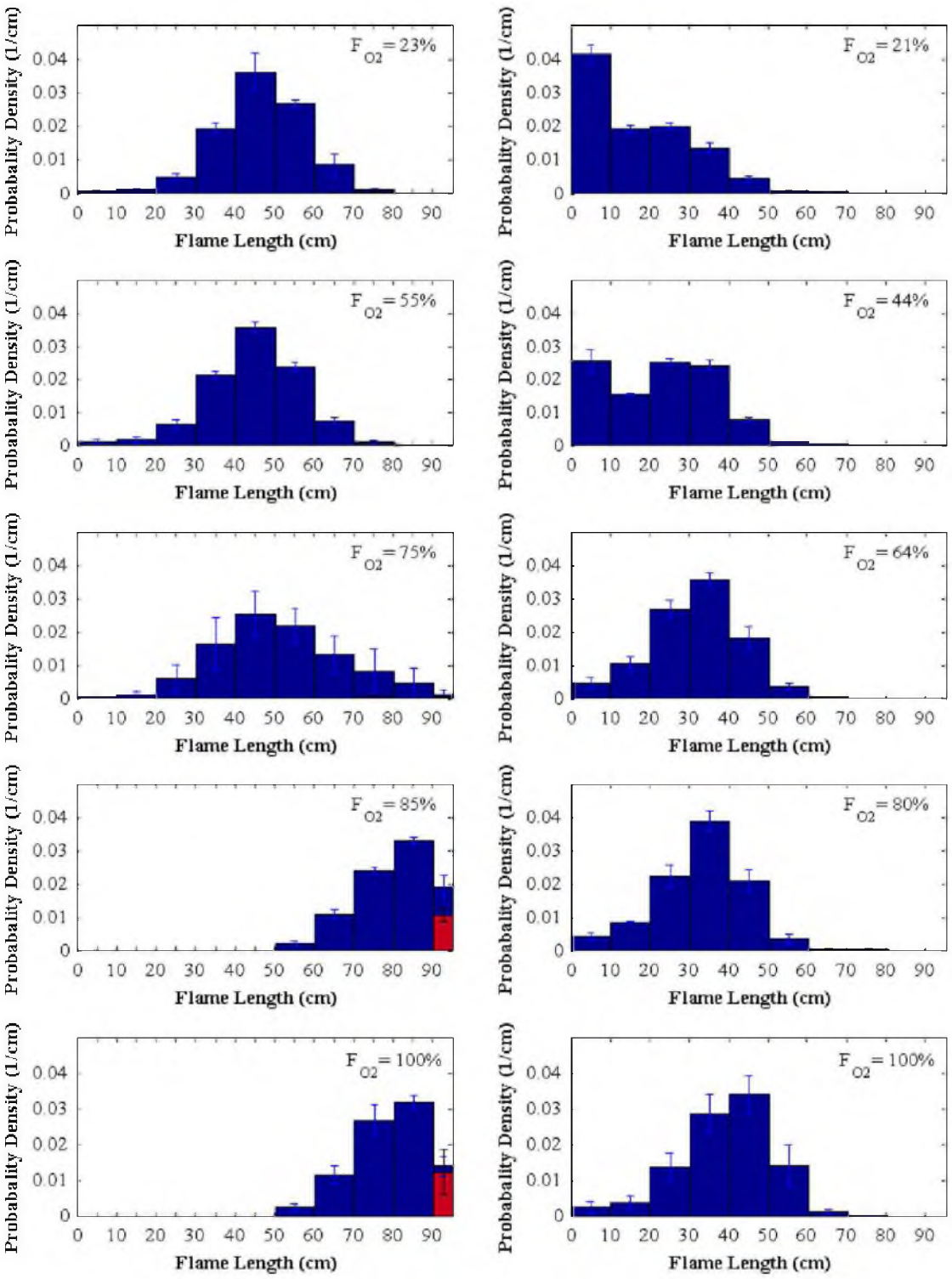

Figure 58. Flame length PDFs. Left: Configuration A, Right: Configuration B

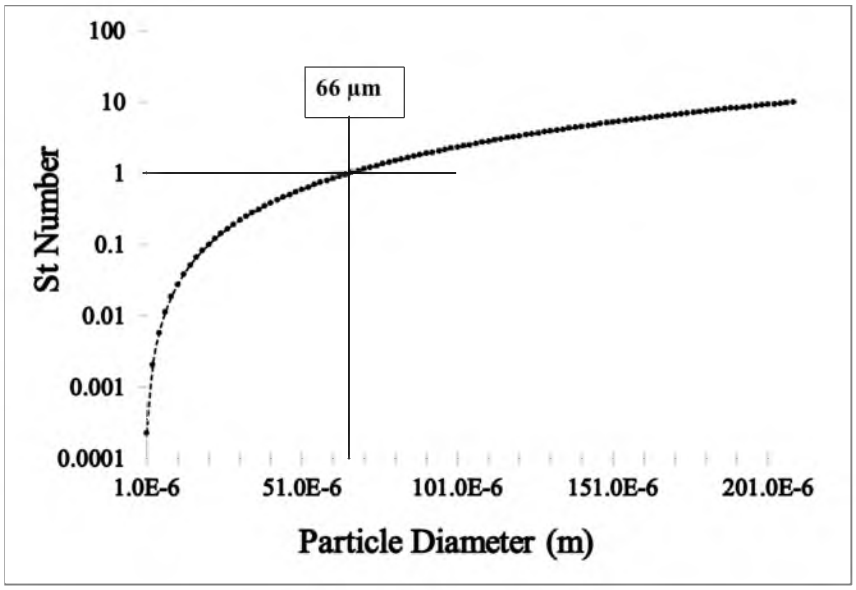

Figure 59. Stokes number vs. particle diameter at nozzle exit

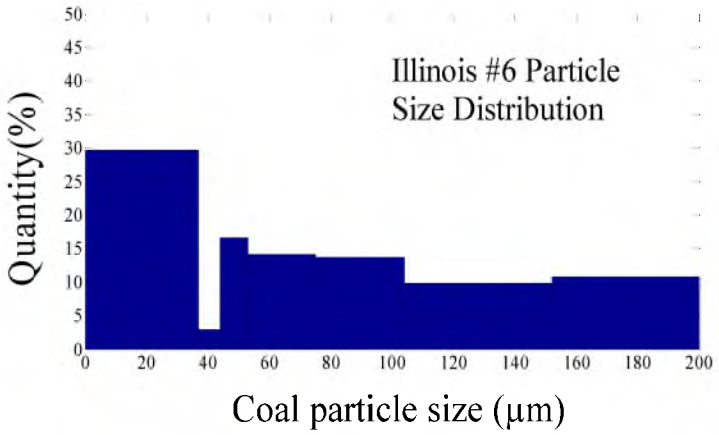

Figure 60. Illinois #6 coal particle distribution

Table 11. Constant parameter of combustion operating conditions

Parameter	Quantity
Total S.R.	1.15
Pri. Stream Vel.	305 K
Pri. Stream Temp.	6.3 (m/s)
O2 Stream Vel.	305 K
O2 Stream Temp.	6.3 ± 0.3 (m/s)
Sec. Stream Vel.	15.4 ± 1.4 (m/s)
Sec. Stream Vel.	489 K
Wall Temp.	1283 K
Overall O2 V.F.	40%
Flame Tadb	2485.5 K

Vel., Velocity
Temp., Temperature
V.F., Volume Fraction
Tadb., Adiabatic Temperature

Table 12. Flame aerodynamic conditions for burners with inner annular oxygen stream (Configuration A)

Case	F_{O2} inner O_2 annulus	Prim. Vel. (m/s)	O_2 stream Vel. (m/s)	Second. Vel. (m/s)	Prim. A_S (cm^2)	O_2 Stream A_S (cm^2)	Second. A_S (cm^2)
1	0.0%	6.37	0.0	14.9	1.9604		6.0744
2	23.0%	6.37	6.10	15.8	1.9604	1.0653	5.0665
3	55.0%	6.34	6.40	15.8	1.9604	2.3788	3.9442
4	75.0%	6.38	6.10	14.6	1.9478	3.2475	3.9515
5	85.0%	6.38	6.70	14.6	1.9478	3.5059	3.6361
6	100.0%	6.38	6.50	15.0	1.9478	4.2651	3.0994

Table 13. Flame aerodynamic conditions for burners with central oxygen stream (Configuration B)

Case	F_{O2} center O_2 stream	Prim. Vel. (m/s)	O_2 stream Vel. (m/s)	Second. Vel. (m/s)	Prim. A_S (cm^2)	O_2 Stream A_S (cm^2)	Second. A_S (cm^2)
1	0.0%	6.37	0.0	14.9	1.9604		6.0744
2	21.0%	6.40	6.28	16.43	1.9801	0.9066	4.9498
3	44.0%	6.32	6.22	16.27	2.0005	1.9604	4.3723
4	64.0%	6.00	6.26	15.8	1.9883	2.9267	3.9442
5	80.0%	6.26	6.27	16.21	1.9883	3.5244	3.4077
6	100.0%	6.30	6.26	16.17	1.9883	4.3825	2.8689

7. ADDENDUM TO CHAPTER 6

7.1 Flame Radiant Heat Flux

In order to study radiant heat transfer in a system with pure oxygen injection, three wide angle (WA) radiometers were employed. These radiometers were built at the University of Utah with the assistance of Praxair. The details of the mechanism of these radiometers are provided in the experimental section. These radiometers were calibrated using a blackbody radiator at different temperatures. The temperatures were close to the furnace temperature to simulate the environment of the furnace. The positions of these WA radiometers are shown in Figure 61 and Figure 62. These radiometers detect all the radiation from both the wall and flame. It is important to note that wall temperature was maintained constant in all the cases, and what is observed is due to the changes in the radiation of the flame. The peak of radiation depends on where the peak of soot radiation is located. These regions can be obtained from the images. The region that has the highest amount of luminosity creates the highest amount of radiation, considering the fact that the region has the highest temperature. The increase of the temperature due to complete combustion in regions of the flame can increase the radiation of both the soot and gaseous products of the combustion, mainly CO_2 and H_2O. Four conditions of each configuration were chosen to investigate the change in the radiant heat flux of the flame. In order to compare the results for Configurations A and B, the F_{O2} for both

configurations were chosen to be nearly identical. For the experimental design limitation (maintaining the velocities) and the restrictions of material, the oxygen fractions are not exactly the same. However, these values are chosen similar enough such that the results are comparable. Radiant heat flux for four cases: F_{O2}=0.0%, F_{O2}=23%, F_{O2}=75%, and F_{O2}=100% were measured in three locations of the flame zone of the OFC.

As shown in Figure 63, by increasing the amount of F_{O2} in the pure oxygen injection, the radiant heat flux was raised. In the same manner, four cases from the Configuration B burners were chosen. The oxygen fractions of these cases are the following: F_{O2}=0.0%, F_{O2}=21%, F_{O2}=64%, and F_{O2}=100%. The results of this test are provided in Figure 64. The radiant heat flux shows a growth trend by increasing the amount of FO2 in the pure oxygen stream. However, all of the heat flux lines in Configuration B have smaller values compared to their similar case in Configuration A. As it was discussed, due to the orientation and configuration of the streams in Configuration A, a more complete combustion occurs. Therefore, the flame temperature and consequently the radiation of the flame increased, resulting in higher heat flux in Configuration A.

7.2 NOx Formation

In addition, NO_x formation in both Configuration A and B were measured. Different oxygen fractions in the oxygen stream resulted in different NO_x emissions. Wendt and Pershing [69,70] investigated the effects of flame stability on NO_x formation for Type 0 coaxial turbulent diffusion flames in O_2/N_2 environment. For high volatile bituminous coals, when the flame was attached, NO formation was much less than when

the flame was detached from the burner. When the coal flame is attached, the nitrogen of the volatile matter is released in the near burner zone of the jet where there is an insufficient amount of oxygen to generate NO due to its consumption for the combustion process. However, in a detached flame, the nitrogen of coal volatile is released after mixing has occurred. The nitrogen species in this case have a direct contact with oxygen, leading to higher NO_x formation. In addition, they showed that the conversion of char nitrogen to NO_x is independent of the near field aerodynamics; the char nitrogen conversion occurs slowly along the furnace for both attached and detached flames. In addition, low NO_x operations require the ignition zone to be very oxidant lean, but still enough to permit devolatilization of coal volatiles. Increasing the injected oxygen in the burner zone next to coal particles increases the oxidation of nitrogen, leading to an increase of NO_x. The same scenario can be implemented in a O_2/CO_2 environment. Figure 65 shows the increase of NO_x formation versus the total fraction of oxygen in the central oxygen stream. The amount of NO_x grows as the amount of oxygen increases in the pure oxygen stream with Configuration B.

As shown in Figure 56 the stand-off distance of the flames with Configuration B shortens as the oxygen fraction increases in the pure oxygen streams; however, it is important to note that the flame never becomes attached. In this system, adding the oxygen to a stream near the primary stream creates an oxidant rich environment that results in high NO_x formation. In Configuration A, although the concentration of oxygen causes an oxidant rich environment in the near burner zone, the flame becomes stable, lowering the NO_x formation.

In this system, there is competition between the negative effects of oxygen increase in the near burner zone and the attachment of the flame. As shown in Figure 66, NO_x emission decreases with a small slope compared to Configuration B. However, when the flame becomes stable, the NO_x formation reduces such that it becomes the governing factor in reduction of NO_x compared to oxygen-rich zone effects.

7.3 Additional Information on the Second Hypothesis

The second hypothesis to explain why Configuration A was more stable than Configuration B is related to radiant heat transfer effects. It has been proven in previous studies that the effect of wall temperature on coal ignition is very important [47,49]. As shown in Figure 67, a portion of coal particles are facing the wall, and the other portion of the coal particles are moving along the reaction layer where oxygen is located. The coal particles can be assumed as a blackbody that can absorb radiant heat from the wall.

The existence of oxygen makes the ignition process occur faster to an appreciable extent. However, as the model shows in Figure 67, not only are the portion of the particles that are receiving the radiation of the wall not exposed to oxygen in the near burner zone, but also they are shielding the heat to be transferred to the particles that are moving along the oxidant zone. In Configuration A, the particles are located in the center of the jet, and the oxygen stream flows along the outer side of the particles. This configuration causes the coal particles to be exposed to both heat and oxygen. Therefore, the flame in Configuration A was stable compared to that of Configuration B.

7.4 Sample Images of Flame from Configurations A and B Burners

Figure 68 provides samples of the images taken for image analysis. These images exhibit how the flame stability or coal ignition is a function of the fraction of oxygen in the pure oxygen stream. In addition, the images show how the luminosity intensity of the flame image increases from the flame with FO2 = 100% compared to FO2 = 21%. As previously discussed, the luminosity of the flame is caused by the radiation of hot soot particles. Emissivity of coal particles can be assumed to be the emissivity of a blackbody. A complete combustion in near burner zone creates a flame with a higher temperature. Therefore, the flame luminosity from flames with higher temperatures is more intense. Figure 70 contains sample images of the flames from both Configuration A and B. Both of these flames have FO2 = 100%. The flame with Configuration A shows a very stable and long flame; however, the flame with Configuration B never became attached. In addition, the length of the flames in Configuration B was short.

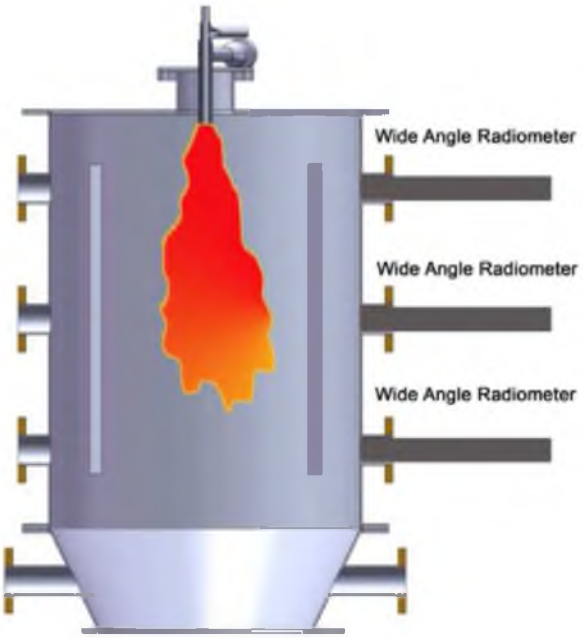

Figure 61. Positions of wide angle radiometers

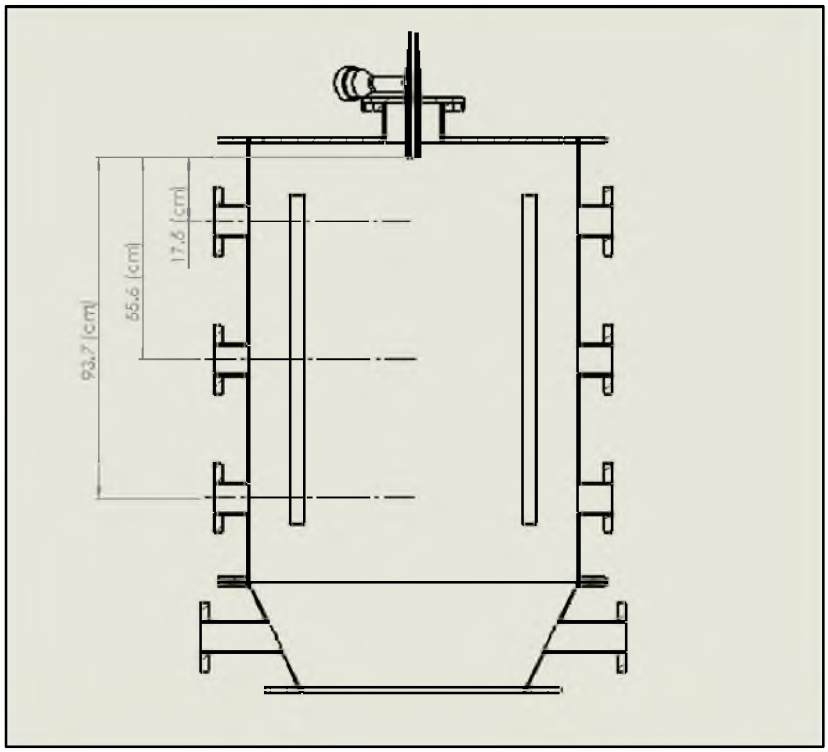

Figure 62. Distance from burner tip to wide angle radiometers

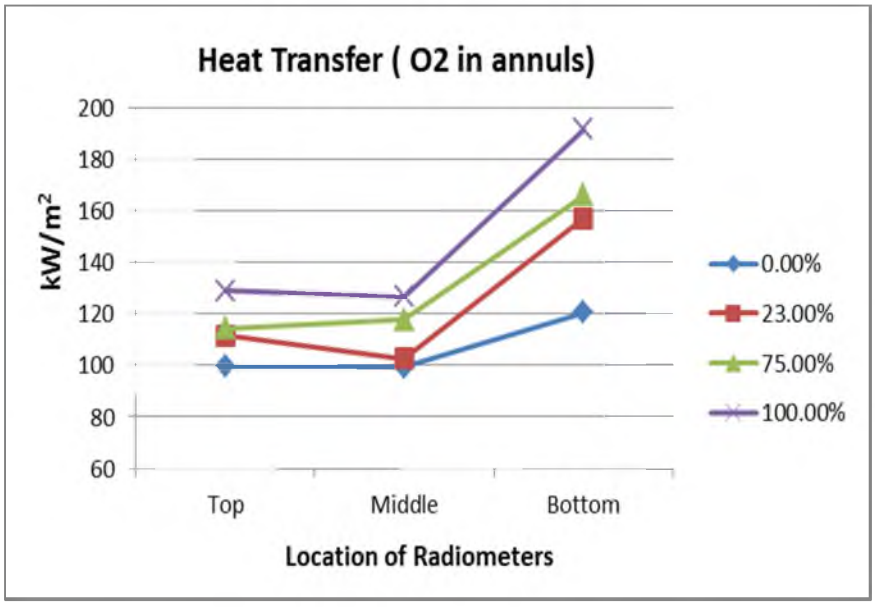

Figure 63. Radiant heat flux from flames with directed pure oxygen injection (Configuration A)

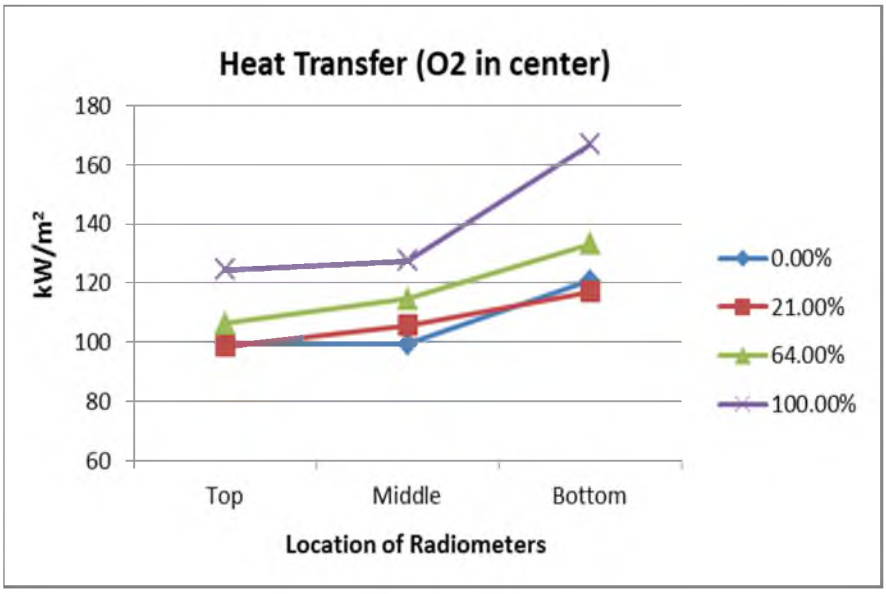

Figure 64. Radiant heat flux from flames with directed pure oxygen injection (Configuration B)

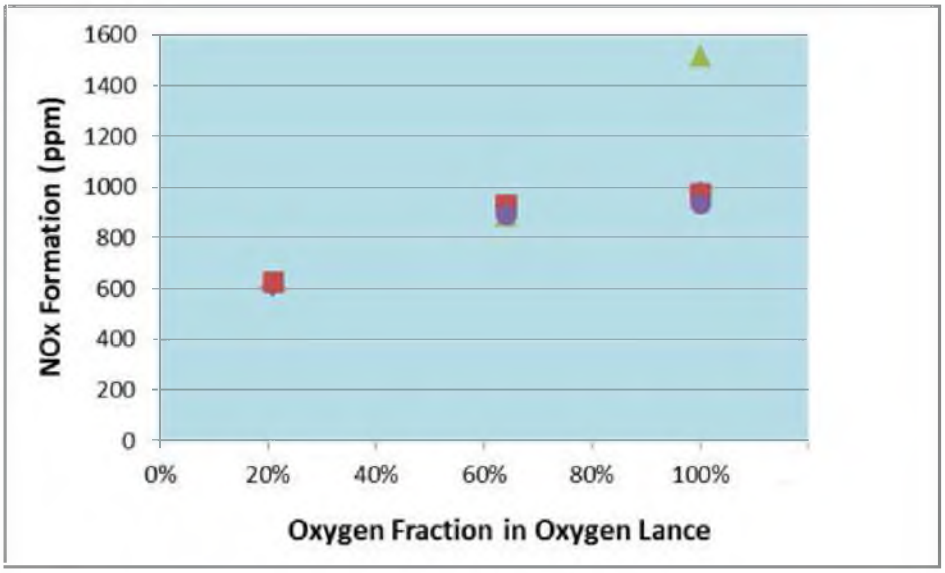

Figure 65. NOx formation vs. F_{O2} in center oxygen stream

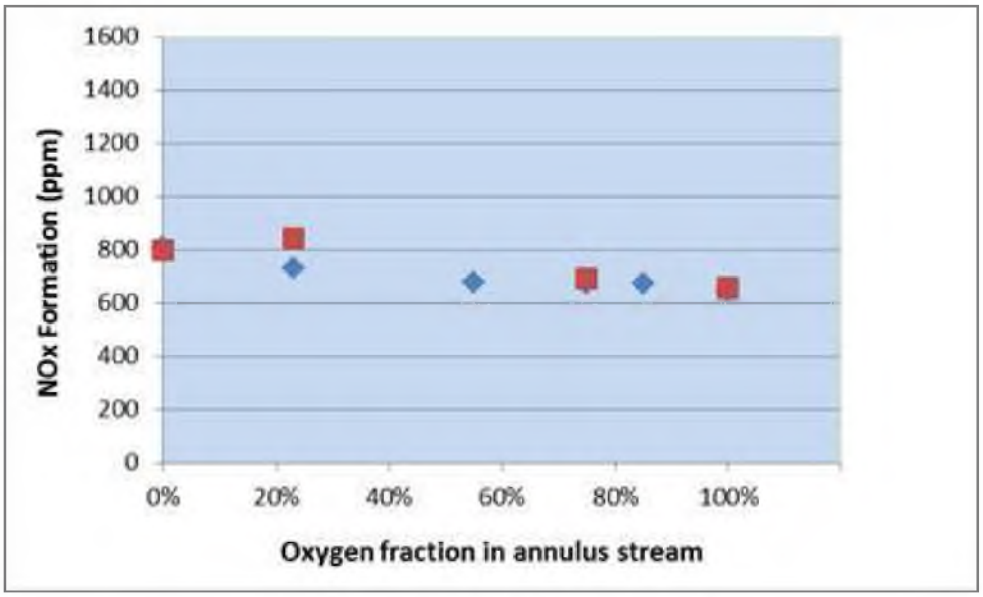

Figure 66. NOx formation vs. F_{O2} in annulus oxygen stream

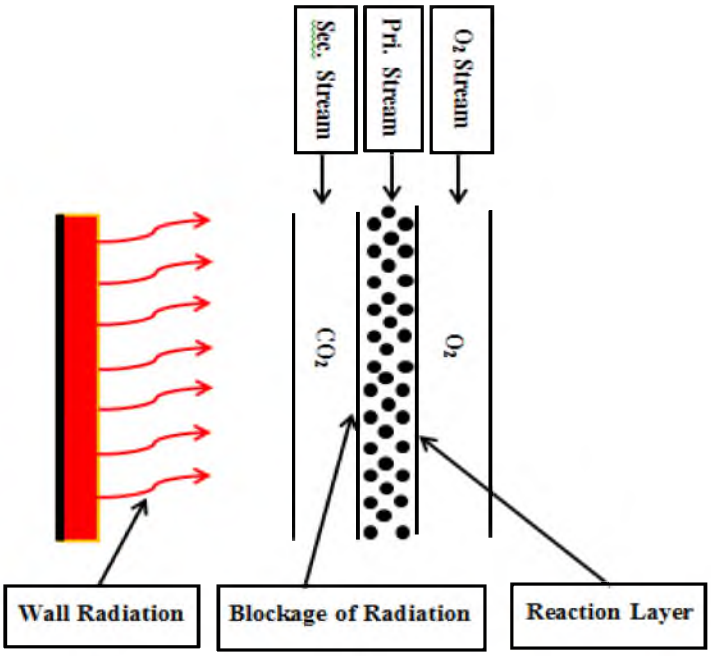

Figure 67. Radiant heat transfer mechanism to coal particles in configuration B.

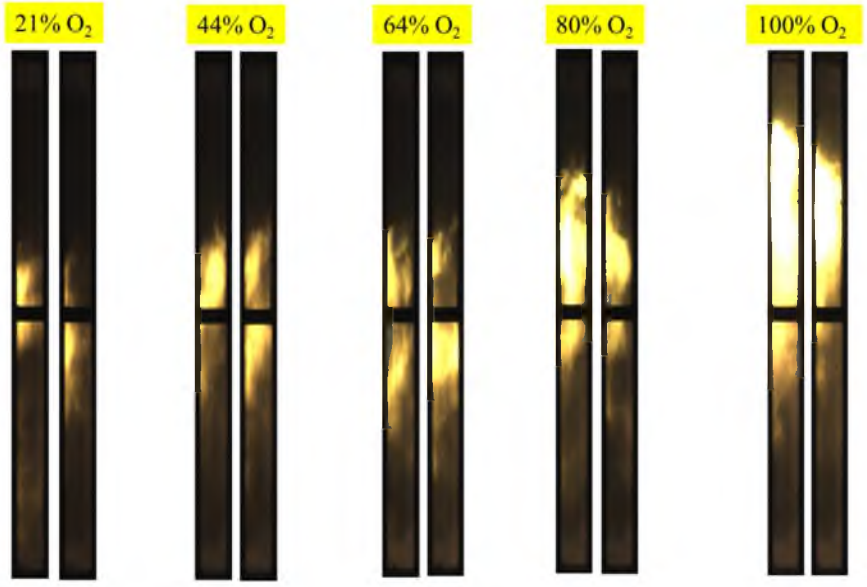

Figure 68. Flame images and change of stand-off distance as a function of F_{O2}: Configuration B

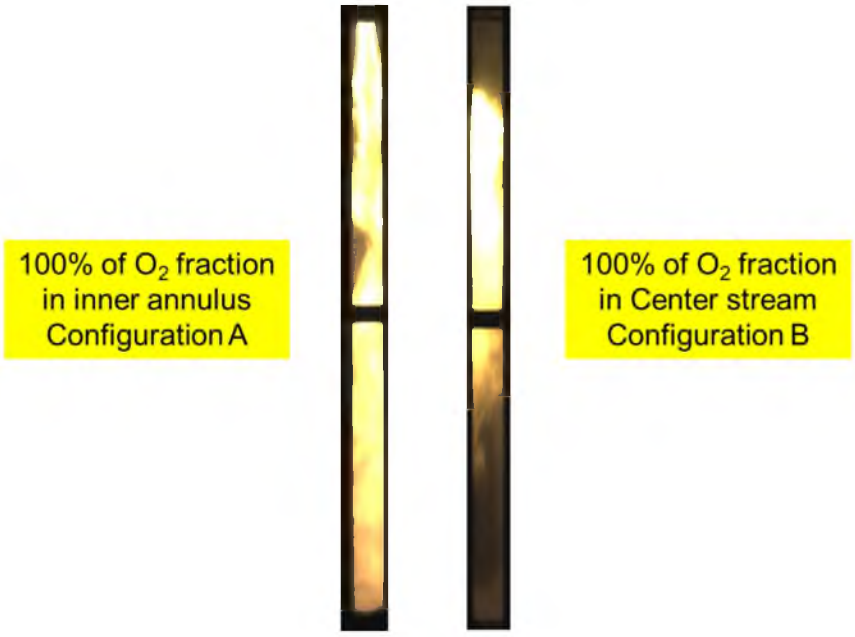

Figure 69. Comparison of effects of pure O_2 stream location on flame stability

8. MINIMIZATION OF CO2 IN OXY-COAL COMBUSTION WITH PURE O2 INJECTION IN CO-AXIAL TURBULENT DIFFUSION FLAMES

8.1 Introduction

The first generations of oxy-coal power plants are believed to be operated in a manner such that the same flame temperature and heat of combustion can be obtained [71]. However, the development of oxy-coal combustion techniques nowadays not only exceeded this level, but also much effort has been put into this research in order to enhance the efficiency of oxy-coal combustion. Smart et al. reported that a similar adiabatic combustion temperature to the conventional air-firing is obtained at a flue gas recycle ratio of 69% [26]. This value depends on the coal composition; however, the range is from 68% to 72%. In addition, Andersson et al. at Chalmers University conducted an oxy-coal combustion with 29% oxygen in a 100 kW oxy-combustor, and matched lignite-fired air and oxy-flame temperatures [28,72]. The increase of the partial pressures of CO_2 and H_2O in oxy-fuel combustion compared to air combustion leads to higher emissivity of the gaseous products of combustion. In oxy-combustion, the most dominant gaseous products are CO_2 and H_2O. Both of these two gases are radiates to an appreciable extent. N_2 for its nonpolar symmetrical molecular structure is almost a transparent gas and does not have an effect on combustion gas emissivity. Wall et al. showed that in air combustion soot alone can contribute 90 % of the radiation in the

visible range and 60% of the radiation in the total range of wavelength [73]. Andersson and his colleagues investigated the differences in total emissivity of combustion products (including soot) and emissivity of gas in oxy-coal combustion compared to air combustion. They reported that particle radiation has a significant impact on the radiation of flame, and the amount of radiation is not considerably different for air combustion. Estimations in their research showed that the overlapping of the emissivities of soot and gas reduced the total emissivity nearly 20% in air combustion and 25% in oxy-combustion. Additionally, they calculated that the gas radiation would contribute about 35-40% of the radiation on the combustor wall and in air combustion, this number reduces to 30%. Wall and Khare predicted oxygen concentration at the burner inlet to range from 25% dry recycle and 38% wet recycle to achieve similar predicted furnace heat transfer as the air case. Also, coal properties such as its heating value and ash had significant impacts on the heat transfer of the furnace. They reported that the total combination of higher concentration of gaseous products of oxy-combustion and soot (function of coal composition) changes the radiative properties of the gas mixture and ultimately heat transfer of the furnace [74].

In the previous study, the effects of the configuration of a pure oxygen stream and the consequences of injecting all the oxygen in one pure oxygen stream were investigated. As explained, by increasing the oxygen in the pure oxygen stream, the stability of the flame improved. These effects were more significant when the oxygen stream was located in the inner annuls. In addition, the data from the radiometers showed that the burner with Configuration A carrying all the oxygen generates the highest amount of radiation.

This study is the continuation of previous work, but now focuses on the effects of the reduction of CO_2 as much as possible on the heat of radiation in a 100 kW pilot-scale oxy-coal combustor using burners with *directed pure* oxygen in a *segregated* stream. It is important to note that in this study, the RFG is not recycled, and CO_2 is supplied from a tank. Reduction of the amount of CO_2 in the OFC resembles the reduction of RFG recycle ratio in oxy-coal combustors. This study explores how changes in the composition and temperature of gaseous products of combustion due to different recycle ratio can have impacts on the total emissivity of gas and ultimately the radiation heat of oxy-furnaces. The directed oxygen stream contains all the required oxygen and is located in an inner annulus between primary and secondary streams. The coal carrier in this study is pure CO_2 and it is located in the primary stream. The CO_2 in the primary stream is kept constant. The secondary stream is a stream located in the outer annulus of the burners that contains pure CO_2. The secondary stream plays the role of recycled flue gas stream in this system, and CO_2 gradually becomes reduced in each step of the experiment. Three wide angle radiometers were employed in three different locations along the flame zone of the OFC to measure the radiation heat from the flame and furnace wall. In parallel with the radiation heat measurements, three thermocouples were installed in the furnace to measure the gas temperature. The change in total gas emissivity was investigated, and a radiation model was applied to relate the heat of radiation and the average gas temperature.

8.2 Coal Selection and Sample Preparation

The coal applied for this study was Illinois #6 Bituminous coal. The ultimate, proximate, and ash analysis of the coals are provided Table 3 and Table 4. The particle size distribution has been calculated and is summarized in Figure 36. According to data shown in Figure 36, we calculated the mass averaged particle size diameter to be 68.5 μm for the Illinois #6 coal particles. According to particle size distribution plot of the coal used in this experiment, the maximum particle size was in the range of 150μm to 200μm.

8.3 Burners and Combustion Operating Conditions

The purpose of this research was to investigate the effects of a reduction of CO_2, or ratio of recycled flue gas. Ultimately, this study can be extended to another generation of oxy-fuel combustion with which fuel can be burned in a combustor without RFG. In this level of oxy-fuel combustion, pure oxygen will be injected into the system. Therefore, in this research, all the burners contain a directed oxygen stream that carries all the required oxygen into the furnace. The primary stream is a transport medium carrying pulverized coal into the chamber and for the experiments here contained only CO_2. As discussed before, the amount of CO_2 in the primary stream is maintained constant and only CO_2 in the secondary gradually becomes reduced. Combustion and burner operating conditions are provided in Table 14 and Table 15. Multiple burners allowed primary stream, oxygen stream, and secondary stream velocities to be kept constant as much as possible, in order to minimize aerodynamic changes, as oxygen distribution was varied. In this manner, the residence time is constant as well. In addition, it was decided to keep the velocity of the primary and oxygen streams as similar as possible. A large velocity ratio of these two streams will create a large mixing. However,

a slow mixing will cause all the combustion reactions to not happen in a short period of time; therefore, the chance for the creation of a longer flame becomes higher. All of the streams, primary, secondary, and directed pure oxygen, were injected at nearly room temperature (20° C to 30° C). As shown in Table 14, the overall feed gas CO_2 concentration in this test decreased from 60% (OF 40) to 41.5% (OF 60). These cases resemble an oxy-fuel combustion process when the recycle ratio decreases from 67% to 49%. Based on the limitation of the system (aerodynamic limitation of the burners), the amount of CO_2 injected to the furnace was minimized to 41.5%. The amount of CO_2 in the primary stream was chosen to be 15.1 (lb/s) in order to be able to carry the coal.

Therefore, this amount had to be kept constant in all the cases. As shown in Table 14, the very last case contains only 8.8 (lb/s) of CO_2, and the next imaginary case would result in a burner without a secondary stream, leading to flames affected by the jet aerodynamics that could have different radiation behaviors. Thus, the experiments were limited to the addressed cases. The gas temperature in the top section of the furnace was measured and monitored using K-Type thermocouples located at three different locations of the furnace. The locations and the distances of these thermocouples from the burner are provided in Table 16 and Figure 70.

In addition, K-Type thermocouples were embedded in the combustor wall to measure the wall temperatures. The thermocouples were installed at the same level as the ports, so that they have the same distance from the burner.

Flue gas composition data consisting of O_2, CO_2, and CO concentration were measured by a gas suction probe located in the end of the convective section of the furnace. The flue gas compositions are measured simultaneously by two analyzers for

higher reliability of the results. The line that carries the gas from the suction probe to the analyzers consists of two condensation sections to remove the water from the flue gas. In addition, using three filters, all the particulate will be filtered from the gas to be fed into the analyzers.

The radiation intensity measurements were performed using three wide angle radiometers. The locations of these probes were at the same level of the gas thermocouples. The distances of these probes from the tips of the burners are provided in Figure 70.

8.4 Radiation Calculation in Oxy-Fuel Combustion

8.4.1 Radiation Calculation Method

The purpose of this method is to correlate the radiometer data to the average gas temperature. Additionally, the effect of the recycle ratio on the value of gas and soot emissivity can be evaluated. Schmidt suggested a model of calculating the total emissivity of a flame on the basis of three radiation intensity measurements using the total radiation viewed by a radiometer [51]. The total radiation received by the radiometer is the summation of following intensities:

1- E1 = Radiation intensity of the flame alone at T_g

2- E2 = Radiation intensity measured by viewing a *hot blackbody* at the temperature T_w through the flame (what is being viewed by a radiometer)

3- E3 = Radiation intensity due to the blackbody calculated from its temperature (Radiation of the wall that can be transmitted into gas along the given distance L)

Considering that the transmissivity of the gas is τ and the emissivity of the gas is ε, one

can calculate the total received radiation. It is assumed that the gas is not reflecting and the furnace wall is a blackbody.

$$\tau_g + \epsilon_g = 1 \tag{6}$$

$$E_2 = E_1 + \tau_g E_3 \tag{7}$$

$$E_2 = \epsilon_g \sigma T_g^4 + (1 - \epsilon_g)\sigma T_w^4 \tag{8}$$

where T_g is the gas temperature. This result can be derived in a more precise way, using the total radiation heat balance that reaches the probe [29,51,75]. At constant temperature and wall emissivity, the amount of radiant energy received by the radiometer at a certain specified wavelength is defined as

$$dE_{T\lambda} = \epsilon_{g\lambda}\, E_{\lambda T_g} d\lambda + \tau_{g\lambda}\, \epsilon_w E_{\lambda T_w} d\lambda + (1 - \epsilon_w)\tau_{g\lambda}\epsilon_{g\lambda} E_{\lambda T_g} d\lambda \tag{9}$$

where E_T is the total energy at wavelength λ. The first term represents the amount of radiation received from the average gas temperature at a certain wavelength. The second term is the amount of radiation from the hot refractory wall. However, some of this radiation is being absorbed by the gas, and only a portion of the radiation that is transmitted through the gas has been considered in the equation. The third term represents the radiation of the gas to the furnace wall that is reflected back in the furnace and then received by the probe. It is important to note here that this method is reliable only based on the assumption that the temperature and concentration of the hot gas in the furnace, being in the view of the radiometer, is averaged. By integrating the equation over the range of wavelengths, the amount of total energy received by the radiometer can be derived to be:

$$E_T = \int_0^\infty \epsilon_{g\lambda} E_{\lambda T_g} d\lambda + \epsilon_w \int_0^\infty \tau_{g\lambda} E_{\lambda T_w} d\lambda + (1-\epsilon_w) \int_0^\infty \tau_{g\lambda} \epsilon_{g\lambda} E_{\lambda T_g} d\lambda \quad (10)$$

In the top section of the OFC where the dominant energy is radiant energy and the convective energy is negligible, with the assumption of an insulated furnace, one can prove that the apparent emissivity of the furnace wall is equal to one. If E is the total outgoing energy or heat flux of an insulated furnace, one can write the heat balance equation as:

$$E = \epsilon_w \sigma T_w^4 + \rho_w E_r \quad (11)$$

where ρ is the reflectivity of the furnace wall, and E_r is the total incident radiation heat flux of the wall surface that is reflected in the proportion of ρ. Assuming the transmissivity of the wall is zero, the total energy can be written as

$$E = \epsilon_w \sigma T_w^4 + (1-\epsilon_w) E_r \quad (12)$$

In this system, the energy exchange is only by radiation, and the furnace is insulated; therefore, the rate of emission must be equal to the rate of absorption:

$$\epsilon_w \sigma T_w^4 = \epsilon_w E_r \quad (13)$$

That is

$$\sigma T_w^4 = E_r \quad (14)$$

Thus

$$E = \epsilon_w \sigma T_w^4 + (1-\epsilon_w)\, \sigma T_w^4 \quad (15)$$

That is

$$E = \sigma T_w^4 \tag{16}$$

This proves that the apparent emissivity of the furnace wall is equivalent to 1, regardless of the actual emissivity of the furnace wall, which is a function of the wall material and the slag on the wall. Assuming the wall emissivity equal to 1, equation 29 can be simplified to:

$$E_T = \int_0^\infty \epsilon_{g\lambda} E_{\lambda T_g} d\lambda + \epsilon_w \int_0^\infty \tau_{g\lambda} E_{\lambda T_w} d\lambda \tag{17}$$

In the absence of the scattering of particles such as soot and ash, and grey body behavior of the hot gas, the gas emissivity becomes independent of the wavelength and equation 37 can be derived.

$$E_T = \epsilon_f \sigma T_f^4 + (1 - \epsilon_f)\, \sigma T_w^4 \tag{18}$$

(ϵ_f) is the total emissivity of the gas in the furnace. The total emissivity (ϵ_f) in coal combustion represents the emission of both soot particles and gas.

$$\epsilon_f = \epsilon_{g+s} \tag{19}$$

One can find the average gas temperature in the furnace by using

$$T_f = \sqrt[4]{\frac{E_T - (1 - \epsilon_f)\, \sigma T_w^4}{\epsilon_f \sigma}} \tag{20}$$

8.4.2 Estimation of Hot Gas Volume Emissivity

H_2O, CO_2, and various hydrocarbon gases radiate to an appreciable extent. These two gases are the most dominant gases in oxy-fuel combustion; therefore, in order to find the gas emissivity in this research, the focus was only on these two gases.

Gases absorb and emit only in narrow wave lengths. Water vapor has an absorptivity of about 0.7 between wavelengths of 1.4 and 1.5 μm, nearly 0.8 between 1.6 and 1.8 μm, about 1.0 between 2.6 and 2.8 μm, and nearly 1.0 between 5.5 and 7.0 μm [76]. Radiation from CO_2 comes particularly from bands at about 2.64 to 2.84 μm, 4.13 to 4.5 μm, and 13 to 17 μm [77]. When there is more than one emitting species in the gas mixture, there is a chance that the emission bands of the two species overlap. Therefore, a correction factor $\Delta\epsilon$ is defined to account for the overlap among the emission bands of the other species in the gas mixture [77]. The emissivity coefficients of CO_2 and H_2O have been carefully measured, correlated, plotted, and tabulated by Hottel and Egbert et al. [76–79] based on several sources of experimental data for different gas compositions, temperatures, and pressures:

$$\epsilon_g = \epsilon_C + \epsilon_H - \Delta\epsilon \tag{21}$$

where ϵ_C is the emissivity of CO_2 and ϵ_H is the emissivity of H_2O. Based on the gas emissivity model explained above, the emissivity of the gas mixture at different recycle ratios and measured averaged gas temperature were calculated. The beam path length can be estimated simply from:

$$L = 3.6\,\frac{V}{A} \tag{22}$$

where V is the volume of the gas and A is the total surface area. The values of L for a limited number of specific geometries are tabulated in references [76,77].

8.4.3 Estimation of Soot Particles Emissivity

As discussed, in the combustion of oil and coal, soot particles contribute an appreciable amount of radiation, and one must account for the soot radiation in coal combustion.

Wall et al. used two pyrometer data outside the triatomic wavelength band, nearly at 0.65 and 0.90 μm, to estimate the absorptivity of soot particles in coal combustion. They reported that soot particles can contribute 90% of the total solid radiation emission at visible wavelengths and 60% of the emission was integrated over the spectrum of the wavelengths [80]. In the same manner that emissivity of gas was obtained using the emissivity of CO_2 and H_2O, the emissivity of total gas including the soot particles can be calculated using the emissivity of the hot gas and soot particles [81]:

$$\epsilon_f = \epsilon_{g+s} = \epsilon_g + \epsilon_s - M\epsilon_g\epsilon_s \tag{23}$$

where $M\epsilon_g\epsilon_s$ accounts for the overlap wavelength bands of gas and soot particles. M is the correction factor that can be calculated with an acceptable error [81]:

$$M = 1.07 + 18\,f_v PL + 0.27\,(\frac{T_g}{1000}) \tag{24}$$

where $\dot{M}$ depends mostly on T_g (average temperature of gaseous media containing soot) and to a much lesser extent on optical density $f_v PL$. P is the total pressure (atm) and f_v is the mole fraction of soot in the gas. In this research, as it is explained in reference [81], only the effect of temperature on the correction factor $\dot{M}$ is accounted for. The method of formulating radiation from soot particle clouds depends on the size of the particle [77]. Soot particles are defined as small particles if they can satisfy the conditions of Rayleigh particles. A particle in Rayleigh regime is considered small if

$$2\pi r < \frac{0.6\lambda}{n} \tag{25}$$

where n is the refractive index, and λ is the wavelength measured in the particle. In this system, the particles acts like a point source of volume. Measurement of soot particle reflective index is not a simple process and efforts have focused on quantifying the refractive index of soot. One study of Henriksen et al. [82] showed the refractive index of soot particles and ultimately optical properties of soot depend not only on temperature, but also on chemical composition and residence time. Different values of the refractive index were reported in this study. In reference [77], the value of 2.0 for the real part of the refractive index was suggested as a characteristic of a carbon black with a low hydrogen content. Based on the soot particles diameter, one can consider the soot particles as Raleigh particles. In this system, the monochromatic absorption of the particle is independent of the particle size and it is function of mole volume fraction of soot particles (f_v), beam length (L), and reciprocal wavelength. K is a function of the refractive index (n) and the absorption index (k).

$$\epsilon_{s\lambda} = 1 - e^{-\left(\frac{K(n,k)\, f_v\, L}{\lambda}\right)} \tag{26}$$

By integrating the monochromatic emissivity coefficient over the whole spectrum of wavelengths, ϵ_s can be obtained.

$$\epsilon_s = 1 - (1 + \frac{K f_v\, LT}{C})^{-4} \tag{27}$$

According to McCartney and Ergun, *K/C* can vary in a range from 5.2 to 2.6 as the atomic H/C ratio varies from 0 to 0.4 [83]. It is important to note that this ratio is not the ratio of H/C of the fuel, but is instead the ratio of H/C of the soot. A tentative value of 5 $cm^{-10}K^{-1}$ is suggested by reference [77]. Thus, the soot emissivity can be derived:

$$\epsilon_s = 1 - (1 + 500 f_v\, LT)^{-4} \tag{28}$$

The next step to find the value of soot emissivity is the value of soot volume mole fraction (f_v). Measurement of f_v is quite complicated for the large uncertainty in optical techniques, and even nowadays, a large number of errors, up to 50%, in the results have been reported.

Brown and Fletcher developed an advanced coal soot model that represents the evolution of the soot [84,85]. The main feature of the model is a transport equation for the soot mass fraction. Tar prediction options include either an empirical or a transport equation approach, which directly impacts the source term for the soot formation. Tar was calculated from the Lagrangian particle phase equations in parallel with application of the CPD model [61] to estimate devolatilization rates and tar yields. Their estimation

had an acceptable consistency with the experimental results of Haneberg et al. [86]. He applied a two-color method in a pilot-scale reactor to determine the average soot volume fractions at various distances and operating conditions across a centerline of a cross-section. Tree [87] provided more soot volume fraction data in a report from his experimental efforts at BYU. The results showed f_0 to be constant when the stoichiometric ratio (S.R.) is kept constant. Based on the job performed at BYU, the amount of soot volume fraction at air-firing case at S.R. = 1.15 is nearly $f_0 = 1.5 \times 10^{-7}$. In another mutual study between the University of Utah and Brigham Young University, it was shown that the same amount of soot volume fraction was obtained for both air-firing and oxy-firing with 29% to 30% oxygen at equal stoichiometric ratios [88]. It is important to note that in the OF29 case, the heat flux ratio becomes similar to the air combustion case [26,74]. In another study, it was shown that by decreasing the amount of CO_2 in oxy-firing, maintaining the S.R., f_0 increased [89]. This increase rate of f_0 was proportional to the rate of decrease of the gas volume in the system. The decrease of the amount of CO_2 increases the concentration of the soot particles in the gas.

As previously discussed, estimation of the soot particle volume fraction is a complicated process and requires very careful and accurate experimental techniques. More experimental investigation is required to predict soot formation in oxy-combustion to have an exact anticipation of soot radiation. However, the method can be conveniently applied to the radiant zone of any type of furnace to estimate the radiant heat flux.

8.5 Results

Figure 71 shows the measurement results of the wall temperature in three different axial locations along the top section of the OFC in various oxy-combustion conditions. The locations are reported as the distance from the tip of the burner to the location of the probe. As shown by the decrease in CO_2, the wall temperature increased. The same increase in temperature was witnessed in the axial locations. The lowest temperature for the OF40 was measured to be 1520 ºF at the top port and the highest was obtained at the bottom thermocouple and was approximately 1600 ºF. As shown in Figure 71, the experiment was conducted for the OF60 as well. The lowest temperature is reported at the top port and the highest temperature was obtained at the bottom port with values of 1600 ºF, and 1675 ºF, respectively. In addition, the total radiation of the wall and flame in the same axial locations were measure using wide angle radiometers. The conclusion of the measurements by the radiometers is provided in Figure 72. As shown, the amount of radiation in the top port was measured to be nearly 82 (kW/m^2) for the OF40, and it increased to be 95.5 (kW/m^2) for the OF60. The highest value of the radiation in each case was measured in the bottom port, and as plotted in the OF40, this value is almost 116 (kW/m^2), and for the OF60 is 139 (kW/m^2). It is important to note that the increase of the radiant heat by minimizing CO_2 is caused by two factors. Not only does the increase of wall temperature contribute to the raise of the radiant heat, but also the increase of the flame or hot gas temperature can have a significant impact on the heat of radiation in oxy-fuel combustion. The increase of gas radiant heat becomes an important factor in oxy-coal combustion due to the existence of soot particles. Heat of radiation is the product of two factors. First is the emissivity of the subject, and second is

the temperature which strongly influences the heat of radiation. Soot particles with a higher temperature can have both higher emissivity and heat of radiation.

In order to investigate the effect of the temperature on the gas, soot, and total emissivities, using the technique described above, their values were calculated and plotted in Figure 74. As presented, the emissivity of the gas mixture (CO2 + H2O) decreased by an increase of the gas temperature. Both CO2 and H2O are emissive gases, and their emissivity depends on their mole fraction and the temperature, with the constant path length assumption. Based on the tabulated emissivity data of these two gases, their emissivity decreased with the increase in temperature. However, the emissivity of the soot particles in the gas mixture follows an opposite manner, and has a significant increase due to the temperature. It is important to note that the emissivity of the soot particle for a constant path length is not only a function of temperature, but is greatly influenced by the volume soot fraction. Thus, the total emissivity of the gas considerably increases with the decrease of the CO_2 volume fraction or recycle ratio. As previously discussed, the emissivity of both hot gas and soot particles is a strong function of the path length, and the path length is defined based on the geometry of the gas enclosure. For large furnaces, the total emissivity of the mixture of hot gas and soot particles can approach one; however, this value is less for shorter path lengths (nearly 0.42 in this study). Based on the calculations discussed above, the spatially mean gas temperature (in the view field of the radiometers) of each location of the top section of the OFC was calculated. These results are presented in Figure 74, Figure 75, and Figure 76. As shown, the mean gas temperature increases in each section when the amount of CO_2 decreased. In addition, the calculated mean gas temperatures were compared to the measured gas

temperatures in the locations of the thermocouples. It is important to note that the calculated mean gas temperatures is the spatially averaged gas temperature in the field of view of the radiometer and is not a radially averaged gas temperature in the determined locations. However, these calculated temperatures manifest the change of the temperature axially, as well as the increase of the temperature due to the decrease of CO_2 in oxy-coal combustion.

The calculation method can be used with the application of narrow angle radiometers to calculated radially averaged gas temperatures. Figure 78, Figure 79, Figure 80, and Figure 81 show the comparison of measured and calculated spatially mean gas temperatures at three locations of the furnace.

8.6 Conclusions

This described research provided an insight into the effects of reduction CO_2 on radiant heat flux in oxy-coal combustion. The coal used in this study was Illinois #6 Bituminous coal. The mole fraction of CO_2 decreased from 60% in the OF40 to 41.5% in the OF60. The total stoichiometric ratio was kept constant in all the experimental cases. The mole fraction of CO_2 or the recycle ratio plays a key role in heat transfer in oxy-coal combustion, and a considerable change in the radiant heat transfer and the temperatures of the furnace wall and gas was witnessed. A model was developed to justify the observations of the experimentation results, leading to a better understanding of the heat transfer phenomena in oxy-coal combustion. More analysis on the gas and soot emissivities sowed that contribution of soot emissivity compared to gas emissivity increase by the decrease of recycle ratio. The total emissivity has a considerable increase

with reduction of CO_2; this change is caused by rise in temperature as well as the increase of soot volume fraction. Assuming there is no overlap between the soot and gas radiation wavelengths at the OF40, the soot particles contribute 55% of the total hot gas radiation in the furnace. However, this contribution increases up to nearly 65% of the total radiation in the OF60. The emissivity of gas (CO_2 + H_2O) radiation had an opposite manner. The emissivity of gas decreased with the increase of temperature; however, this increase is not as significant as the increase of soot particles' emissivity by temperature.

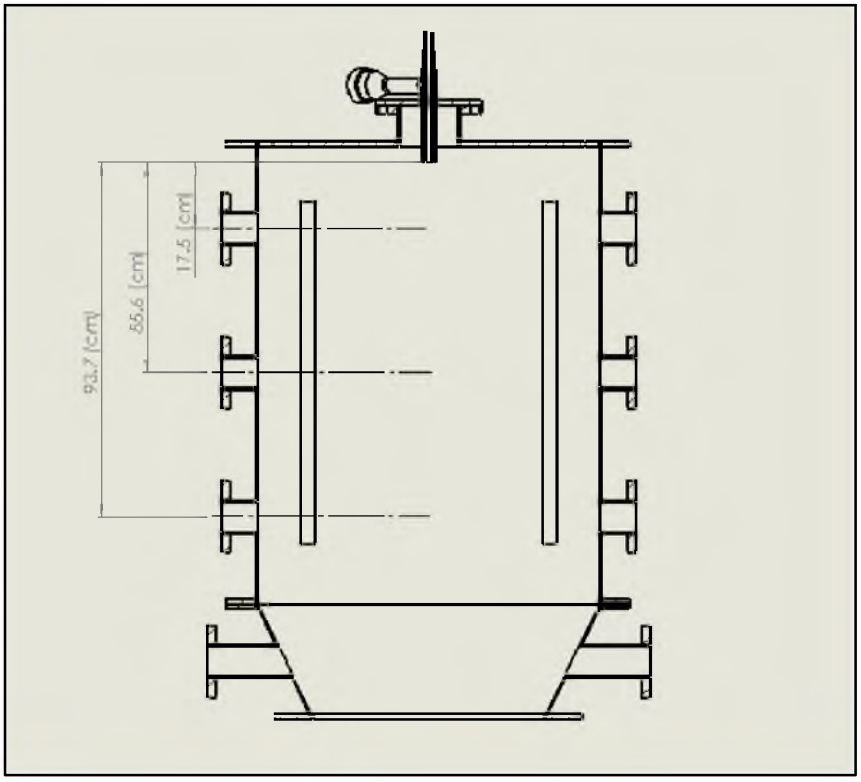

Figure 70. Distances of thermocouples and radiometers from burner

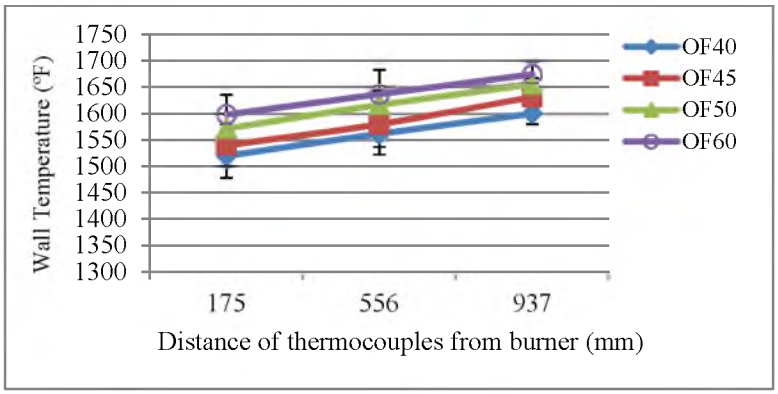

Figure 71. Axial wall temperature variation caused by reduction of CO_2

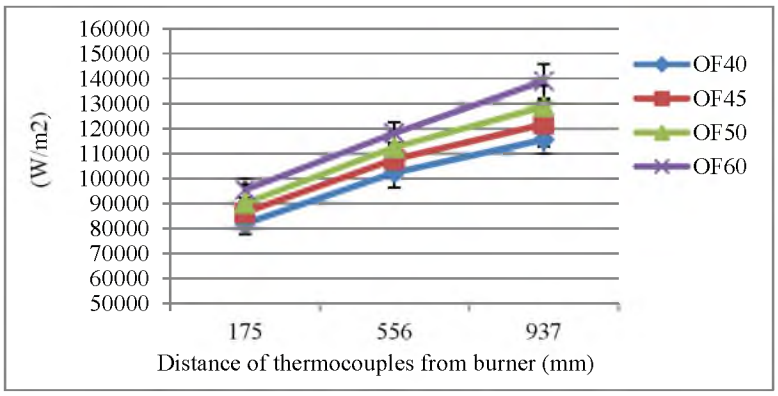

Figure 72. Radiant heat flux variation due to reduction of CO_2 in axial locations of OFC

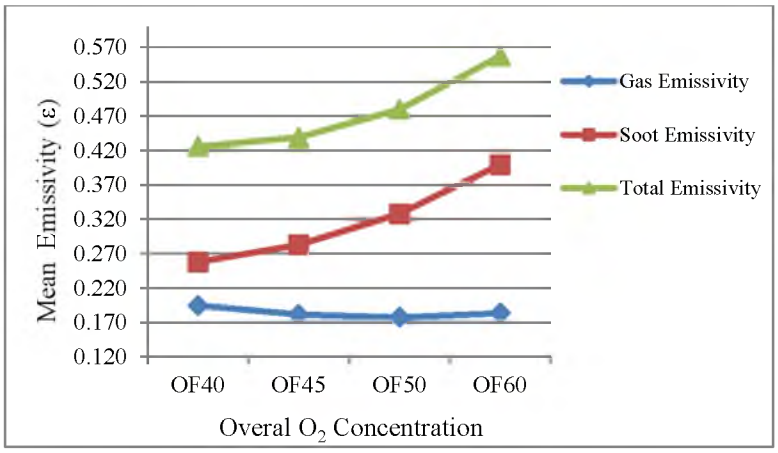

Figure 73. Calculated total emissivities

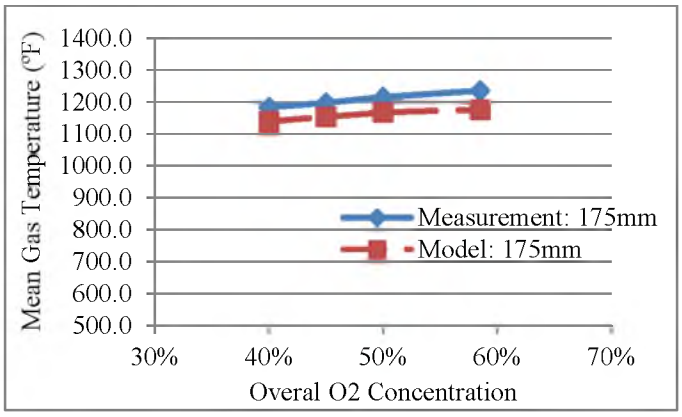

Figure 74. Increase of gas temperature in top port (175 mm from burner)

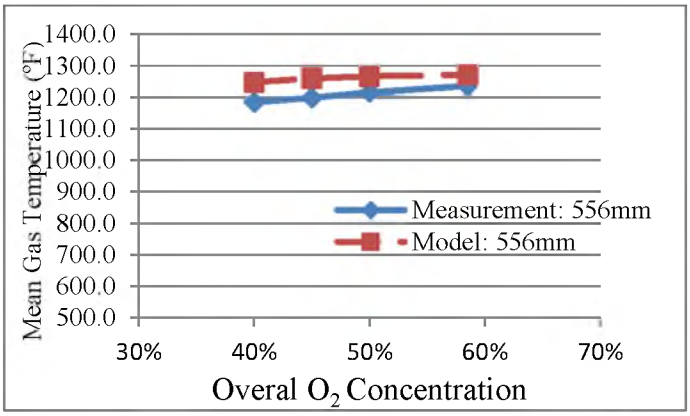

Figure 75. Increase of gas temperature in middle port (556 mm from burner)

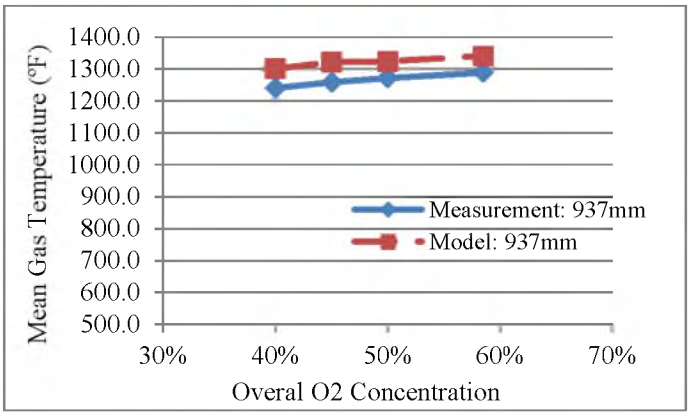

Figure 76. Increase of gas temperature in bottom port (556 mm from burner)

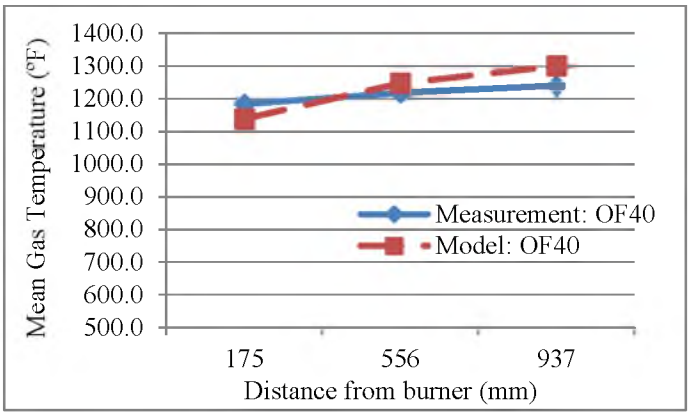

Figure 77. Comparison of calculated and measured gas temperature at OF40

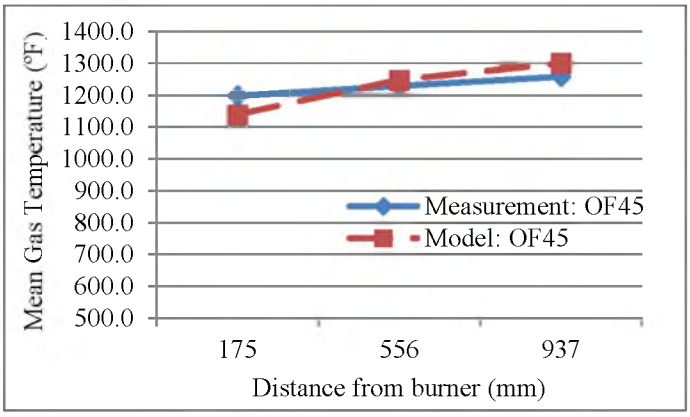

Figure 78. Comparison of calculated and measured gas temperature at OF45

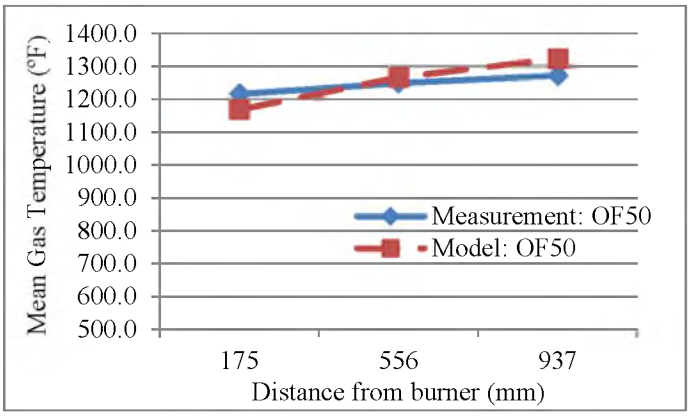

Figure 79. Comparison of calculated and measured gas temperature at OF50

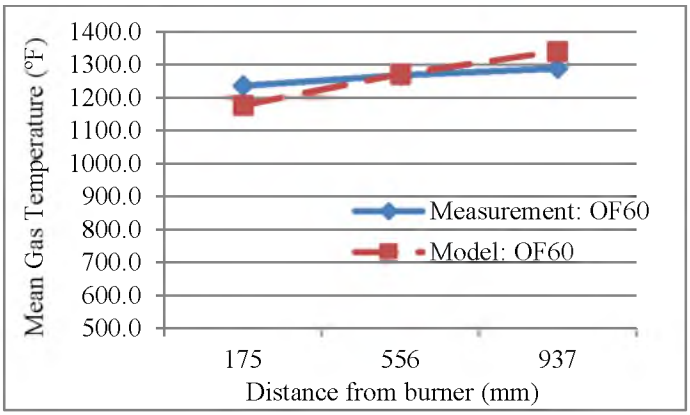

Figure 80. Comparison of calculated and measured gas temperature at OF60

Table 14. Combustion and burners conditions for CO_2 reduction test

Case	Overall O_2	Overall CO_2	Recycle Ratio	Flue gas O_2 concentration	Pri. Vel. (m/s)	O_2 stream Vel. (m/s)	Sec. Vel. (m/s)
OF 40	40%	60%	67%	5.48	6.39	6.48	14.97
OF 45	45%	55%	62%	6.2	6.39	6.48	16.37
OF 50	50%	50%	57%	7	6.39	6.48	15.19
OF 60	58.5%	41.5%	49%	8.2	6.39	6.48	15.48

Table 15. Combustion and burner conditions for CO_2 reduction test (streams flow rate)

Case	Pri CO_2 (lb)	O_2 stream (lb)	Sec O_2 (lb)	Sec CO_2 (lb)	Vel Ratio Pri./O_2 Stream	Vel Ratio Sec./O_2 Stream
OF 40	15.11	24.4	0	35.2	0.99	2.31
OF 45	15.11	24.4	0	25.1	0.99	2.53
OF 50	15.11	24.4	0	18.4	0.99	2.34
OF 60	15.11	24.4	0	8.7	0.99	2.39

Table 16. Measurement positions of thermocouples and radiometers

Port position	Distance from the burner (mm)
Top	175
Middle	556
Bottom	937

9. FUTURE WORK

This study allowed for a better understanding of the effects of coal composition on flame ignition in a pilot scale, as well as the impacts of directed pure oxygen injection on the flame stability, and the changes caused in the heat of radiation caused by the reduction of CO_2 in oxy-coal combustion. Additionally, this research, potentially, contributes several suggestions for future work.

1) High Velocity Directed Pure Oxygen Stream

   In this study, the velocity ratio of the O_2 stream and the primary stream was maintained equal to one being nearly 2.5 times smaller than the secondary stream. However, it has been suggested to explore the effects of the oxygen stream when it is located in the outer stream with higher velocities. Additionally, high velocity oxygen injection in the center of the burner and its effects on the migration direction of the coal particles should be investigated. Also, the injection of oxygen with supersonic velocity in different configurations could have advantages on the flame stability, flame length, and the heat distribution of the flame that need be studied.

2) Minimization of CO_2 in Primary Stream

   As discussed in this study, in order to reduce the amount of CO_2 or the recycle ratio, CO_2 was reduced from the secondary stream, leading to lowering the total

mole fraction of CO_2 down to 41.5%. However, in order to investigate the heat transfer in oxy-coal combustion at lower recycle ratios, CO_2 in the primary stream needs to be reduced. It is recommended to maintain the stream velocities to minimize the aerodynamic effects. The reduction of the primary stream can increase the particle residence time, leading to a different flame type. Different flames might not have the same the heat distribution.

3) Application of IR Camera to Measure Heat of Radiation

Radiometers were employed in this research to measure the differences in the heat of radiation for several oxy-coal combustion conditions. The wide angle radiometers collect the averaged total radiation coming from its field of view. The narrow angle radiometers have small angle filed of views; however, there are only a limited number of ports for the radiometers based on the size of the furnace. An IR camera can be applied to capture the radiant heat of the whole length of flame. Each pixel, with a good estimation, provides data of the radiant heat being received from a small element of the flame captured by the camera on the pixel. These data can be valuable for the validation of simulation results.

4) Measurement of Soot Volume Fraction

The radiation of soot particles has large impacts on the radiant heat in oxy-coal combustion. As discussed before, the soot volume fraction plays a key role on the emissivity of flame. More research on the measurements of flame soot volume fraction in different coal compositions and combustion conditions is suggested. In addition, the effects of reduction of CO_2 on the soot volume fraction should be studied in detail. Inventing a more accurate technique with less uncertainty

compared to the previous methods to measure the soot volume fraction can be very helpful.

5) Effects of Coal Rank on Radiant Heat Transfer

According to the previous studies, coal rank can have a big impact on the heat of oxy-combustion. Various several recycle ratios in oxy-coal combustion were obtained to obtain a similar heat of combustion to air combustion. One of the main reasons for the variety in the reported data was suggested to be the coal composition. In this study, the effect of minimization of CO_2 was tested on Illinois #6 coal; however, it is recommended to conduct an experiment on a coal with different rank, such as Powder River Basin (PRB) coal.

6) Application of PIV and PSV

As mentioned in this study, the migration direction of the coal particles has a significant impact on the stability of flame. The Particle Image Velocimetry (PIV) or Particle Shadow Velocimetry (PSV) can be applied to capture the direction of the coal particles in the near burner zone. In addition, these two techniques can provide a better insight about the mixing process of flame streams by presenting a velocity map of the flame.

APPENDIX A

FLAME STAND-OFF DISTANCE PDFS OF CONFIGURATION A

As discussed in Chapter 6, PDF plots of the stand-off distance of flames obtained from Configuration A burners were provided. The PDFs were averaged over the replicates of these experiments and the detail of each replicate could be obscure for some of the plots. Therefore, the PDF plots are individually provided here for each case of configuration A presented in Chapter 6. Five replicates were performed for three main cases at F_{O2} = 0%, F_{O2} = 55%, and F_{O2} = 100%. All the cases resulted in very similar replicates except F_{O2} = 75%. This case was a transient case for unstable flames to stable flames, and showed a very sensitive behavior to all the possible effects of wall temperature. The flame was stable and attached in one of the replicates.

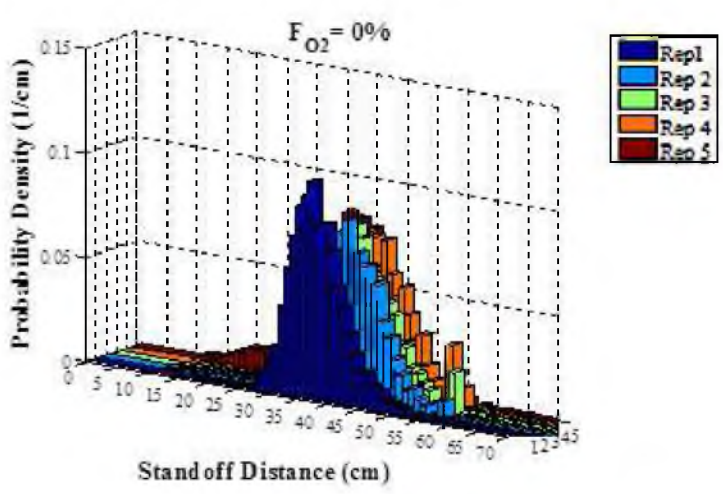

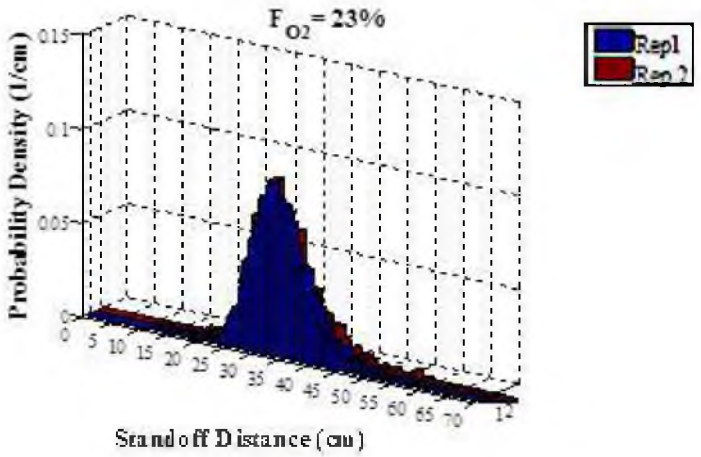
F_{O2} = 23%
Probability Density (1/cm)
0.15
0.1
0.05
0
0 5 10 15 20 25 30 35 40 45 50 55 60 65 70
Standoff Distance (cm)
Rep1
Rep 2

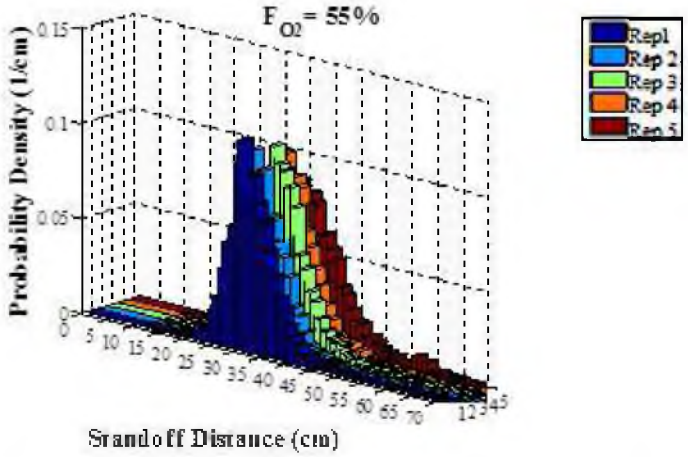
F_{O2} = 55%
Probability Density (1/cm)
0.15
0.1
0.05
0
0 5 10 15 20 25 30 35 40 45 50 55 60 65 70
Standoff Distance (cm)
Rep1
Rep 2
Rep 3
Rep 4
Rep 5

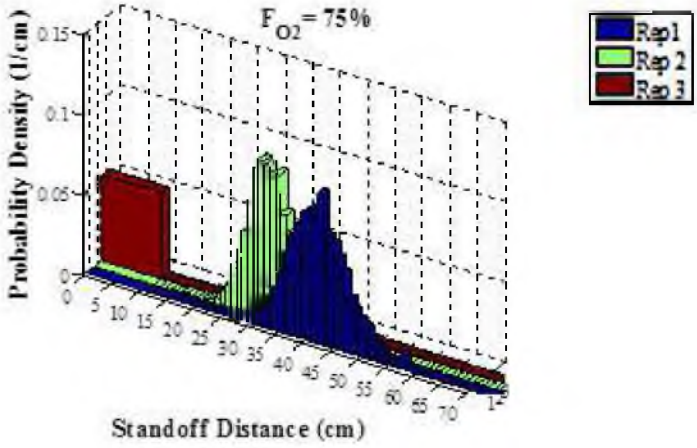
F_{O2} = 75%
Probability Density (1/cm)
0.15
0.1
0.05
0
0 5 10 15 20 25 30 35 40 45 50 55 60 65 70
Standoff Distance (cm)
Rep1
Rep 2
Rep 3

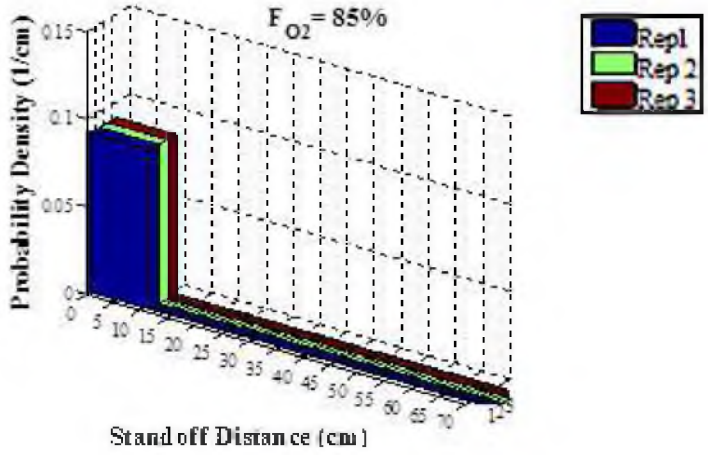
F_{O2} = 85%
Probability Density (1/cm)
0.15
0.1
0.05
0
0 5 10 15 20 25 30 35 40 45 50 55 60 65 70
Standoff Distance (cm)
Rep1
Rep 2
Rep 3

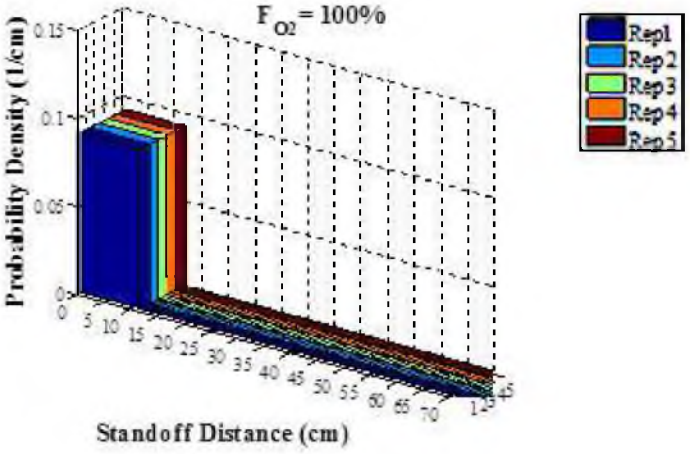
F_{O2} = 100%
Probability Density (1/cm)
0.15
0.1
0.05
0
0 5 10 15 20 25 30 35 40 45 50 55 60 65 70
Standoff Distance (cm)
Rep1
Rep 2
Rep 3
Rep 4
Rep 5

APPENDIX B

FLAME STAND-OFF DISTANCE PDFS OF CONFIGURATION B

The Configuration B PDF plots presented in Chapter 6 were averaged over the experiment replicates. In order to have better understanding of the detail of the PDFs obtained from the experiments with the Configuration B burners, the PDF plots are individually provided here for each case.

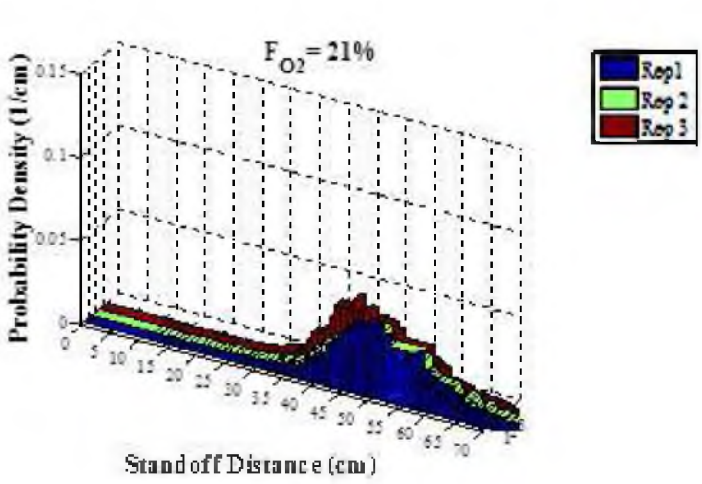

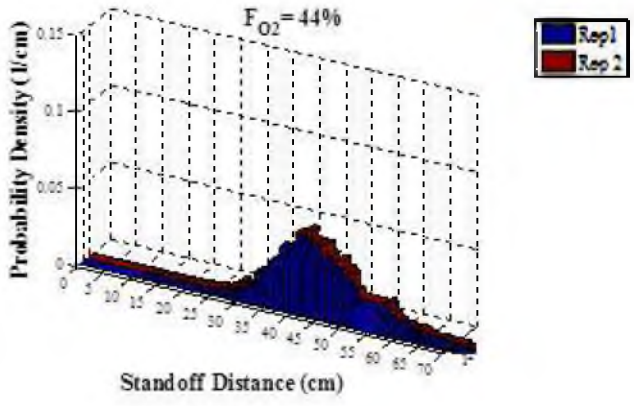

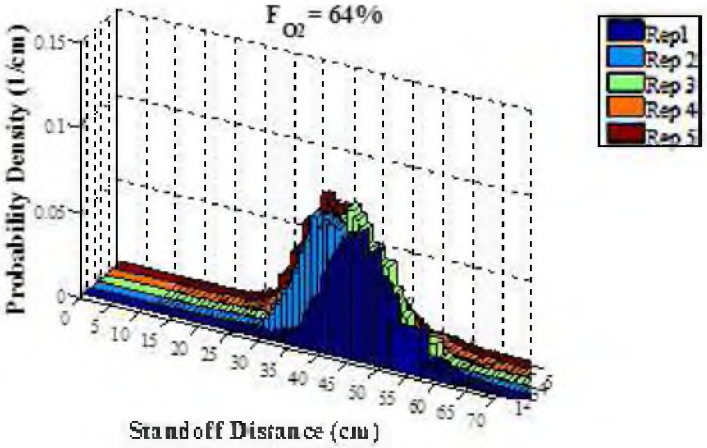
F O2 = 64%
Probability Density (1/cm)
0.15
0.1
0.05
0
0 5 10 15 20 25 30 35 40 45 50 55 60 65 70
Standoff Distance (cm)
Rep1
Rep 2
Rep 3
Rep 4
Rep 5

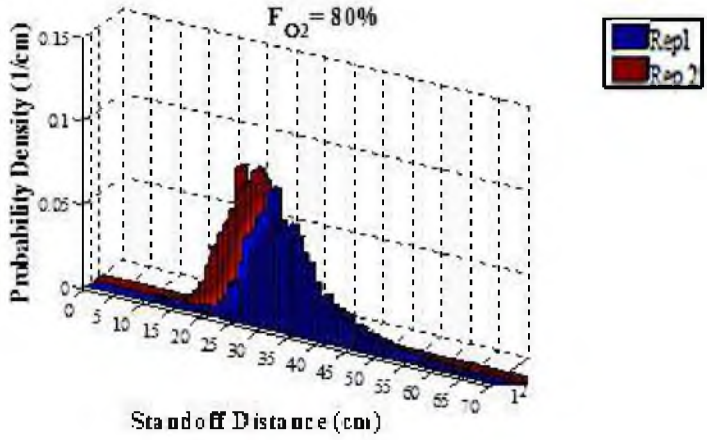
F O2 = 80%
Probability Density (1/cm)
0.15
0.1
0.05
0
0 5 10 15 20 25 30 35 40 45 50 55 60 65 70
Standoff Distance (cm)
Rep1
Rep 2

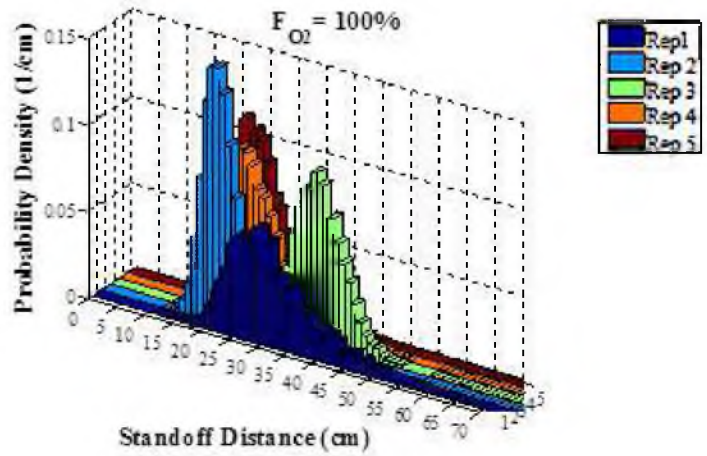
F O2 = 100%
Probability Density (1/cm)
0.15
0.1
0.05
0
0 5 10 15 20 25 30 35 40 45 50 55 60 65 70
Standoff Distance (cm)
Rep1
Rep 2
Rep 3
Rep 4
Rep 5

APPENDIX C

DESIGN THEORY OF CONFIGURATIONS A AND B

Multiple burners allowed primary stream, oxygen stream, and secondary stream velocities to be kept constant as much as possible, in order to minimize aerodynamic changes, as oxygen distribution was varied. In addition, it was decided to keep the velocities of the primary and oxygen streams as similar as possible. A large velocity ratio of these two streams will create a large mixing.

A large mixing will cause all the combustion reactions to happen in a short period of time; therefore, the chance of a creation of a short flame becomes higher. Different methods to create similarity in combustion systems were introduced by Spalding et al. [90], Beer and Chigier et al. [31–34]. The first argument was the effect of very large Reynolds numbers. If the Reynolds number is high enough, mixing is controlled by large turbulent mixing and molecular diffusion could be neglected. Assuming that the fluid is not transported by molecular diffusion but also by turbulent velocity fluctuations, we derive:

$$\frac{\partial C}{\partial t} + \frac{\partial u_j C}{\partial x_j} = D \frac{\partial^2 C}{\partial x_j x_j} \tag{29}$$

$$Re = \frac{UL}{\upsilon} \tag{30}$$

$$D\frac{\partial^2 C}{\partial x_j x_j} = D\frac{\Delta C}{L^2} \tag{31}$$

$$\frac{\partial u_j C}{\partial x_j} = U\frac{\Delta C}{L} \tag{32}$$

In order to compare the effect of convective term with molecular diffusive term, one can look at the ratio of these two values:

$$\frac{Convection}{Diffusion} = \frac{UL}{D} \tag{33}$$

This ratio is the Peclet (Pe) number, and for turbulent flows, this quantity has large values. Also, it shows that greater values of Reynolds number will result in a large turbulence; therefore, diffusion forces become negligible. The second factor is the momentum ratio of the burner streams. Additionally, in swirl burners, a number called the Swirl number was defined. This number is required to be maintained constant for scaling purposes.

John Smart et al. in his PhD dissertation at the University of London 1992 [91], compared different approaches for modeling and scaling combustion systems and burners. In his study, he emphasized the importance of consideration of the two factors of burner and furnace for scaling of a combustion system. The approaches are listed below

1. Constant Reynolds number
2. Constant inlet velocity
3. Constant residence time

Constant velocity scaling is "historically" the most applied approach in combustion scaling. Beer and Chigier [31–34] have applied this approach in most of their works. In this method, the convective and the turbulent diffusion time scale decreases and specific mixing rate increases as scale is reduced and fixed to the diameters ratio. Let us consider:

$$u_i = \bar{u}_i + \acute{u}_i \tag{34}$$

Applying this equation in the Navier Stokes equation we derive:

$$\rho \frac{\partial \bar{u}_i}{\partial t} + \rho \frac{\partial \bar{u}_i \bar{u}_j}{\partial x_j} = \frac{\partial}{\partial x_j} (\bar{\sigma}_{ij} - \overline{\acute{u}_i \acute{u}_j}) \tag{35}$$

The unsolvable part of the equation is called the Reynolds stress term which is due to fluctuation of the turbulence flow. For the first time, Boussinesq et al. [92] suggested a model by which viscous stress in laminar flow should be a function of mean velocity gradient. He named the constant of this equation, Eddy Viscosity:

$$-\overline{\acute{u}_i \acute{u}_j} = \upsilon_T \left(\frac{\partial \bar{u}_i}{\partial x_j} + \frac{\partial \bar{u}_j}{\partial x_i} \right) - \frac{2}{3} k \delta_{ij} \tag{36}$$

The next level, which is defining the quantity of turbulent or eddy viscosity, was achieved by analogy of molecular viscosity and turbulent viscosity. Prandtle et al. [93] suggested eddies in a turbulence flow can be assumed as gas molecules in a gas. Molecular viscosity is the result of the collision of molecules leading to a moment exchange between the species. The viscosity of gases is proportional to the multiplication

of velocity and the mean free path of molecules. The same scenario was applied to define turbulent viscosity:

$$v_T \propto VL \tag{37}$$

$$V = L_m\left(\frac{\partial \bar{u}_i}{\partial x_j}\right) \tag{38}$$

$$v_T = L_m^2\left(\frac{\partial \bar{u}_i}{\partial x_j}\right) \tag{39}$$

Each stream exiting the burner jet is assumed to have such an individual core. Considering applying constant inlet velocity and turbulent mixing theory, one can derive a mathematical relationship for some distance downstream of the flow where two streams combine and completion of mixing occurs. Merging of the separated streams happens due to the mixing process. Mixing is a function of gradient between the two streams and the area normal to mixing surfaces. The gradient between two streams can be caused by momentum, heat, or mass concentration. The constant of this proportionality is the turbulent kinematic viscosity in turbulent flows. Therefore, one can derive the rate of mixing in turbulent jets:

$$Mixing\ surface = xL \tag{40}$$

$$concentration\ gradient = \frac{\Delta C}{L} \sim \frac{1}{L} \tag{41}$$

$$Mixing\ Rate = (xL)\left(\frac{1}{L}\right)(uL) = xuL \tag{42}$$

Considering all the materials that will be mixed in the jet or burner is:

$$Q_t \sim uA \sim uL^2 \tag{43}$$

Dividing the mixing rate by the total mixing will provide the fraction of mixing downstream of the flow:

$$f_m \sim \frac{xuL}{uL^2} = \frac{x}{L} \tag{44}$$

Therefore, applying the constant velocity approach at constant f_m the degree of mixing is the same. Thus, if any difference in flame stability and reactant mixing occur, it will be caused by other factors, which in this case are a fraction of oxygen in oxygen stream, configuration of oxygen stream, and the heat of radiation. This analysis required modification in the case of swirl flow. Thus, for the sake of discussion and analysis of flame mixing in this study, it was decided to employ coaxial turbulent diffusion burners with zero swirls.

APPENDIX D

TEMPORAL CHANGES OF WALL TEMPERATURE AT OF45

More investigation was performed on the temporal change of wall temperatures in the test of effects of minimization of CO_2. For each case, the combustion operating conditions were maintained nearly 150 minutes to reach the steady state of the case. In this study, only one case was chosen (OF45) and the case was maintained for almost 5 hour to look at the derivation of temperatures by time. Based on the plot, the change in the wall temperatures after150 minutes to the end of the experiments that is nearly 300 minutes are obtained to be 15 ° F for the top, 16 ° F for the middle, and only 7 ° F for the bottom thermocouple. The results of this test showed that the change in the wall temperature reported in the experiment is due to the change of the combustion operating conditions (minimization of CO_2) and it is not due to the temporal changes of the heat flux in the furnace.

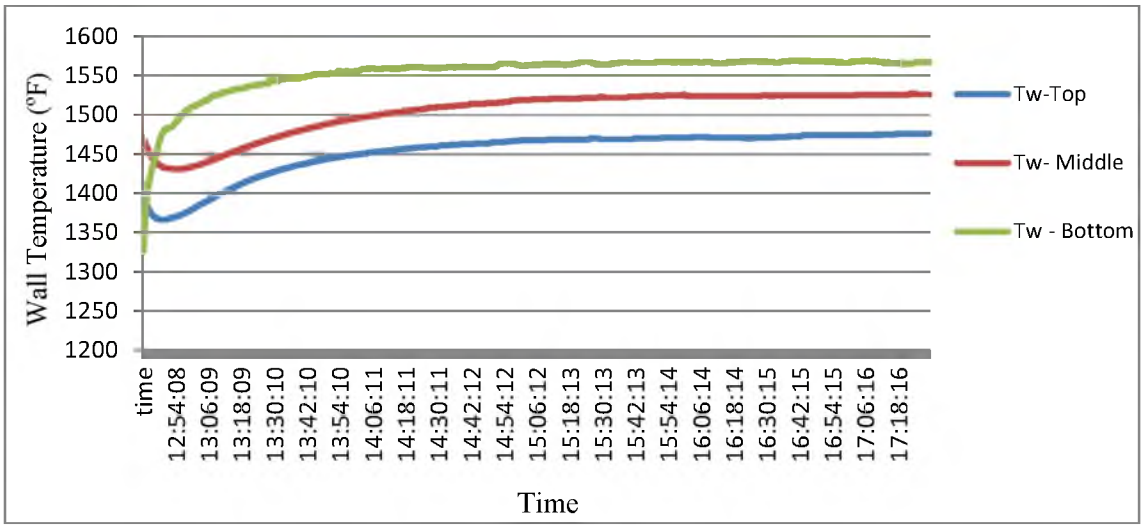
Wall Temperature (°F)
1600
1550
1500
1450
1400
1350
1300
1250
1200
time
12:54:08
13:06:09
13:18:09
13:30:10
13:42:10
13:54:10
14:06:11
14:18:11
14:30:11
14:42:12
14:54:12
15:06:12
15:18:13
15:30:13
15:42:13
15:54:14
16:06:14
16:18:14
16:30:15
16:42:15
16:54:15
17:06:16
17:18:16
Time
Tw-Top
Tw- Middle
Tw - Bottom

APPENDIX E

RADIANT HEAT FLUX DATA WITH STANDARD DEVIATION

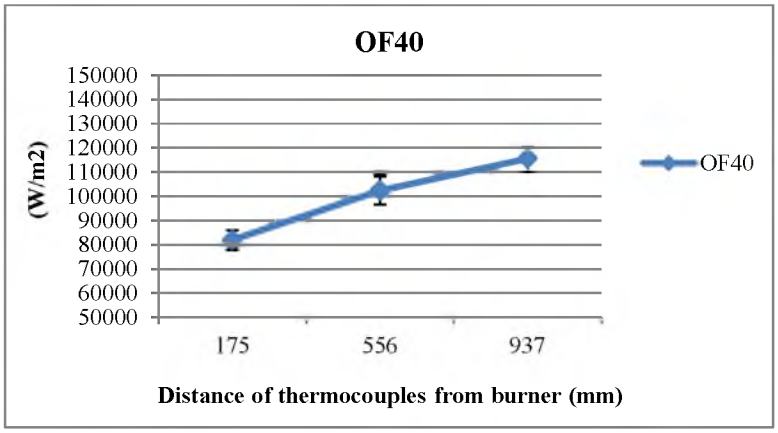

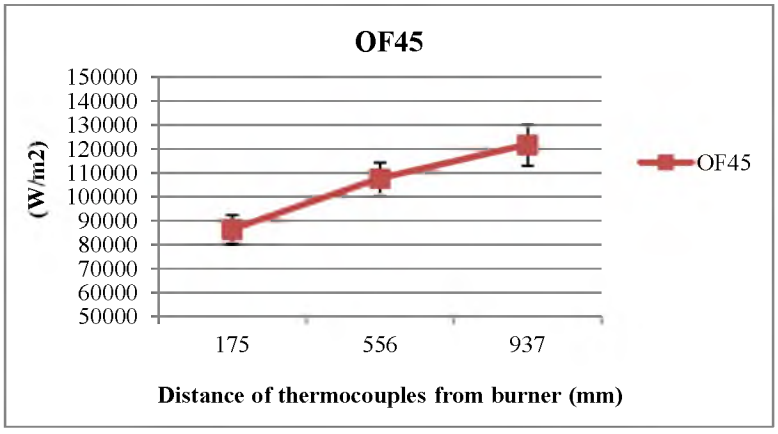

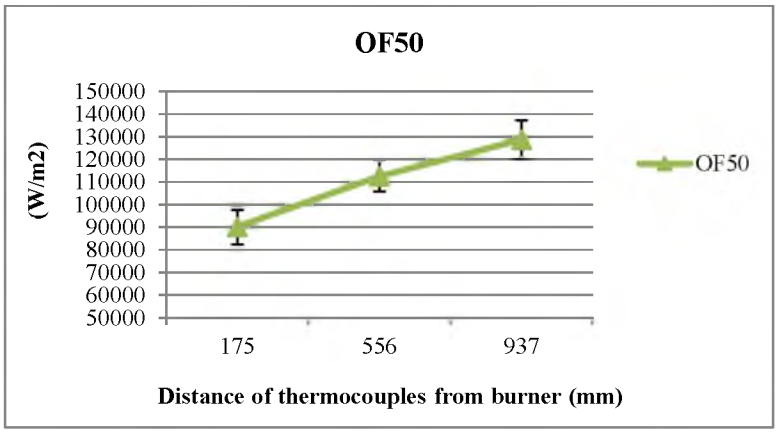
OF50
150000
140000
130000
120000
110000
100000
90000
80000
70000
60000
50000
(W/m2)
175
556
937
Distance of thermocouples from burner (mm)
OF50

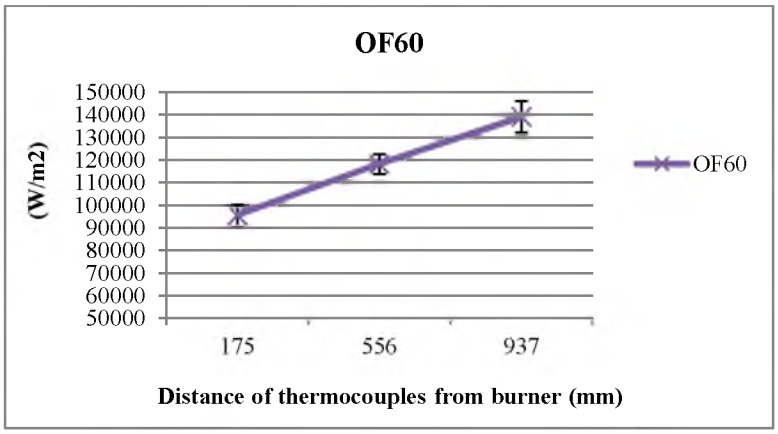
OF60
150000
140000
130000
120000
110000
100000
90000
80000
70000
60000
50000
(W/m2)
175
556
937
Distance of thermocouples from burner (mm)
OF60

APPENDIX F

WALL TEMPERATURE DATA WITH STANDARD DEVIATION

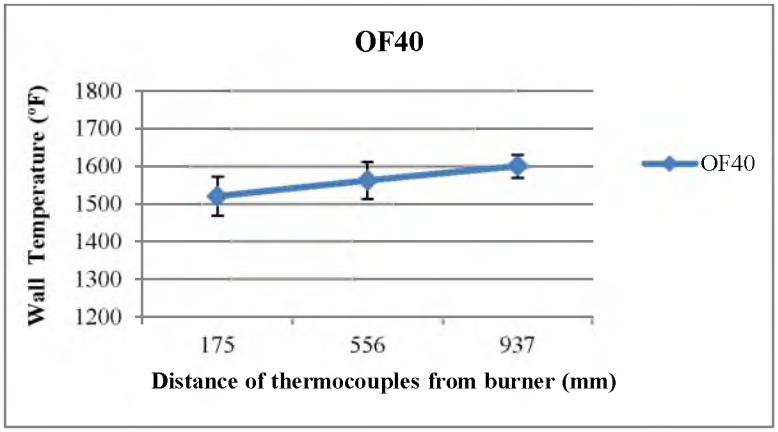

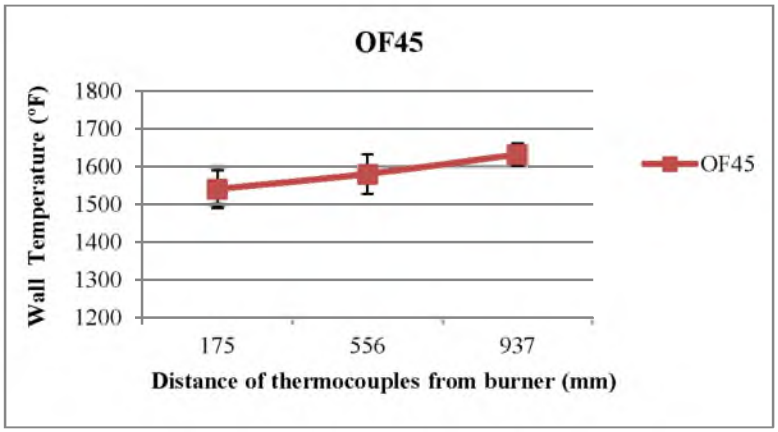

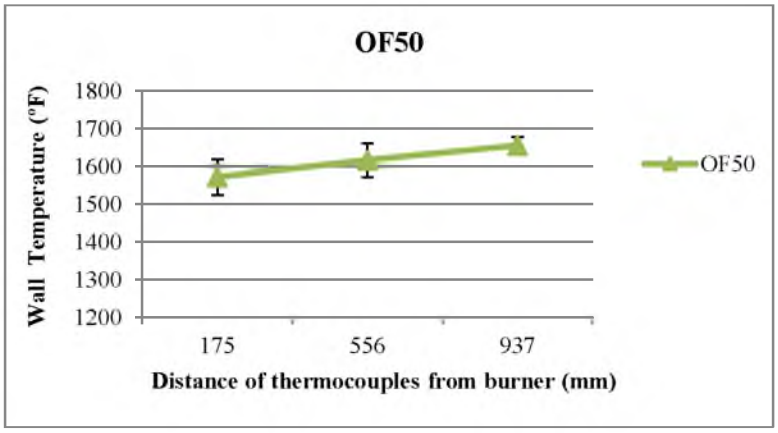
OF50
Wall Temperature (°F)
1800
1700
1600
1500
1400
1300
1200
175
556
937
Distance of thermocouples from burner (mm)
OF50

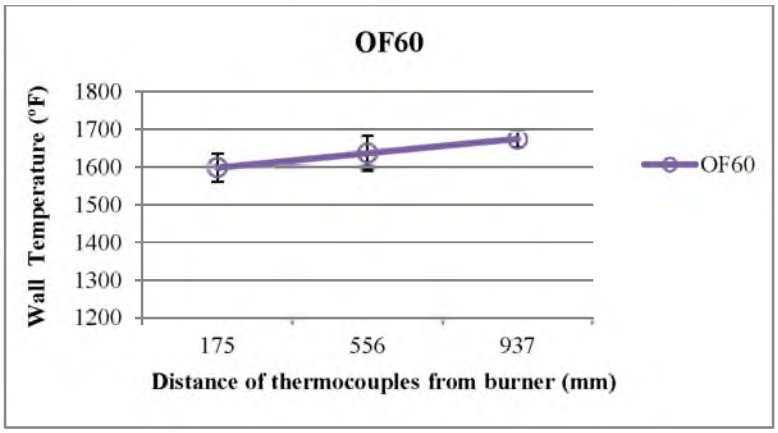
OF60
Wall Temperature (°F)
1800
1700
1600
1500
1400
1300
1200
175
556
937
Distance of thermocouples from burner (mm)
OF60

REFERENCES

[1] B.J.P. Buhre, L.K. Elliott, C.D. Sheng, R.P. Gupta, T.F. Wall, Oxy-fuel combustion technology for coal-fired power generation, Progress in Energy and Combustion Science. 31 (2005) 283–307.

[2] B.M. Abraham, J.G. Asbury, E.P. Lynch, A.P.S. Teotia, Coal-oxygen process provides CO2 for enhanced recovery, Oil and Gas Journal. 80:11 (1982) 68–70, 75.

[3] C.S. Wang, G.F. Berry, K.C. Chang, A.M. Wolsky, Combustion of pulverized coal using waste carbon dioxide and oxygen, Combustion and Flame. 72 (1988) 301–310.

[4] C.R. Shaddix, A. Molina, Particle imaging of ignition and devolatilization of pulverized coal during oxy-fuel combustion, Proc. Combust. Inst. 32 (2009) 2091–2098.

[5] Vattenfall, http://www.encapco2.org/sp3.htm, (n.d.).

[6] E. Kharbat, K. Annamalai, C. Gopalakrishnan, Ignition and combustion of isolated and binary array of coal particles, Science. 421 (1995) 413–421.

[7] H. Katalambula, J. Hayashi, T. Chiba, K. Kitano, K. Ikeda, Dependence of single coal particle ignition mechanism on the surrounding volatile matter cloud, Energy & Fuels. 11 (1997) 1033–1039.

[8] M. Sami, K. Annamalai, M. Wooldridge, Co-firing of coal and biomass fuel blends, (2001) 171–214.

[9] X. Du, K. Annamalai, The transient ignition of isolated coal particle, Combustion and Flame. 97 (1994) 339–354.

[10] Y. Qiao, L. Zhang, E. Binner, M. Xu, C.-Z. Li, An investigation of the causes of the difference in coal particle ignition temperature between combustion in air and in O2/CO2, Fuel. 89 (2010) 3381–3387.

[11] C.R. Shaddix, E.S. Hecht, A. Molina, Ignition of a group of coal particles in oxy-fuel combustion with CO2 recirculation, in: 34th International Technical Conference on Coal Utilization and Fuel Systems, Clearwater, FL, 2009.

[12] T. Kiga, S. Takano, N. Kimura, K. Omata, M. Okawa, T. Mori, et al., Characteristics of pulverized-coal combustion in the system of oxygen/recycled flue gas combustion, Energy Conversion and Management. 38 (1997) 129–134.

[13] T. Nozaki, S.-I. Takano, T. Kiga, K. Omata, N. Kimura, Analysis of the flame formed during oxidation of pulverized coal by an O2/CO2 mixture, Energy. 22 (1997) 199–205.

[14] R. Stanger, T. Wall, Sulphur impacts during pulverized coal combustion in oxy-fuel technology for carbon capture and storage, Progress in Energy and Combustion Science. 37 (2011) 69–88.

[15] T. Ochs, C. Summers, D. Oryshchyn, D. Gross, Oxy-fuel combustion systems for pollution free coal fired power generation, (2004).

[16] T. Wall, Y. Liu, C. Spero, L. Elliott, S. Khare, R. Rathnam, et al., An overview on oxyfuel coal combustion—State of the art research and technology development, Chemical Engineering Research and Design. 87 (2009) 1003–1016.

[17] H. Li, J. Yan, M. Anheden, Impurity impacts on the purification process in oxy-fuel combustion based CO2 capture and storage system, Applied Energy. 86 (2009) 202–213.

[18] M.B. Toftegaard, J. Brix, P. a. Jensen, P. Glarborg, A.D. Jensen, Oxy-fuel combustion of solid fuels, Progress in Energy and Combustion Science. 36 (2010) 581–625.

[19] A.C. Bose, J.O.L. Wendt, Pulverized coal combustion: fuel nitrogen mechanisms in the rich post-flame, in: Symposium (International) on Combustion, Elsevier, 1989: pp. 1127–1134.

[20] K. Okazaki, T. Ando, NOx reduction mechanism in coal combustion with recycled CO2, Energy. 22 (1997) 207–215.

[21] F. Normann, K. Andersson, B. Leckner, F. Johnsson, High-temperature reduction of nitrogen oxides in oxy-fuel combustion, Fuel. 87 (2008) 3579–3585.

[22] D.M. Woyecenko, I. Ikeda, W.L. Van de Kamp, Characterization of flames generated by burneing pulverized coal in a mixture of oxygen and recycle flue gas, 1995.

[23] D.M. Woyecenko, I. Ikeda, W.L. Van de Kamp, Combustion of Pulverized Coal in a Mixture of Oxygen and Recycled Flue Gas, 1994.

[24] R. Tan, G. Corragio, S. Santos, Oxy- Coal Combustion with flue gas recycles for the power generation industry, a literature review, 2005.

[25] L. Chen, S.Z. Yong, A.F. Ghoniem, Oxy-fuel combustion of pulverized coal: Characterization, fundamentals, stabilization and CFD modeling, Progress in Energy and Combustion Science. 38 (2012) 156–214.

[26] J.P. Smart, P. O'Nions, G.S. Riley, Radiation and convective heat transfer, and burnout in oxy-coal combustion, Fuel. 89 (2010) 2468–2476.

[27] G. Scheffknecht, L. Al-Makhadmeh, U. Schnell, J. Maier, Oxy-fuel coal combustion—A review of the current state-of-the-art, International Journal of Greenhouse Gas Control. 5 (2011) S16–S35.

[28] K. Andersson, R. Johansson, S. Hjartstam, F. Johnsson, B. Leckner, Radiation intensity of lignite-fired oxy-fuel flames, Experimental Thermal and Fluid Science. 33 (2008) 67–76.

[29] K. Andersson, F. Johnsson, Flame and radiation characteristics of gas-fired O2/CO2 combustion, Fuel. 86 (2007) 656–668.

[30] W. Forstall, A.H. Shapiro, Momentum and mass transfer in coaxial gas jets, Journal of Applied Mechanics. 18 (1951) 219–228.

[31] N. Chigier, J. Beer, The flow region near the nozzle in double concentric jets, Journal of Basic Engineering. 86 (1964) 797.

[32] N. Chigier, J. Beer, Velocity and static-pressure distributions in swirling air jets issuing from annular and divergent nozzles, Journal of Basic Engineering. 86 (1964) 788.

[33] J. Beer, N. Chigier, Impinging jet flames, Combustion and Flame. 12 (1968) 575–586.

[34] J. Beer, N. Chigier, K. Lee, Modeling of double concentric burning jets, Proc. Combust. Inst. 9 (1963) 892–900.

[35] D. Durao, J. Whitelaw, Turbulent mixing in the developing region of coaxial jets, Journal of Fluids Engineering. 95 (1973) 467.

[36] N.W.M. Ko, A.S.H. Kawn, The initial region of subsonic coaxial jets, Journal of Fluid Mechanics. 73 (1976) 305–332.

[37] C.T. Crowe, R.A. Gore, T.R. Troutt, Particle dispersion by coherent structures in free shear flows, Particulate Science and Technology. 3 (1985) 149–158.

[38] I.M. Kennedy, M.H. Moody, Particle dispersion in a turbulent round jet, Experimental Thermal and Fluid Science. 18 (1998) 11–26.

[39] J. Pedel, J. Zhang, J. Thornock, J.O.L. Wendt, P. Smith, Ignition of coaxial turbulent oxy-coal jet flames: Experiments and simulations collaboration, Clearwater, Florida, 2011.

[40] S.G. Budilarto, An experimental study on effects of fluid aerodynamics and particle size distribution in particle laden flows, Purdue University, West Lafayette, Indiana, USA, 2003.

[41] S. Khare, T. Wall, A. Farida, Y. Liu, B. Moghtaderi, R. Gupta, Factors influencing the ignition of flames from air-fired swirl pf burners retrofitted to oxy-fuel, Fuel. 87 (2008) 1042–1049.

[42] N. Oka, T. Murayama, H. Matsuoka, S. Yamada, T. Yamada, S. Shinozaki, et al., The influence of rank and maceral composition on ignition and char burnout of pulverized coal, Fuel Processing Technology. 15 (1987) 213–224.

[43] S. Su, J.H. Pohl, D. Holcombe, J.A. Hart, A proposed maceral index to predict combustion behavior of coal, Fuel. 80 (2001).

[44] S. Su, J.H. Pohl, D. Holcombe, J.A. Hart, Techniques to determine ignition , flame stability and burnout of blended coals in p . f . power station boilers, Progress in Energy and Combustion Science. 27 (2001) 75–98.

[45] M. Cloke, E. Lester, Characterization of coals for combustion using petrographic analysis: a review, Fuel. 73 (194AD) 315–320.

[46] V. Halatte, Rank and maceral composition on coal combustion characteristics, Fuel Processing Technology. 20 (1988) 297–306.

[47] J. Zhang, K.E. Kelly, E.G. Eddings, J.O.L. Wendt, Ignition in 40kW co-axial turbulent diffusion oxy-coal jet flames, Proc. Combust. Inst. 33 (2011) 3375–3382.

[48] J. Zhang, K.E. Kelly, E.G. Eddings, J.O.L. Wendt, CO2 effects on near field aerodynamic phenomena in 40kW co-axial, oxy-coal, turbulent , diffusion flames, International Journal of Greenhouse Gas Control. 5 (2011) S47–S57.

[49] J. Zhang, Oxy-coal combustion: Stability of coaxial pulverized coal flames in O2/CO2 environments, University of Utah, 2010.

[50] W. Morris, An examination of pulverized coal combustion aerosols in air and in retrofit oxy-fired combustion environments, University of Utah, 2011.

[51] J. Chedaille, Measurements in flames, Crane Russak, New York, 1972.

[52] a. V. Murthy, I. Wetterlund, D.P. DeWitt, Characterization of an ellipsoidal radiometer, Journal of Research of the National Institute of Standards and Technology. 108 (2003) 115.

[53] E. Villermaux, H. Rehab, Mixing in coaxial jets, Journal of Fluid Mechanics. 425 (2000) 161–185.

[54] E.B.C. Schettini, The density field of coaxial jets with large velocity ratio and large density differences, International Journal of Heat and Mass Transfer. 44 (2001) 1913–1924.

[55] S.P. Khare, T.F. Wall, A.Z. Farida, Y. Liu, B. Moghtaderi, R.P. Gupta, Factors influencing the ignition of flames from air-fired swirl pf burners retrofitted to oxy-fuel, Fuel. 87 (2008) 1042–1049.

[56] S. Pregermain, Rank and maceral effects on coal combustion characteristics, Fuel Processing Technology. 20 (1988) 297–306.

[57] S. Su, J.H. Pohl, D. Holcombe, J.A. Hart, A proposed maceral index to predict combustion behavior of coal, Fuel. 80 (2001) 699–706.

[58] D.M. Grant, R.J. Pugmire, T.H. Fletcher, A.R. Kerstein, Chemical model of coal devolatilization using percolation lattice statistics, Energy & Fuels. 3 (1989) 175–186.

[59] M.S. Solum, R.J. Pugmire, D.M. Grant, 13C solid-state NMR of Argonne premium coals, Energy & Fuels. 3 (1989) 187–193.

[60] T.H. Fletcher, A.R. Kerstein, R.J. Pugmire, D.M. Grant, Chemical percolation model for devolatilization. 2. Temperature and heating rate effects on product yields, Energy. 4 (1990) 54–60.

[61] T.H. Fletcher, A.R. Kerstein, R.J. Pugmire, M.S. Solum, D.M. Grant, Chemical percolation model for devolatilization . 3 . Direct use of 13C NMR data to predict effects of coal type, Energy. 6 (1992) 414–431.

[62] R.J. Pugmire, M.S. Solum, D.M. Grant, S. Critchfield, T.H. Fletcher, Structural evolution of matched tar-char pairs in rapid pyrolysis experiments, Fuel. 70 (1991) 414–423.

[63] T.H. Fletcher, M.S. Solum, D.M. Grant, S. Critchfield, R.J. Pugmire, Solid state 13C and 1H NMR studies of the evolution of the chemical structure of coal char and tar during devolatilization, Symposium (International) on Combustion. 23 (1991) 1231–1237.

[64] H. Huang, K. Wang, D.M. Bodily, Density Measurements of Argonne Premium Coal Samples, Energy & Fuels. 9 (1996) 20–24.

[65] C. Crowe, J. Chung, Particle mixing in free shear flows, Progress in Energy and Combustion. 14 (1988) 171–194.

[66] E. Longmire, J. Eaton, Structure of a particle-laden round jet, Journal of Fluid Mechanics. 236 (1992) 217.

[67] Y. Hardalupas, A.M.K.P. Taylor, J.H. Whitelaw, Velocity and particle-flux characteristics of turbulent particle-laden jets, Proceedings of the Royal Society A: Mathematical, Physical and Engineering Sciences. 426 (1989) 31–78.

[68] C.J. Call, I.M. Kennedy, Measurements and simulations of particle dispersion in a turbulent flow, International Journal of Multiphase Flow. 18 (1992) 891–903.

[69] J.O.L. Wendt, Mechanisms governing the formation and destruction of NOx and other nitrogenous species in low NOx coal combustion systems, Combustion Science and Technology. 108 (1995) 323–344.

[70] D.W. Pershing, Nitrogen oxide formation in pulverized coal flames., University of Arizona, 1976.

[71] T. Wall, R. Stanger, S. Santos, Demonstrations of coal-fired oxy-fuel technology for carbon capture and storage and issues with commercial deployment, International Journal of Greenhouse Gas Control. 5 (2011) S5–S15.

[72] S. Hjärtstam, K. Andersson, F. Johnsson, B. Leckner, Combustion characteristics of lignite-fired oxy-fuel flames, Fuel. 88 (2009) 2216–2224.

[73] T.F. Wall, I.M. Stewart, The measurement and prediction of solids- and soot-absorption coefficients in the flame region of an industrial P.F. chamber, Symposium (International) on Combustion. 14 (1973) 689–697.

[74] T. Wall, S. Khare, Radiative transfer in oxy-fired furnaces and impact of coal properties, technical note 27, 2007.

[75] S.A. Varma, Mathematical model for radiation heat transfer during combustion of pulverized coal in an absorbing, emitting, and anisotropically scattering medium, University of Utah, 1981.

[76] J.P. Holman, Heat Transfer, 8th ed., McGraw-Hill, 1997.

[77] H.C. Hottel, Radiative Transfer, McGraw-Hill, 1967.

[78] H.C. Hottel, R.B. Egbert, Radiant Heat Transmission from Water Vapor, AIChE Trans. 38 (1942) 531–565.

[79] B. Leckner, Spectral and total emissivity of water vapor and carbon dioxide, Combustion and Flame. 19 (1972) 33–48.

[80] T.F. Wall, I.M. Stewart, The measurement and prediction of solids- and soot absorption coefficients in a flame region of an industrial p.f. chamber, Symposium (International) on Combustion. 14 (1973) 689–697.

[81] J.G. Knudsen, O. State, H.C. Hottel, A.F. Sarofim, P.C. Wankat, Perry's Chemical Engineers' Handbook, Section 5: Heat and Mass Transfer, 8th Editio, 1999.

[82] T. Henriksen, T. Ring, D. Call, E. Eddings, A. Sarofim, Determination of soot refractive index as a function of height in an inverse diffusion flame, in: 5th U.S. Combustio Meeting, University of California at San Diego, 2007: pp. 1795–1803.

[83] J.T. McCartney, S. Ergun, Optical properties of graphite and coal, 1967.

[84] A.L. Brown, T.H. Fletcher, Modeling soot derived from pulverized coal, Energy & Fuels. 12 (1998) 745–757.

[85] A. Brown, Modeling soot in pulverized coal flames, Brigham Young University, 1997.

[86] A.L. Haneberg, Soot volume fraction determined by two-color extinction in a practical scale pulverized coal flame, Brigham Young University, 1997.

[87] D.R. Tree, On line measurement of primary fine particulate matter, 1999.

[88] C. Stimpson, T. Reeder, D. Tree, A. Fry, Soot measurements in an air and oxy-fired coal flame, in: 24th Annual ACERC Conference, Provo, Utah, USA, 2010.

[89] C. Stimpson, T. Blanc, D.R. Tree, W. Morris, J.O.L. Wendt, A. Fry, Line of sight soot measurements in oxy- and air-fired pulverized coal flames, 2012.

[90] D.B. Spalding, H.C. Hottel, S.L. Bragg, A.H. Lefebvre, D.G. Shepherd, A.C. Scurlock, The art of partial modeling, Symposium (International) on Combustion. 9 (1963) 833–843.

[91] J.P. Smart, On the effect of burner scale and coal quality on low NOx burners performance, The University of London, 1992.

[92] J. Boussinesq, Essai sur la théorie des eaux courantes, 26 Ème Édn Acad Sci Paris. 23 (1877) 1–680.

[93] L. Prandtle, Eine Beziehung zwischen Wärmeaustausch und Strömungswiderstand der Flüssigkeiten, Physics. 11 (1925) 1072–1078.